Rubisco's chiropractor: a study of higher plant Rubisco activase

A thesis submitted in partial fulfilment of the requirement for the Degree of Doctor of Philosophy in Biochemistry

2015

Jeremy Russell Keown
University of Canterbury

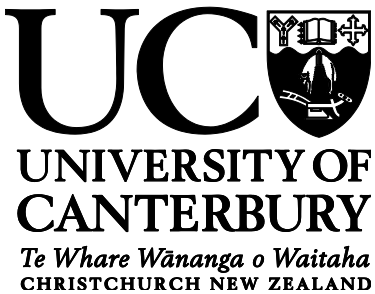

Table of Contents

Acknowledgements

First and foremost I must thank my supervisor Grant for his support and constant encouragement to think for myself. His tireless efforts to educate me on so many biophysical techniques helped me to gain an understanding of not just how everything works, but also why it sometimes doesn't. The long discussions about science, cricket, or the weekend made my PhD studies a relaxed and enjoyable experience.

I wish to thank Jackie for her infallible assistance in whatever I was doing, helping with everything from TEM to cake production. Ren and Mike, thank you for assistance with AUC or crystallography whenever it was required. To Haydyn and Nigel of the Australian Synchrotron SAXS beam line thank you for all your effort. Your troubleshooting at the beam line all hours of the day and night was always greatly appreciated, and without this help this thesis would be much more brief.

To my mum, dad, brothers, and grandparents thank you for always taking an interest in my studies, and for listening when I was trying to explain why an experiment didn't work. I was never lacking in encouragement at home.

Finally to my fellow lab members (in no particular order) Eric, Mo, Kathy, Rachel, Amy 1 and 2, Akshita, Dylan, Sarah, Jenn, Jared, Nivas, Luigi, Penel and other 6th floor lab members. You have all made it such a great place to learn, have coffee, play Frisbee, sing karaoke, and go to conferences together. I am so lucky to count all of you as great friends and to have spent so much time with this stellar bunch of people. Without you all this thesis would never have been possible. Thank you.

Abbreviation list

Å	Angstrom
B-ME	β-mercaptoethanol
µM	Micromolar
µL	Microlitre
°C	Degrees Celsius
3PG	D-3-phosphogylcerate
AAA+	ATPases associated with diverse cellular activities
ADP	Adenosine diphosphate
AMP-PNP	Adenosine 5′-(β,γ-imido) triphosphate
ANS	8-anilino-1-naphthalalenesulfonic acid
ATP	Adenosine triphosphate
ATPγS	Adenosine 5'-(γ-thio) triphosphate
AUC	Analytical ultracentrifugation
BTP	Bis-tris propane
c(M)	Continuous mass distributions
c(S)	Continuous Svedberg distributions
CA1P	2-carboxy-D-arabinitol-1-phosphate
CBB	Calvin-Bensen-Bassham
CD	Circular dichroism
cDNA	Complementary deoxyribonucleic acid
D_{max}	Maximum dimension

DSF	Differential scanning fluorometry
DTT	Dithiothreitol
EDTA	Ethylenediaminetetraacetic acid
EM	Electron microscopy
FCS	Fluorescence correlation spectroscopy
IPCC	Intergovernmental Panel on Climate Change
IMAC	Immobilised metal affinity chromatography
K_A	Association constant
K_D	Dissociation constant
kDa	Kilodalton
kV	Kilo volts
L	Litre
NAD^+/NADH	Nicotinamide adenine dinucleotide (reduced/oxidised)
nm	Nano metre
nanoESI-MS	Nano ElectroSpray Ionisation Mass Spectroscopy
MDa	Megadalton
mL	Millilitre
mM	Millimolar
mm	Millimetre
LB	Lysogeny broth
LDS	Lithium dodecyl sulfate
LSU	Large subunit
p	Poise

PCR	Polymerase chain reaction
PEG	Polyethylene glycol
PEP	Phosphoenolpyruvate
PMSF	phenylmethanesulfonylfluoride
ppm	Parts per million
ppt	Precipitate
psi	Pounds per square inch
Rca	Rubisco activase
RFU	Relative fluorescent units
Rpm	Revolutions per minute
RuBP	Ribulose 1,5-bisphosphate
Rubisco	Ribulose 1,5-bisphosphate carboxylase/oxygenase
Rubisco activase	Ribulose 1,5-bisphosphate carboxylase/oxygenase activase
$S_{20,w}$	Sedimentation coefficient at 20°C in water
SAXS	Small angle X-ray scattering
SDS-PAGE	Sodium dodecyl sulfate polyacrylamide gel electrophoresis
SEC	Size exclusion chromatography
SEC-SLS	Size exclusion chromatography – static light scattering
SE	Sedimentation equilibrium
SSU	Small subunit
SV	Sedimentation velocity
TEM	Transmission electron microscopy
TEV	Tobacco etch virus

USP	Ubiquitin serine protease
UV	Ultraviolet
v/v	Volume per volume
w/v	Weight per volume
XuBP	Xylulose 1,5-bisphosphate

Publications

During the course of my PhD studies two sections of work were published.

Keown, J. R., Griffin, M. D. W., Mertens, H. D. T. & Pearce, F. G. Small oligomers of ribulose-bisphosphate carboxylase/oxygenase (Rubisco) activase are required for biological activity. *The Journal of Biological Chemistry* **288**, 20607-20615 (2013).

I contributed all protein samples, collected all data and contributed to manuscript preparation. I carried out the SEC-SLS data analysis and was guided through the analysis of AUC and SAXS modelling by Dr Mike Griffin and Dr Haydyn Mertens, respectively.

Keown, J. R. & Pearce, F. G. Characterisation of spinach ribulose 1,5-bisphosphate carboxylase/oxygenase activase isoforms reveals hexameric assemblies with increased thermal stability. *Biochemical Journal* **464,** 413-424 (2014).

I carried out all experiments involving the wild type and variant tobacco Rubisco activase. Additionally I carried out the SAXS modelling for both the tobacco and spinach proteins. I contributed to experimental design and manuscript preparation with my supervisor Dr Grant Pearce.

Abstract

Rubisco activase operates as the chaperone responsible for maintaining the catalytic competency of Ribulose 1,5-bisphophate carboxylase oxygenase (Rubisco) in plants. Rubisco is notoriously inefficient, rapidly self-inactivating under physiological conditions. Rubisco activase uses the power released from the hydrolysis of ATP to power a conformational change in Rubisco, reactivating it. Rubisco activase has been previously shown to form a large range of species in solution; however, little has been done to relate the size of oligomeric species and physiological activity.

In this thesis data is presented from a range of biophysical techniques including analytical ultracentrifugation, static light scattering, and small angle X-ray scattering combined with activity assays to show a strong relationship between oligomeric state and activity. The results suggest that small oligomers comprising 2-4 subunits are sufficient to attain full specific activity, a highly unusual property for enzymes from the AAA+ family. Studies utilising a number of Rubisco activase variants enabled the determination of how Rubisco and Rubisco activase may interact within a plant cell. A detailed characterisation of the α-, β-, and a mixture of isoforms further broadened our knowledge on the oligomerisation of Rubisco activase. Of particular importance was the discovery of a thermally stable hexameric Rubisco activase variant.

It is hoped that these findings may contribute to development of more heat tolerant Rubisco activase and lead research into more drought resilient crop plants.

Chapter One: **Introduction**

Ribulose 1,5-bisphosphate carboxylase/oxygenase (Rubisco) activase is a key chaperone protein in the CO_2 fixation pathway in plants. Rubisco activase uses the power of ATP hydrolysis to reactivate Rubisco, the enzyme which catalyses the first step of the carbon fixation pathway. The tendency of Rubisco to catalytically misfire necessitates the need for the reactivating protein, Rubisco activase.[1] Rubisco activase aggregates *in vitro* at temperatures of approximately 38 °C, this means that above these temperatures the lability of Rubisco activase limits the photosynthetic potential of the plant.[2]

Rubisco activase is a member of the ATPases associated with diverse cellular activities (AAA+) family of ATPases which couple the chemical hydrolysis of adenosine triphosphate (ATP) to mechanical force to achieve rearrangement within a target protein. Recent structural studies have added much needed atomic resolution data[3,4]; however, much is still unknown about the oligomeric state in solution. Early studies suggested a more dynamic oligomeric state than commonly found in AAA+ proteins.[5]

A greater understanding of the interaction between Rubisco and Rubisco activase would allow for modification of either protein with the goal of increasing both the carbon fixation and energy production in crop plants. Due to the effect of climate change on the environment, an improved awareness of the role of Rubisco and Rubisco activase within higher plants will become valuable both socially and economically.

This thesis aims to characterise Rubisco activase from higher plants to elucidate the effect of physiologically relevant conditions on the oligomeric state, the effect of interface mutations to the oligomeric state, and differences between the two plant isoforms.

1.1 Discovery of Rubisco activase

In 1982 an *Arabidopsis thaliana* (arabidopsis) mutant, was shown to accumulate ribulose 1,5-bisphosphate (RuBP), among other Calvin-Benson-Bassham (CBB) cycle intermediates.[6] The Rubisco appeared structurally identical to other plants, though it was inactive.[6] The mutant plant was missing the protein responsible for reactivating Rubisco, this protein was named ribulose 1,5-bisphosphate carboxylase activation (Rubisco activase).[7] Salvucci *et al.* (1985) demonstrated the necessity of two approximately 40 kDa proteins for maintaining Rubisco activity.[8] Subsequent experiments showed that the Rubisco activase proteins were necessary to facilitate the removal of sugar-phosphates from the active site of Rubisco.[7]

Rubisco activase has two activities, the hydrolysis of ATP and the activation of Rubisco, both of these activities have been characterised from a number of species.[5,9-12] Discoveries in recent years utilising mass spectrometry[13], transmission electron microscopy[3] (TEM), size exclusion chromatography[5,11] (SEC), and X-ray crystallography[3] have elucidated some structural detail of Rubisco activase.

1.2 Rubisco activase plays an important role in the biosphere

1.2.1 *The light dependent and light independent reactions of photosynthesis*

Photosynthesis acts as the main route of carbon fixation into the biosphere, functioning in bacteria, algae, and plants. This pathway serves as the major entry point for energy for most life on earth, sequestering 100, 000, 000, 000 metric tons of CO_2 globally each year.[14]

Photosynthesis is divided into two sets of reactions the light dependent, and the light independent. The light reactions involve the harvesting of light using photosystem I and photosystem II, which shuttles protons across the thylakoid membrane creating an electrochemical potential. This potential is used by ATP synthase to create ATP from adenosine diphosphate (ADP) and P_i, later used to power activities within the cell. The light independent reactions occur independently of the light harvesting complexes and fix CO_2 using the CBB pathway. Rubisco is the first enzyme in this pathway and catalyses the formation of two three carbon sugars from the five carbon sugar, RuBP and CO_2.

The high abundance of Rubisco in plants means that a build up of inactive Rubisco is a major drain on carbon and nitrogen in the plant. Approximately 1% of reactions catalysed by Rubisco undergo catalytic misfire, creating sugar phosphate inhibitors which bind tightly in the active site, creating a "dead end" complex. To maintain Rubisco activity when photosynthesis is occurring higher plants use the chaperone protein Rubisco activase to remove these inhibitors

1.2.2 *The function and structure of Rubisco*

The first step of the carboxylation reaction is the carbamylation of an active site lysine.[15] Magnesium is then coordinated to the carbamate and stabilised by two active site residues, aspartate and glutamate, activating Rubisco.[16,17] RuBP, a 5 carbon sugar phosphate, binds to Mg^{2+}, causing movement of loop 6 closing the active site.[1] Carbon dioxide is then lyased RuBP to producing a six-carbon intermediate. This intermediate rapidly undergoes lysis between carbons three and four giving two molecules of 3-phosphoglycerate (3PG).

In 25% of reactions undertaken by higher plant Rubisco the oxygenation rather than the carboxylation reaction occurs. This results in the production of a single molecule of 3PG and a molecule of the two carbon sugar phosphate, phosphoglycolate.[18] Recycling of phosphoglycolate through photorespiration is costly with regards to both energy and the loss of carbon.[19,20]

Rubisco is found in four distinct structural arrangements; Form I, II, III, IV (Reviewed in Tabita *et al.,* 2008).[21] Form I Rubisco are hexadecameric, comprising eight large (~55 kDa) and eight small subunits (~15 kDa) across eukaryotes and bacteria.[21-23] The large subunit (LSU) dimerises, this dimer is the minimal catalytic unit used by all Rubisco forms.[16,24-26] A tetramer of LSU dimers forms the catalytic core of Form I higher plant Rubisco.[27-29] The small subunit (SSU) forms a tetramer which caps the LSU octamer at each end.[26] The SSU is highly variable between species and organisms where it plays a poorly understood role in CO_2/O_2 specificity.[30]

1.2.3 *The role of inhibitors in Rubisco activity*

Rubisco can be inhibited by several ligands, some produced by the plant as a means of regulation, and some that are produced as a by-product of catalysis. Some plant species, including *Solanum tuberosum* (potato) and *Phaseolus vulgarus* (common bean), produce the nocturnal inhibitor 2-carboxy-D-arabinitol 1-phosphate (CA1P) which down regulates Rubisco activity.[31,32] During daylight CA1P is degraded by CA1P-phosphatase allowing the reactivation of Rubisco, and the continuation of the dark reactions.[33] This provides an effective means of Rubisco regulation.

Additionally catalytic misfire occurs in ~1% of reactions resulting in a five carbon sugar-phosphate inhibitor becoming tightly bound in the active site, locking Rubisco in a closed conformational state.[1,34,35] In combination the production of these inhibitors provides effective short to medium term regulation of Rubisco activity; however, the removal of these inhibitors is also important. Rubisco activase is able to effectively and rapidly remove these inhibitors, reactivating Rubisco.

1.2.4 *Why does green type Rubisco require a reactivating chaperone?*

A comparison of Rubisco from a variety of kingdoms by Savir *et al.* (2010) found that there was a strong negative correlation between rate of reaction and specificity of CO_2.[36] Cyanobacterial Rubisco has a higher catalytic rate though lack of CO_2/O_2 specificity, while the highly specific non-green algae Rubisco have a much slower catalytic rate.[37,38] Rubisco with low CO_2 specificity produce higher levels of inhibitors; however, they are less tightly bound and are released more quickly. Rubisco which are more specific produce inhibitors at a much lower level[39], thus organisms at both extremes have a similarly low net occupancy of inhibitors at a given point in time. Higher plants, green algae, and photosynthetic bacteria fall between these two extremes.[36] The processes of fallover, where inhibitors build up in the active site of Rubisco, drive the need for Rubisco activase.[9,35,40,41]

For organisms populating this intermediary region the accumulation of inhibitors occurs with high enough frequency, and they remain bound sufficiently long to inactivate a large net amount of Rubisco. For higher plants it is also important to inactivate Rubisco, so it can respond to the light/dark cycle, and the corresponding changes in

CO_2/O_2 concentration. For this reason higher plants have a chaperone protein capable of reactivating Rubisco.[42,43]

1.2.5 *Importance of Rubisco activase on a global scale*

The Intergovernmental Panel on Climate Change (IPCC) 2013 report proposes that man-made global warming will increase the global surface temperature by between 1 and 3.7 °C by the end of the 21st century. Over the last 50 years atmospheric CO_2 concentrations have increased from 320 to 400 ppm and surface temperatures have increased by 1 °C. The report on climate change further suggests that not only will the operating temperatures for leaves in many environments increase, it is likely many environments will become more arid.

A study by Sage *et al.* (2008) showed that the limiting process controlling photosynthesis was not a declining capacity of the electron transport chain to regenerate RuBP, rather that Rubisco was not fully activated.[44] The study investigated black spruce, a common tree found in the boreal region of North American forests. They found that above 30 °C the activity of Rubisco activase becomes the rate limiting factor in photosynthesis.[44] The IPCC (2007) report showed that the predicted increase in temperature in the boreal region in Canada would be between 3-10 °C.[45]

A greater understanding of how Rubisco and Rubisco activase function in increasingly extreme and rapidly changing environments could lead to the development of a more tolerant Rubisco activase. New breeds of crop plants able to grow in more extreme climates will allow food production in a wider range of environments.

1.3 Thermal stability of Rubisco activase

1.3.1 *High thermal lability of Rubisco activase*

The thermolability of Rubisco activase has been well documented and is a cause of Rubisco inactivation at higher temperatures, and thus a potent "off switch" for photosynthesis.[44,46-50]

The β-isoform from a number of different species denature at ~40 °C in the absence of nucleotide, upon addition of either ADP or ATP/ATPγS the protein is stabilised by ~6 °C.[2,50] The α-isoform; however, is highly unstable, for example the α-isoforms from arabidopsis and spinach have melting points of around ~30 °C. Upon the addition of ATPγS they are stabilised by 11 °C and 25 °C, respectively.[51,52] Analysis of leaf extracts from arabidopsis, tobacco, and cotton show that there is a strong correlation between the temperature at which a plant lives and the temperature at which maximal Rubisco activation activity is achieved.[47,53-55] Thus Rubisco activases from tobacco and cotton have a greater Rubisco activation activity and are active to a higher temperature than Rubisco activase from arabidopsis. Leaf extracts from plants belonging to Solanaceae and non-Solanaceae families alike lose full ATPase and Rubisco activities before ~45 °C.[47] This inactivation of activase could have a useful physiological role by decreasing the reactivation of Rubisco under undesirable and inefficient photosynthetic conditions.

1.3.2 *Denaturation of Rubisco activase is responsible for inactivation of Rubisco at high temperatures*

It is important to control Rubisco activity and plants have a mechanism linked to a diurnal cycle. As previously mentioned Rubisco activase activity is reduced by a high ADP:ATP ratio, and by a poorly understood mechanism involving the redox-active α-isoform. Changes to the redox potential and the ADP:ATP ratio occur within the stroma in response to the diurnal light/dark cycle. Once Rubisco activase has been inactivated the inhibitors produced by the plant like CA1P and xylulose 1,5-bisphosphate (XuBP) inactivate Rubisco overnight.[44]

For over 30 years it has been shown that photosynthesis in higher plants is inhibited at temperatures of ~55 °C.[56] Higher temperatures destabilise the enediol intermediate within the Rubisco active site causing a six fold increase in XuBP with a rise in temperature from 20 to 45 °C.[57] However the increase in temperature also increases the flexibility of Rubisco leading to a net reduction in fallover.[57] Thus it appears that the major factor in Rubisco inactivation, and thus photosynthesis, at higher temperatures is the loss of Rubisco activase activity.

1.4 Rubisco activase is a AAA+ protein

1.4.1 *General AAA+ characteristics*

Sequence alignments of AAA+ proteins carried out by Neuwald *et al.* (1999) and others confirmed that Rubisco activase is a member of the AAA+ family of proteins.[58-60] AAA+ proteins are a large family of proteins found across all kingdoms of life, characterised by the presence of ATP binding sites.[61,62] AAA+ proteins share a conserved ATPase domain of around 200-250 amino acids in length.[63] The ATPase domain is comprised of three

canonical motifs the Walker A; Walker B; Sensor 1; and in some proteins a fourth motif, the Sensor 2.

The location of these motifs in *Nicotiana tabacum* (tobacco) Rubisco activase are shown in **Fig. 1.1**. Collectively the motifs constitute a Rossman fold which is responsible for nucleotide binding and hydrolysis.[58,64-68] The nucleotide binding pocket lies at the interface between two adjacent protomers within the AAA+ oligomer. This allows two arginine residues, a so called arginine finger, from the adjacent protomer to enter the active site and facilitate hydrolysis of the γ-phosphate.[69]

The AAA+ family have a number of highly conserved residues. A key active site lysine from the Walker A motif interacts with the β- and γ- phosphates of the nucleotide. Mutation of this residue prevents nucleotide hydrolysis and thus the protein loses its function.[59,70] Within the Walker B motif are glutamate and aspartate residues which prepare a water molecule for nucleophilic cleavage of the γ-phosphate of ATP.[71]

The Sensor 1 region is involved in a hydrogen-bonding network which assists in positioning a water molecule required in γ-phosphate cleavage, and as such is closely associated with the Walker B motif.[69] The Sensor 1 region also contains the arginine finger.

```
G.hirsutum α1    MAAEKEIDEETQTEKDRWKGLAYDISDDQQDITRGKGMVDSLFQAPMNDG 50
G.hirsutum β     ---AKEIDEDTQTDQDRWKGLAYDISDDQQDITRGKGMVDSLFQAPMNDG 47
N.tabacum        --EEKDADPKKQTDSDRWKGLVQDFSDDQQDITRGKGMVDSLFQAPTGTG 48
                     *: * ..**:.******. *:********************** . *

G.hirsutum α1    THYAVMSSYEYLSQGLKTYNLDNNMDGFYIAPAFMDKLVVHITKNFMSLP 100
G.hirsutum β     THYAVMSSYEYISQGLRTYDLDNNMDGFYIAPAFMDKLVVHITKNYMTLP 97
N.tabacum        THHAVLQSYEYVSQGLRQYNLDNKLDGFYIAPAFMDKLVVHITKNFLKLP 98
                 **:**:.****:****: *:***::**********************::.**

G.hirsutum α1    NIKVPLILGIWGGKGQGKSFQCELVFAKMGINPIMMSAGELESGNAGEPA 150
G.hirsutum β     NIKVPLILGIWGGKGQGKSFQCELVFAKMGINPIMMSAGELESGNAGEPA 147
N.tabacum        NIKVPLILGIWGGKGQGKSFQCELVFRKMGINPIMMSAGELESGNAGEPA 148
                 ************************ ***********************
                              Walker A
G.hirsutum α1    KLIRQRYREAADIIKKGKMCALFINDLDAGAGRMGGTTQYTVNNQMVNAT 200
G.hirsutum β     KLIRQRYREAADIIKKGKMCCLFINDLDAGAGRMGGTTQYTVNNQMVNAT 197
N.tabacum        KLIRQRYREAAEIIRKGNMCCLFINDLDAGAGRMGGTTQYTVNNQMVNAT 198
                 ***********:**:**:**.****************************
                                     Walker B
G.hirsutum α1    LMNIADNPTNVQLPGMYNKEENPRVPIIVTGNDFSTLYAPLIRDGRMEKF 250
G.hirsutum β     LMNIADNPTNVQLPGMYNKEENPRVPIIVTGNDFSTLYAPLIRDGRMEKF 247
N.tabacum        LMNIADNPTNVQLPGMYNKQENARVPIIVTGNDFSTLYAPLIRDGRMEKF 248
                 ******************:**.****************************
                                              Sensor 1     Arginine finger
G.hirsutum α1    YWAPTRDDRVGVCKGIFRTDGIPDEDIVKLVDTFPGQSIDFFGALRARVY 300
G.hirsutum β     YWAPTREDRIGVCTGIFRTDNVPVDDIVKLVDTFPGQSIDFFGALRARVY 297
N.tabacum        YWAPTREDRIGVCTGIFRTDNVPAEDVVKIVDNFPGQSIDFFGALRARVY 298
                 ******:**:***.******.:* :*:**:**.*****************
                                                                Sensor 2
G.hirsutum α1    DDEVRKWISDVGVAGVGKKLVNSRDGPPTFEQPKMTIEKLLEYGNMLVAE 350
G.hirsutum β     DDEVRKWIGEVGVNSVGKKLVNSREGPPSFEQPTMTIEKLLEYGNMLVAE 347
N.tabacum        DDEVRKWVSGTGIEKIGDKLLNSFDGPPTFEQPKMTIEKLLEYGNMLVQE 348
                 *******:. .*:  :*.**:** :***:****.************** *

G.hirsutum α1    QENVKRVQLADKYLSEAALGEANEDSINRGTFYGKAAQQVGVPVPEGCTD 400
G.hirsutum β     QENVKRVQLADKYLSEAALGNANDDAIKRGAF----------------- 379
N.tabacum        QENVKRVQLADKYLKEAALGDANADAINNGSFFAS--------------- 383
                 **************.*****:** *:*:.*:*

G.hirsutum α1    PNADNFDPTARSDDGTCTYKF 421
G.hirsutum β     ---------------------
N.tabacum        ---------------------
```

Figure 1.1. **Comparison of sequences for mature proteins used in this thesis detailing AAA+ motifs and key interface residues**. Highly conserved residues (*), semi conserved (:), and not conserved (.) are indicated. Residues involved in binding were found using PISA. Key salt bridge and hydrogen bonding residues from tobacco Rubisco activase (AAA78277) are shown and mapped onto the Rubisco activase α1 and β isoforms (ABB20913, AAG61120) from *Gossypium hirsutum (*cotton*)*. The alignment was performed using Clustal W2.[72]

The Sensor 2 region consists of a conserved arginine residue that interacts with the β- and γ-phosphate. Mutation of this residue significantly decreases ATPase activity.[73] The importance of this arginine is not fully understood; however, any mutation causes a complete loss of ATP binding and hydrolysis.[74] It is thought the arginine residue is involved in nucleotide hydrolysis, not nucleotide binding.[75,76] Currently it is purported that the residues are involved in hydrolysis, and increase the protein's stability through intersubunit contacts.[73]

A catalytically competent AAA+ active site requires the contribution of residues from an adjacent protomer, these dimers then typically assemble into a ring comprising five, six, or seven subunits.[59,77] In most cases a catalytically active closed ring is formed which increases thermal stability and optimises the number of competent nucleotide binding sites. It has been suggested that the shared residues allows some degree of nucleotide regulation of the oligomeric state and co-operativity between protomers.[63] Some AAA+ proteins, such as ClpA and FtsH, undergo a change from a stable closed ring structure to a spiral form upon addition of ADP.[78,79] The closed ring form is biologically active in many AAA+ proteins.

The formation of a ring creates a central pore to insert a part of a target protein for degradation or remodelling. For example, ClpA binds to target proteins and unravels them by threading through the central pore into the associated ClpP for proteolysis.[80] The ability of the protein complex to remain in contact with the target protein greatly increases the remodelling efficiency and allows optimal use of the mechanical force generated by the hydrolysis of ATP.

1.4.2 *CbbX, a red-type Rubisco activase*

In 2011 Mueller-Cajar *et al.* published the full length structure of the ~35 kDa protein AAA+ protein CbbX, a red algal Rubisco activase from the purple bacteria *Rhodobacter sphaeroides.*[43] CbbX, along with CbbY and CbbZ, are found downstream of the Rubisco genes.[81] Previous studies did not indicate that CbbX was phylogenetically similar to the green-type Rubisco activases.[35] Form I Rubiscos are divided into a green branch comprising higher plants, cyanobacteria and green algae, and a red branch present in photosynthetic bacteria and red algae.[21] The grouping of red and green type Rubisco activase follows that of the Rubisco. While the green-type Rubisco activases constitutively hydrolyse ATP, CbbX requires both the target Rubisco and the allosteric activator RuBP to be maximally active. The necessity of RuBP to activate CbbX means that CbbX will be active when photosynthesis is occurring and Rubisco is at risk of inactivation, providing an additional measure of control over the ATPase activity.

CbbX formed hexameric rings in the presence of ATP/RuBP and large fibrillar structures in the range of 0.6-10 MDa, in the presence of ATP alone.[43] Many AAA+ proteins form active ring structures and act by translocation of a substrate protein through the central pore. Ultimately this study was able to show that CbbX was able to pull on to the C-terminus of Rubisco which stimulated ATPase activity and reactivated Rubisco. It was suggested that the fibrillar state of CbbX is an inactive storage form of the enzyme caused by a low concentration of RuBP when photosynthesis is not occurring.

1.4.3 *The structure of Rubisco activase*

Currently two atomic structures of Rubisco activases have been published, both in 2011. Higher plant Rubisco activase (~380 residues) is comprised of three discrete domains, the N-termini, AAA+, and C-terminal domains (**Fig. 1.2A**). The N-terminal domain, (~70 residues) is important for interaction with the substrate, Rubisco.[3,82] The central AAA+ domain (~290 residues) comprises a Rossman fold containing the α/β subdomain and the smaller α-helical subdomain. The structure of the α-helical subdomain has been solved for both *Larrea tridentate* (creosote) and tobacco.[4] The structures show high similarity in the core architecture with a central four helix bundle as seen in many AAA+ domains, though one helix from the creosote structure appears as two in the tobacco structure (**Fig. 1.2B**).

The C-terminal extension (~20 residues), is necessary for both the ATPase and Rubisco reactivation activity.[3] The tobacco crystal structure lacks the N- and C- termini and some electron density in four flexible loop segments.[3] The C-terminal domain is important for the recognition of Rubisco from different families.

Tobacco Rubisco activase crystallised as a six subunit per turn spiral ($P6_5$), common for many AAA+ proteins.[83-85] Interface analysis of the proposed biologically relevant hexameric arrangement showed a large intersubunit interface with a buried surface area of ~1140 $Å^2$.[86] Interaction at the interface includes a salt bridge and a hydrogen bond network (**Table 1.1**).

A

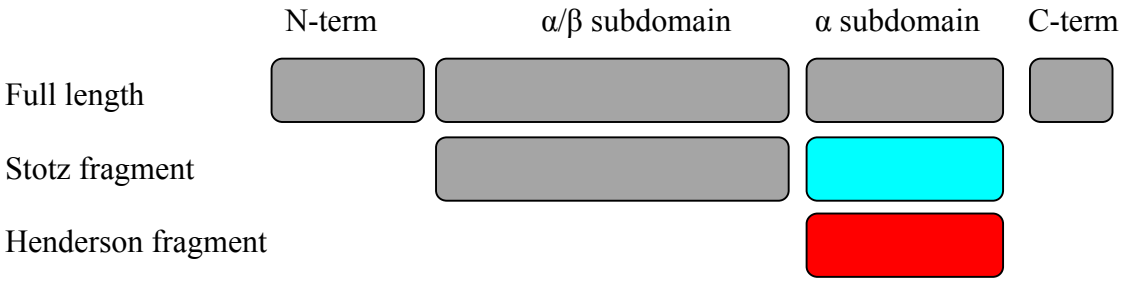

B

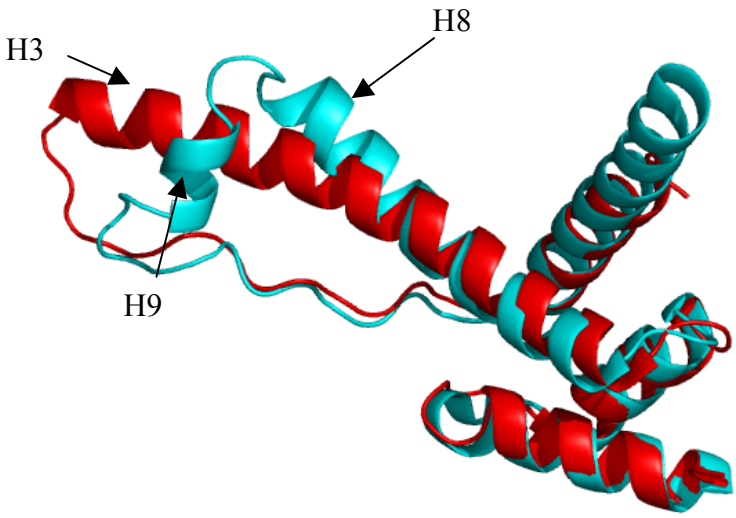

Figure 1.2. **Tobacco Rubisco activase has a split helix while creosote Rubisco activase has a single helix**. A) Domain arrangement in green type Rubisco activases, mapped against pieces for which atomic resolution structures have been solved. B) Comparison of the α-helical subdomains from creosote (red, PDB 3THG) and tobacco (cyan PDB 3T15). In creosote Rubisco activase the helix responsible for specificity, H3, is a single contiguous helix. In tobacco Rubisco activase the helix has been shortened and the helix is now two helicies, H8 and H9.

Hydrogen bonds			Salt-bridge		
Residue 1	Distance (Å)	Residue 2	Residue 1	Distance (Å)	Residue 2
Lys92	**2.91**	**Asp299**	**Lys92**	**3.88**	**Asp299**
Asn166	3.48	Asn320	**Lys92**	**2.91**	**Asp299**
Tyr249	3.84	Val355	Asp84	3.91	Arg303
Asn99	**2.9**	**Arg294**			
Asn99	**2.93**	**Arg294**			
Asn99	3.71	Tyr298			
Asn99	3.1	Gln330			

Table 1.1. **A number of residues provide stability at the intersubunit interface.** List of interface residues and bonds found in the $P6_5$ crystal lattice. Shown in bold are the residues that were the focus of this study. Residues participating in bonding at the interface were found using the PISA server.[86]

1.4.4 *Rubisco activase has two isoforms*

Some Rubisco activase enzymes exist in two distinct isoforms; the α-isoform (~420 residues, 46 kDa) and the β-isoform (~380 residues, 42 kDa). The two isoforms share common core architecture; however, the α-isoform is slightly larger with an extended C-terminal tail. The two isoforms are either produced by alternative splicing of the same mRNA or gene duplication events.[87] Most plants (spinach, cotton, and rice) express both isoforms; however, the Solanaceae family (tobacco, tomato, and potato) only contain the redox insensitive β-isoform.[88-91]

The activity of Rubisco activase must be tightly controlled so that it is most active when photosynthesis occurs during the day, while much less active when Rubisco is inactive at night. The activity of the β-isoform is regulated by the ADP:ATP ratio with high levels of ADP causing a loss of activity.[10] The ADP:ATP ratio changes during the day, ATP concentrations are high during the day, while ADP concentrations are high during the night.[92] This changing ADP:ATP ratio causes the β-isoform of Rubisco activase to be much more active during the day when it is required, whilst it is much less active during the night when it is not required.

The α-isoform is able to regulate its activity through formation of a C-terminal disulfide bond obstructing ATP binding.[6,92,93] The disulfide linkage allows the enzyme to be responsive to the changing redox potential within the stroma.[6] Reduction of the disulfide bond allows binding of ADP and ATP at the level seen for the redox insensitive β-isoform.[92,94,95] The redox potential and ADP:ATP ratio within the stroma provides a means of linking the diurnal cycle to Rubisco activase (and thus Rubisco) activity.[96]

1.4.5 *Binding and hydrolysis precede as two independent steps*

The conformational change caused by nucleotide binding has been measured using intrinsic fluorescence. The change in the intrinsic fluorescence in Rubisco activase is from tryptophan residues 109 and 250 (tobacco).[97] These tryptophan residues are located within the nucleotide binding Rossman fold, and have been used to monitor changes in structural arrangement caused by nucleotide binding.[5,11,82,97-99]

Early studies suggested that changes in oligomerisation causes a change in intrinsic fluorescence; however, it was later shown that there is no correlation of oligomerisation with ATP hydrolysis and intrinsic fluorescence.[11] No change in fluorescence is found without the addition of Mg or with the addition of ADP, suggesting only substrate binding causes a change in conformation.[5] Mutation of the arginine finger removed ATPase activity, but retained the change in intrinsic fluorescence upon addition of ATPγS.[11] Substitution of a non-hydrolysable ATP analogue has been shown to cause a change in intrinsic fluorescence.[11] This demonstrates that nucleotide binding, not hydrolysis, causes the change in intrinsic fluorescence.[11]

Hydrolysis of ATP by Rubisco activase is thought to follow three discrete stages. Initially Mg.ATP binds to Rubisco activase, causing movement of the two AAA+ subdomains.[5,100-102] The binding of ATP rearranges Rubisco activase into a state which is able to interact with Rubisco. Rubisco activase can then either interact with Rubisco, and hydrolyse ATP to power the removal of the inhibitor, or hydrolyse ATP without interacting with Rubisco.

It may be that post hydrolysis Rubisco activase rapidly dissociates from Rubisco presumably with ADP bound, how this occurs or which oligomeric state interacts with Rubisco at any stage of this process is currently unknown.

1.5 Rubisco activase has variable oligomeric states

Studies detailing the oligomeric state of Rubisco activase have shown a wide range of higher order species varying with both protein concentration, the presence of nucleotide or magnesium, and temperature.

1.5.1 *Protein concentration affects oligomeric state*

Salvucci *et al.* (1992) first demonstrated that a spinach and tobacco Rubisco activase mixture formed a range of oligomeric states and that addition of the crowding agent polyethylene glycol (PEG) caused a large increase in oligomeric size.[103] Wang *et al.* (1993) expanded these studies using mixed isoforms of spinach Rubisco activase.[5] They found that Rubisco activase eluted from a size exclusion chromatography (SEC) column as an asymmetric peak with a long trailing tail, indicating a range of species in rapid equilibrium was present in solution.[5] They also demonstrated the increase in specific ATPase activity as a function of increasing protein concentration, suggesting that higher order oligomers are required for maximal activity. The specific ATPase activity for the β- and α/β mixed isoforms both reach a maximum at a protein concentration of 1.5 μM.[5,104] Together these results suggest a relationship between oligomeric state and activity, with a plateau in specific activity inferring that a minimal catalytic unit has been reached.

With increasing protein concentrations, the β-isoform from arabidopsis formed species ranging from 280 to 660 kDa.[105] An intriguing find was an inactive, folded, and soluble 2 MDa assembly of activase, which may be analogous to the fibrillar structures seen for CbbX[43]; however, the physiological relevance for the green-type Rubisco activases is unknown. Formation of these large species took hours; however, the addition of nucleotide protected against production of these species.

Fluorescence correlation spectroscopy was used to assess the oligomerisation pathway for the β-isoform of cotton Rubisco activase in the presence of Mg.ADP.[106] It was found that the mostly accurate model for oligomerisation was monomer–dimer–tetramer–hexamer-four stacked hexamers. The monomer dimer equilibrium had a dissociation coefficient of 3.5 μM. The oligomerisation steps up to a hexamer all had dissociation coefficients of 1 μM, and formation of four stacked rings had a dissociation coefficient of 25 μM.[106] This same study found that Rubisco activase was monomeric at concentrations below 0.3 μM.

1.5.2 *Physiological conditions affect oligomeric state*

As Rubisco activase is a AAA+ ATPase it was important to consider the effect that substrate (ADP), product (ATP) and cofactor (Mg) may have on the oligomeric state. Many AAA+ domains, such as the GTPase, PspF and the foot and mouth virus protein, 2C, assemble into the active hexameric rings upon addition of ATP.[107,108]

Much of the molecular weight determination of Rubisco activase has been carried out using SEC.[5,11,103,105,109] Rubisco activase is thermally unstable without nucleotide present, and SEC experiments can take hours. Generally these experiments are carried out

at 4 °C in the absence of nucleotide or 25 °C in the presence of nucleotide. Tobacco β-isoform Rubisco activase appeared insensitive to changes in molecular weight with the addition of any nucleotide in the absence of magnesium.[11] The β-isoform from spinach, in the absence of magnesium, was twice the molecular weight with ATP versus ADP.[11] A mixture of α- and β-isoforms from spinach showed no change in oligomeric state with ADP or ATP in the absence of magnesium; however, Mg.ADP decreased the oligomeric state while Mg.ATP/ATPγS caused an increase relative to the absence of nucleotide.[5] Magnesium alone reduces oligomeric state significantly.[5] These results suggest that the β-isoform from the tobacco (Solanaceae family) has a different nucleotide response to the same isoform from the non-Solanaceae family.

Comparing the most physiologically relevant condition for non-Solanaceae plants, with both isoforms present along with nucleotide and magnesium, it appears that the binding of ATP causes formation of much larger Rubisco activase species. Presumably this is influenced by the α-isoform; however, there is no literature on the oligomeric state of isolated α-isoform. Recent results from our lab show that the spinach Rubisco activase α-isoform and an α/β- isoform mixture can form hexamers in the presence of Mg.ATPγS.[110]

Changes in oligomeric state may be influenced by a second nucleotide binding domain found in the N-termini, where either ADP or ATP could bind.[101] Competitive assays with ADP versus adenosine 5′-(β,γ-imido)triphosphate (AMP-PNP) for tobacco Rubisco activase suggest that ADP binds more tightly in the absence of magnesium; however, in the presence of the cofactor, ADP and ATP bind with equal affinity.[13,98,100]

Blayney *et al.* (2011) found tobacco Rubisco activase oligomers ranging from monomer to hexamer, including all intermediate oligomers with nano electrospray ionisation mass spectrometry.[13] The presence of higher order oligomeric species was noted with increasing ionic strength, though these were less stable. Lilley *et al.* (1997) reported a large decrease in activity when ionic strength is lowered.[111] Together these results suggest that smaller species of Rubisco activase are less catalytically competent.[111]

1.5.3 *Interface mutations of Rubisco activase*

Mutation of a key arginine (R294, tobacco), proposed to interact with ATP, located within sensor 2 have changed the resulting proteins structure and function.[3,13] The R294A variant reduces the maximal ATPase and Rubisco activation activities to approximately 20% of wild type.[11] However mutation of this same residue to valine maintains both activities at wild type levels.[3] R294A was found to form much smaller oligomers (110 vs 250 kDa) than the wild-type enzyme in the presence of ADP.[11] R294A incubated with ATP showed a slight decrease in molecular weight (230 versus 250 kDa) and increased resistance to trypsin digest when compared to the wild-type enzyme.[11]

Further investigation of the R294A variant protein by mass spectrometry showed the protein formed stable hexamers in the presence of the non-hydrolysable analogue Mg.ATPγS.[13] Wild-type tobacco Rubisco activase did not undergo hexamer formation under the same conditions. A doubling in the intrinsic fluorescence yield with ATPγS by R294A[13] compared to the wild-type enzyme has been suggested to be caused by hexamer formation.[11,13]

The valine variant, R294V, in the presence of Mg.ATPγS, also forms a hexamer as shown by negative stain TEM and a low resolution model was solved (EMD 1940).[3] This model was then used as an envelope to fit the atomic resolution structure of truncated wild-type Rubisco activase and build a hexameric atomic resolution model. The hexameric structure proposed in this paper was achieved after reorienting the monomers, essentially twisting the crystal lattice from $P6_5$ to P6 symmetry.

To find the minimally active oligomer, charge switching of a key salt bridge K92–D299 was carried out to create Rubisco activase protomers with an interface which cannot oligomerise. The variant proteins K92D, D299K, D299A and a double mutant K92D/D299K were monomeric and had no activity.[3] Experiments where the total protein concentration was kept constant but the ratio of wild type and variant enzyme was changed was used to approximate the minimally active oligomer. The likelihood of incorporation of a unidirectional variant was used to calculate the likely oligomer in solution, as incorporation of a variant protein effectively terminated oligomer formation at that interface.[109]

This study showed that for all unidirectional variant proteins the minimally active ATPase oligomer was around a trimer.[3] For K92D, D299K, and D299A the minimal oligomer for Rubisco activation was 4, 3, and 5 subunits, respectively. The authors concluded that D299A provided the best model and combined with the structural data proposed that the minimal active oligomeric state for wild-type tobacco Rubisco activase was a closed hexamer as observed for the R294 variant proteins.

1.6 The regulation of Rubisco by Rubisco activase

1.6.1 *Mechanism and site of interaction*

It has long been established that Rubisco activase from the Solanaceae family can only activate Rubisco from the same family, the same is true from non-Solanaceae.[112] Esau *et al.* (1998) found the C-terminus of Rubisco activase confers species specificity between Solanaceae (tobacco) and non-Solanaceae (spinach, rice) plants, and key residues involved in the interaction between Rubisco and Rubisco activase have been proposed.[112-114] Strong evidence suggests a hydrophobic patch of residues on Rubisco and Rubisco activase mediate the interaction between the two enzymes (**Fig. 1.3**).[4,104]

Currently only a single example of the interaction domain from each of the Solanaceae and non-Solanaceae grouping has been solved to atomic resolution (**Fig. 1.2**). Creosote (non-Solanaceae) Rubisco activase has a single helix, H3, with the residues important for the Rubisco recognition, whereas tobacco (Solanaceae) Rubisco activase has split the helix into two separate helices, H8 and H9 (**Fig. 1.2B**). The Rubisco specificity can be switched by mutating residues located near the helices end.[104] Clearly this region is responsible, at least in part, for the species specific recognition of Rubisco activase for Rubisco. The creosote fragment extends by a further 3 turns, suggesting it may not just be the nature of the residues but also the length of the helix which contributes to the specificity between Solanaceae and non-Solanaceae.

Solanaceae Rubisco residues R89, E93, K94 have been shown to interact with Rubisco activase residues L314, K312, and D311, respectively (**Fig. 1.3**).[4,104,113,115] In non-Solanaceae plants residues P89, E93, D(E)94 from Rubisco interact with Rubisco activase residues V314, K(R)312, and K311.[4,104,113,115] Switching of these residues

between species from either Rubisco activase or Rubisco causes changes in species specificity.[104,115-117] Cross species substitution of the Rubisco SSU showed no change in activation by Rubisco activase, suggesting the small subunit plays no role in Rubisco activase recognition.[118] Mutations within the Rubisco solvent channel did not change the reactivation by Rubisco activase.[119] The residues responsible for specificity on Rubisco are located adjacent to the LSU active site.[120] How residues in these regions are able to cause formation of a binary Rubisco activase-Rubisco complex is unknown. No stable interaction of Rubisco activase and Rubisco has been documented using structural or biophysical methods.

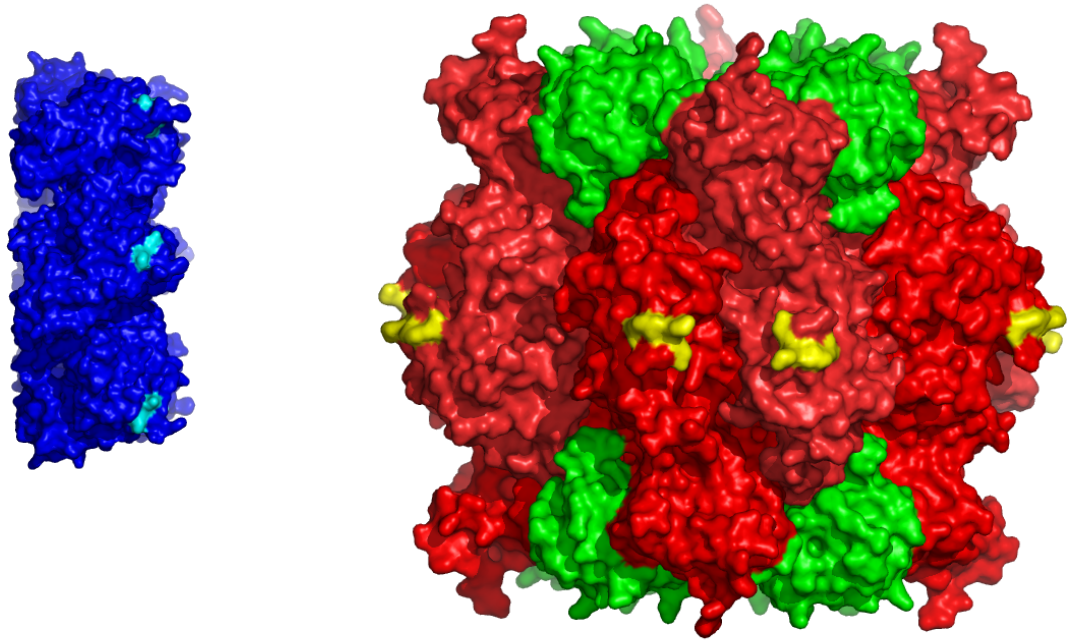

Figure 1.3. **Tobacco Rubisco activase specificity for tobacco Rubisco occurs through specific residues.** Tobacco Rubisco (PDB 1EJ7) interacting with a Rubisco activase hexamer (PDB 3ZW6) from the same species. The orientation of interaction between Rubisco and Rubisco activase is unknown. The Rubisco LSU is shown in red, and the SSU in green, and the residues important for Rubisco activase recognition are in yellow. Rubisco activase is shown in blue with the interacting residues in cyan.

1.6.2 *Mechanism of reactivation of Rubisco by Rubisco activase*

Two mechanisms for the removal of inhibitors from Rubisco have been proposed. Firstly, that it proceeds by the same mechanism as other AAA+ proteins and CbbX, where an activated closed ring structure pulls part of the target protein through the central pore causing loss of secondary structure. The R294 variants suggest that stable hexameric Rubisco activase oligomers can form and that, in the case of R294V, maintain wild type activities.[3] The R294A mutant; however, has much reduced ATPase and Rubisco activation activities.[13,105] Preliminary studies in our lab have shown that the α-isoform from spinach is able to form stable hexamers, and that these can activate Rubisco.[110] It may be that the R294 variants mimic an interaction of the extended α-isoform C-terminus which occurs when ATP binds, causing hexamer formation.

AAA+ proteins commonly achieve remodelling of the target protein by drawing the polypeptide through the central pore, in tobacco Rubisco activase three loop regions facing the central channel appear necessary for both ATPase and Rubisco activation function.[3,59]

The second proposed mechanism postulates that an elongated Rubisco activase oligomer encircles inhibited Rubisco and the hydrolysis of ATP then powers the movement of each subunit relative to others in the ring causing Rubisco rearrangement.[87] After hydrolysis, the presence of ADP in the active site causes dissociation.[87] Early EM studies suggested Rubisco activase spiraled around Rubisco; however, this result has not been replicated.[121] Helix 8 and 9 (tobacco), which are responsible for the specificity of Rubisco activase for Rubisco, are located on the exterior of the hexameric crystal

structure.[3,4] This suggests a side on interaction to bring these residues into contact with their counterparts on Rubisco.

1.7 Aim of this study

Currently two theories exist around the oligomerisation of Rubisco activase and its active oligomeric state. The first theory proposes a closed hexameric oligomer is necessary for activity. The second theory requires an open oligomer where small oligomers are able to reactivate Rubisco.

The primary aim of this study is to characterise the oligomerisation and activity of Rubisco activase using the model Rubisco activase β-isoform from tobacco. To further the molecular basis for oligomerisation site directed mutagenesis of key interface residues will be used to probe the role of individual residues. These variant proteins will also be used to investigate how oligomerisation and activity are linked.

The second aim of this thesis is to examine how the β- and redox sensitive α-isoforms interact, specifically what is the role of the α-isoform in hetero oligomer formation. There is currently no literature on the oligomerisation of the α-isoform.

With an understanding of how oligomerisation and activity are related I will look to define a single oligomer or range of oligomers which are required for activity. This will strengthen the case for one of the two oligomerisation theories proposed above. An increased understanding of how Rubisco activase functions *in vivo* will give insights as to how it interacts with Rubisco *in planta*.

Chapter Two: **Materials and methods**

2.1 Materials

All materials, unless otherwise stated, were obtained from Sigma-Aldrich (St. Louis, Missouri, United States of America) or Invitrogen/Life Technologies (Victoria, Australia). Chromatography resin and prepacked columns were from GE Healthcare Lifesciences (Auckland, New Zealand). Ultrapure water (Milli-Q, Millipore) was used for preparation of all media and buffers. Extinction coefficients were calculated from amino acid sequence using the online server PROTPARAM.[122] A_{280} readings were made using a Nanodrop 1000, or for analytical ultracentrifugation (AUC) using a wavelength scan using a CARY 100 Bio UV/Vis spectrometer. Nucleotide concentrations were calculated from the A_{260} where 1 mM adenosine nucleotide gives an absorbance of 15.4 (Sigma).

2.2 Nucleotide purity

2.2.1 *ATPγS contains contamination*

This work was carried out with the help of Mr Dion Thompson (Callaghan Innovation). Both ADP and ATP have previously been seen to affect the oligomeric state of Rubisco activase differently.[5] Thus it was important to assess the purity of ATPγS from Sigma (America) or Bio-Ryte (England). High performance liquid chromatography was chosen as the method of purity assessment. Samples were run on a Dionex 3000 system comprising Dionex p680 pump, integrated with an ASI-180 autosampler, a TCC-100 temperature controller and Diode Array Detector (DAD-3000RS). A Phenomenex Luna 5 μm C18(2), 100 Å, 250 x 4.6 mm column was used, run at a flow rate of 1 $mL.min^{-1}$.

All nucleotides were reconstituted in ultrapure water, a running buffer of 50 mM NaPi, pH 7.4 was used. Absorbance at 260 nm was recorded for detection of the adenosine ring. Samples were run at 40 °C. Twenty microlitre injections of the given nucleotide were used at a concentration 1 mM. Pure samples of AMP, ADP, ATP and Pi were run as standards. The ATPγS samples showed purities of 87 and 44% for Sigma and Bio-Ryte, respectively (**Fig. 2.1**). The major contaminant in both samples was ADP.

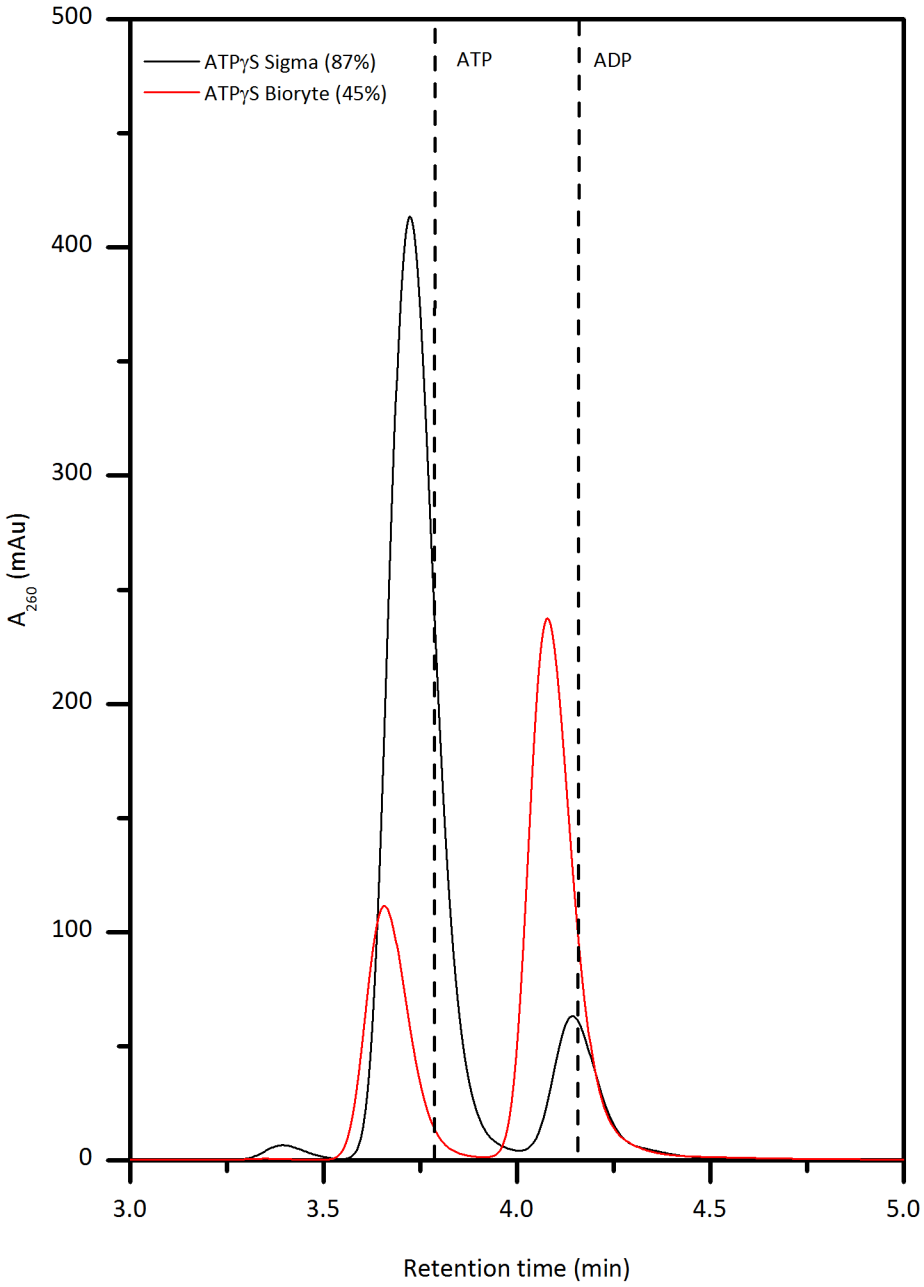

Figure 2.1**. Supplies of ATPγS are contaminated with ADP**. A comparison of ATPγS from Sigma and Bio-Ryte indicates the Bio-Ryte is much less pure. Samples were both loaded at a concentration of 1 mM and were run in 50 mM NaPi. Pure standards of ATP and ADP have been run for comparison.

2.3 Rubisco activase cloning and purification

2.3.1 *General molecular biology*

2.3.1.1 Bacterial Rubisco activase constructs

Wild-type tobacco Rubisco activase was cloned from cDNA into pET28a with a His-tag and was a kind gift from Dr Spencer Whitney (ANU). The R294A variant was cloned into pHUE with a His-tag fused to ubiquitin. His-ubiquitin was cleaved using ubiquitin serine protease (USP).[123] The R294A and USP constructs were kind gifts from Dr. Spencer Whitney (ANU). Rubisco activase variants with a hexahistidine-tag and a tobacco etch virus (TEV) protease cleavage site cloned into pET28a were bought from Epoch. Cotton α- and β- isoforms cloned into pET23a were a gift from Prof. Michael Salvucci (USDA).

2.3.1.2 Transformation and glycerol stock preparation

Briefly, 50 μg of plasmid was added to 50 μL of chemically competent BL21-DE3 pLysS cells. The cells were heat shocked for 30 s at 42 °C and placed on ice for 2 min. Two hundred microlitres of Lysogeny Broth (LB) (Invitrogen) was added and allowed to recover at 37 °C for 1 h. The total reaction volume was then plated out on LB-agar supplemented with either 0.03 $g.L^{-1}$ kanamycin (pET28a), 0.1 $g.L^{-1}$ ampicillin (pHUE), or 0.1 $g.L^{-1}$ ampicillin and 0.1 $g.L^{-1}$ chloramphenicol (pET23a). Plates were grown overnight at 37 °C. The following morning single colonies were picked and used to inoculate 10 mL cultures which were grown to an OD_{600} of 0.4 - 0.6. Seven hundred microlitres of culture were then added to 300 μL of sterile 50% glycerol and snap frozen using liquid nitrogen to serve as glycerol stocks for protein expression.

2.3.2 *Protein purification for His-tagged tobacco Rubisco activase variants*

Protocols for purifying pHUE and pET28a constructs were developed based on Baker *et al.* (2005).[124] A scraping of the frozen glycerol stock was added to 10 mL of LB with the appropriate antibiotic and grown overnight at 37 °C.

Four millilitres of starter culture was added to 400 mL of LB with the appropriate antibiotic and grown to an OD_{600} of 0.6 – 0.8 at 37 °C. Cultures were then cooled to 26 °C and 0.1 $g.L^{-1}$ isopropyl β-D-1-thiogalactopyranoside (IPTG) was added, and the cultures incubated for 16 h.

All purification steps were carried out at 4 °C. Cells were harvested at 15,000 g for 10 min at 4 °C. Pellets were resuspended in Buffer A (20 mM NaPi, pH 8.0, 30 mM imidazole, 1 M NaCl). The cells were then lysed by sonication (UP200S, Hielser Ultrasound Technology) for 12 min at 50% pulsing, 75% strength. The lysate was clarified of cell debris by centrifugation at 35,000 g for 15 min.

The lysate was then applied at 2 $mL.min^{-1}$ using an AKTA Explorer (GE) to a 5 mL HisTrap FF (GE Life Sceinces) immobilised metal affinity column (IMAC) which had been equilibrated with 6 column volumes of Buffer A. After loading the lysate 10 column volumes of Buffer A were used to wash unbound compounds. Protein was eluted with an single step increase to 100% of Buffer B (20 mM NaPi, pH 8.0, 300 mM imidazole, 0.5 M NaCl), and protein was detected using the absorbance at 280 nm. Fractions were then assessed for Rubisco activase content using sodium dodecyl sulfate – polyacrylamide gel electrophoresis (SDS-PAGE). Fractions with Rubisco activase present were pooled and dialysed against 2 L of cleavage buffer (10 mM NaPi, pH 7.4,

50 mM NaCl) overnight at 4 °C. For Rubisco activase variants with a cleavable His tag 1 mg of TEV protease was added to the dialysis tubing along with 4 mM β-mercaptoethanol (β-ME) in the buffer. For ubiquitin tagged Rubisco activase variants, 1 mg ubiquitin serine protease (USP) was added to the Rubisco activase, along with β-ME to 1 mM in the dialysis buffer.[124]

For variants with a cleavable His-tag the protein was mixed to IMAC resin pre-equilibrated with Buffer A and mixed for 1 h at 4 °C. Gravity flow columns were used to collect cleaved protein, while the uncleaved protein and the His-tagged proteases bound to the IMAC resin.

The collected flow through was then mixed with equal volumes of saturated ammonium sulfate and allowed to stand for 1 h. The precipitate was collected by centrifugation at 45000 g for 12 min. The precipitate was resuspended in dialysis buffer and filtered using a 0.22 micrometer sterile filter. Two millilitres was loaded onto a HiPrep 16/60 GE Superdex 200 column equilibrated with 3 column volumes of storage buffer (10 mM NaPi, pH 7.4, 50 mM NaCl, 1 mM EDTA) and eluted with the same buffer. Fractions containing Rubisco activase were then pooled and snap frozen after addition of 10% v/v glycerol and stored at -80 °C. Protein purity and quality was verified by SDS-PAGE and mass spectrometry.

2.3.3 *Purification of cotton isoforms*

The protocol used is a variation on that used by Barta *et al.* (2011).[125]

The pET23a construct was grown as above; however, the media was changed to M9ZB (for 1 L); 1 g NH_4Cl, 3 g KH_2PO_4, 6 g Na_2HPO_4, 10 g bacto-tryptone, and 5 g NaCl. This

media was supplemented with 10 mL glucose (40% w/v) and $MgSO_4$ to 1 mM. The cell pellet was resuspended in 40 mL cell extraction buffer (50 mM HEPES-KOH, pH 7, 5 mM $MgCl_2$, 1 mM EDTA, 0.1% (w/v) Triton X100, 2 mM ATP, 10 mM β-ME, 1 mM phenylmethanfulfonylfluoride (PMSF)).

Briefly, clarified lysate was applied to a 16 mL Hitrap Q HP anion exchange column pre equilibrated with buffer A (50 mM HEPES-KOH, pH 7.2, 20 mM KCl, 10 mM βME, and 10 mM $MgCl_2$). The column was then washed with 5 column volumes of buffer A. The protein was eluted with a linear 0-100% gradient using the same buffer supplemented with 1 M KCl over 10 column volumes. Fractions containing Rubisco activase were then pooled and saturated ammonium sulfate was added to 37.5% drop wise at 4 °C. The precipitate was collected by centrifugation at 45000 g for 15 min. The pellet was resuspended with 2 mL buffer A and applied to a HiPrep SEC 16/60 GE Superdex 200 column equilibrated with 3 column volumes of storage buffer (50 mM HEPES-KOH, pH 7.4, 10 mM $MgCl_2$). Purity was assessed using SDS-PAGE. Fractions containing Rubisco activase were pooled, supplemented with 10% glycerol and snap frozen to be stored at -80 °C.

2.3.4 *Tobacco Rubisco purification*

This protocol is based on that used by Servaites (1985).[126] Tobacco Rubisco was purified from the Petit Havana variety of tobacco. From seeds, plants were grown at ambient atmospheric conditions in a temperature controlled growth room under artificial lighting at 25 °C, leaves were harvested after 6-8 weeks. ~50 g of leaves were collected, deveined, snap frozen using liquid nitrogen and ground into a fine powder. The powder

was then added to 50 mL of extraction buffer (50 mM Tris-HCl, pH 7.4, 20 mM $MgCl_2$ 20 mM $NaHCO_3$, 0.5 mM EDTA, 50 mM βME, 0.5 g casein, 1 g poly-vinyl-polypyrrolidone, 1 mM PMSF, and 10% glycerol).

The solution was filtered through cheesecloth and clarified by centrifugation at 12000 g for 10 min at 4 °C. 60% w/v PEG_{3350} was added drop wise to a final concentration of 10% over 30 min, before being centrifuged as before. Again 60% PEG_{3350} was added to a final concentration of 20% and centrifuged again. The resulting white pellet was resuspended in 25 mL resuspension buffer (50 mM Tris-HCl, pH 7.4, 20 mM $MgCl_2$ 20 mM $NaHCO_3$, 0.5 mM EDTA). The solution was then applied to a HiPrep Q FF 16/10 anion exchange column equilibrated with Buffer A (10 mM NaPi, pH 7.6, 50 mM NaCl, 1 mM EDTA). Buffer B (buffer A +1 M NaCl) was used to elute Rubisco using a linear gradient over 6 column volumes. Fractions were checked for Rubisco using SDS-PAGE and pooled.

The fractions were concentrated using 30 kDa cut-off spin concentrators and loaded on a HiPrep 16/60 GE Superdex 200 column equilibrated with Buffer A. Fractions containing Rubisco were pooled, supplemented with 10% glycerol and snap frozen to be stored at -80 °C.

2.4 General protein characterisation techniques

2.4.1 *Buffers*

All studies used Rubisco activase which had been first buffer exchanged into 20 mM Bis-tris phosphate (BTP), pH 8, 20 mM KCl, 0.2 mM EDTA, unless otherwise noted.

Nucleotide stocks were made in water with the concentration calculated from the A_{260} before being added to the indicated concentration.

2.4.2 *SDS-PAGE*

Protein samples were run on SDS-PAGE under reducing conditions to judge protein purity and estimate protein size. All reagents mentioned here are proprietary Invitrogen technology (St Louis, USA) unless otherwise stated. Novex Sharp Prestained Protein Standard was used to approximate protein molecular weight. Into a microfuge tube 1.5 μL sample buffer, 1 μL reducing buffer, 1-5 μL protein solution depending on concentration, and water to 10 μL was mixed and heated for 2 min at 90 °C.

Each sample was then loaded onto a premade 4-12% Bis-tris gel and run at 160 V for 35 min in NuPAGE MES SDS running buffer. At completion, the gel was placed into 100 mL water, microwaved for 1 min, and shaken for 1 min. The cycle was repeated three times. Fifty millilitres of Simply Blue Protein Stain (Life technologies, Victoria, Australia) was added, microwaved for 45 s and allowed to shake for 20 min. The stain was poured off and the gel placed into water. The gel was imaged using a gel dock.

2.4.3 *Sequence alignments*

Sequence alignments on the mature Rubisco activase used in this thesis were carried out using ClustalW2 server published by EMBL-EBI.[72] Protein accession numbers were tobacco (AAA78277), and cotton α1 and β isoforms (ABB20913, AAG61120).

2.4.4 *ATPase and Rubisco activation assays*

All assays were carried out in a Cary100 Bio UV/Vis spectrophotometer, equipped with a heat block set at 25 °C. Assays were temperature equilibrated for 10 min prior to the assay being carried out. Assays were carried out in 1 mL cuvettes.

2.4.4.1 ATPase coupled assay

This assay has previously been published by Robinson *et al.* (1989). The rate of ATP hydrolysis by Rubisco activase was measured by coupling the hydrolysis of ATP to ADP to the oxidation of NADH. NADH absorbs at 340 nm, $\varepsilon = 6.22 \times 10^3\ M^{-1}$, while NAD^+ does not absorb. Hydrolysis of 1 molecule of ATP causes oxidation of 1 molecule of NADH. In this assay the production of ADP was coupled to the oxidation of NADH. Pyruvate kinase and lactate dehydrogenase were the coupling enzymes used.

Briefly, Rubisco activase was firstly desalted in assay buffer (50 mM Tricine, pH 8, 20 mM KCl, 5 mM $MgCl_2$).[104] The concentration of protein was measured using the Nanodrop and serial dilutions from this stock were used to achieve the appropriate assay concentrations. The reaction mixture contained: 50 mM Tricine, pH 8; 20 mM KCl; 5 mM $MgCl_2$; 1 mM phosphoenol pyruvate (PEP); 0.2 mM NADH; 12 $units.ml^{-1}$ pyruvate kinase; 12 $units.ml^{-1}$ lactate dehydrogenase, and 2.5 mM ATP. The reaction was initiated by the addition of Rubisco activase.

As a lag in activity of around 90 s is observed, the first linear part of the curve was used. For ATPase assays carried out at pH 7 the buffer was changed from 50 mM Tricine pH 8, to 50 mM BTP, pH 7 or 8 as indicated.

2.4.4.2 Rubisco activation assay

This assay has been published by Kallis *et al.* (2000).[52] Rubisco activity was measured using a spectrophotomeric assay by coupling the consumption of 3-phosphoglycerate, the product of the carboxylation reaction of Rubisco, to the oxidation of NADH.[127] This allows the calculation of the number of carboxylation reactions, four molecules of NADH are reduced per RuBP used. RuBP was synthesised and purified by F. G. Pearce.[128] Rubisco was inactivated prior to addition to the reaction mixture in buffer containing, 100 mM EPPS-NaOH, pH 8, 1 mM EDTA, 0.5 mM RuBP at room temperature for 60 min.

The reaction mixture contained: 100 mM EPPS-NaOH, pH 8; 20 mM $MgCl_2$; 1 mM EDTA; 0.5 mM DTT; 0.2 mM NADH; 2 mM ATP; 10 mM phosphocreatine; 5-20 units.ml^{-1} 3-phosphoglycerate kinase; 20 units.ml^{-1} glyceraldehyde-3-phosphate dehydrogenase; 50 units.ml^{-1} triphosphate isomerise, and 20 units.ml^{-1} glycerol-3-phosphate dehydrogenase. Rubisco activase was added at the indicated concentration 30 s prior to the addition of 1.5 μM Rubisco. Rates were measured after 3 min.

2.4.5 *Size exclusion chromatography static light scattering*

A Viscotek 302-040 Triple Detector GPC/SEC (Malvern, Malvern, England) with a Superdex 200 10/300 SEC column attached was used to carry out size exclusion chromatography – static light scattering (SEC-SLS). The flow rate was 0.5 mL.min^{-1} and experiments were carried out at 28 °C. Sample volumes of 100 or 200 μL at the indicated protein concentration were injected. Molecular weight profiles were calculated using the refractive index, intrinsic viscosity and either right or low angle scattering detectors as appropriate. A bovine serum albumin standard (Sigma, St. Louis, USA) was run before

and after each set of experiments for molecular weight calibration and as a system stability control. OMNISEC v4.7 (Malvern, Malvern, England) was used for analysis.

2.4.6 *Analytical ultracentrifugation*

2.4.6.1 General considerations

All sedimentation velocity (SV) samples were buffer matched using a 5 mL HiTrap Desalting column prepacked with Sephadex G-25 Superfine or overnight dialysis or SEC. For sedimentation equilibrium (SE) experiments samples were dialysed overnight, then gel filtered using a Superdex 200 10/300 GL equilibrated in the same buffer to remove aggregates. All experiments were carried out using a Beckman Coulter model XL-I analytical ultracentrifuge equipped with UV-visible scanning optics. Wavelength scans were recorded between 200 and 300 nm at 1 nm step sizes for each cell.

All buffers used had the same viscosity (0.0121 p) and density (1.005 $g.mL^{-1}$) calculated using SEDNTERP.[129] The partial specific volume of the protein was calculated from the primary sequence using SEDNTERP.[129] SV data were analysed using SEDFIT and all values were transformed to $S_{20,w}$, normalising data to standard conditions for accurate comparison [130,131] Sedimentation equilibrium (SE) data were analysed using both HETEROANALYSIS and SEDPHAT.[132,133]

2.4.6.2 Sedimentation velocity

Four hundred microlitres of reference material and 380 µl of sample were loaded into 12 mm double-sector cells with quartz windows. Both four hole (An-60) and eight hole (An-50) rotors were used and temperatures are as indicated in the results sections. A minimum

of 1000 counts difference between sample and reference were recorded for each sample. Proteins were centrifuged at various speeds, with the aim of the protein reaching the bottom of the cell after approximately 40 scans. For low protein concentrations wavelengths around 230 nm were used, for samples containing nucleotide wavelengths around 290 nm were recorded. Data were analysed using the c(S) model in SEDFIT. The c(S) model was chosen over c(M) because c(M) relies on an accurate frictional ratio, which cannot be found for a highly polydisperse system as was the case for most Rubisco activase samples. Stable Rubisco activase oligomers were analysed using a c(M).

2.4.6.3 Sedimentation equilibrium

To characterise the equilibrium of species in solution sedimentation equilibrium studies were carried out. The eight hole An-50 rotor was used for all SE experiments. The reference sector was loaded with 130 µl BTP buffer. The sample sector was first loaded with 10 µl of FC-43 (3M), an opaque oil, followed by 100 µl of sample. Wavelengths were chosen so the cell with the highest protein concentration had an absorbance of no more than 0.3. Speeds were chosen so that at least three speeds could be recorded, while the maximum absorbance stayed below 1.5. The approach to equilibrium was monitored using MATCH, a program within HETEROANALYSIS.[134] No interaction with the FC-43 was seen, as would have been indicated by an inability of the system to reach equilibrium. Data were first analysed using HETEROANALYSIS. SEDPHAT was used for the final analysis in an attempt to get k_{on} and k_{off} values, and refine the fit.

2.4.7 *Small angle X-ray scattering*

Measurements were performed at the Australian Synchrotron SAXS/WAXS beamline equipped with a Pilatus 1M detector (170 X 170 m, effective pixel size, 172 X 172 μm). The wavelength of the x-rays was 1.0332 Å.[135] For most measurements a sample-detector length of 1576 mm was used providing a q range of 0.006-0.4 $Å^{-1}$, where q is the magnitude of the scattering vector, which is related to the scattering angle (2θ) and the wavelength (λ) as follows: $q = (4\pi/\lambda)\sin\theta$). Wild-type tobacco Rubisco activase in the absence of additives was also collected at 7000 mm changing the low q range to 0.0015-0.09 $Å^{-1}$.

Data was collected directly from a 96 well plate using a 1.5 mm glass capillary at 12 °C under continuous flow at 2 s exposures. Samples of low polydispersity, were run through an inline chromatography system equipped with a Superdex 200 5/125 SEC column at a flow rate of 0.2 $mL.min^{-1}$, with 2 s exposures. Protein concentrations are indicated in the relevant sections. SCATTERBRAIN was used to create two-dimensional radially averaged intensity plots, normalised to sample transmission, and background subtracted.[136]

The ATSAS software package was used for data analysis. Where two camera lengths were used the data was merged using PRIMUS.[137] Data quality was assessed using the Guinier region with PRIMUSQT.[137] PRIMUSQT was used to create the distance distribution (P_r) profile and D_{max} values. *Ab initio* bead models were built using GASBOR.[138,139] Rigid body modelling was carried out using BUNCH or CORAL.[139,140] Theoretical scattering curves were generated using CRYSOL, and compared to experimental SAXS data.[141]

Two methods were used to approximate molecular masses. For direct capillary measurements where protein concentration is accurately known, the I(0) is used to calculate protein molecular weight. This method has been found to be within 10% of the actual molecular weight.[142] Two equations are used to find the molecular weight, these are described below.

In Equation (1) $\rho_{M,prot} = 3.22 \times 10^{23}$ the number of electrons per dry mass weight, $\rho_{solv} = 3.34 \times 10^{23}$ e cm^{-3} is the number of electrons per volume of the aqueous solvent, $\bar{\upsilon}$ is the proteins partial specific volume and $r_o = 2.8179 \times 10^{-13}$ cm is the scattering length of an electron. $\bar{\upsilon}$ is consistently ~0.73 for all proteins.[143]

In equation (2) I(0)/c is the forward scattering contrast against concentration $N_A = 6.023 \times 10^{23}$ mol^{-1} is the Avagadros number. The molecular mass is given in kDa.

For samples run through the chromatography, without knowing the eluting concentration at each data point a approximation of MM = Porod volume $Å^3$ x 0.625 was used. Where 0.625 has been found experimentally to be a reasonable approximation of the relationship between mass and volume.[139]

$$\Delta\rho_{M} = [\Delta\rho_{M,prot} - (\Delta\rho_{solv}\bar{\upsilon})]r_o \qquad \text{Equation (1)}$$

$$MM = [N_A I(0)/c]/\Delta\rho_M^2 \qquad \text{Equation (2)}$$

2.4.8 *Circular dichroism*

All experiments were collected using a Jasco J-815 circular dichroism (CD) spectrophotometer. Protein solutions were prepared in BTP buffer and blanked with the

same solution. A path length of 10 mm was used for all experiments. Wavelength scans were recorded from 190 to 250 nm with 0.5 nm increments. Results were analysed, and buffer subtractions carried out using Spectra Analysis v2 (Jasco). The Jasco – 432S/15 attachment was used to carry out thermal melts. The temperature was increased from 20 to 50 °C in 1 °C increments, with a dwell time at each temperature of 1 min. The wavelength was recorded at 222 nm to measure α-helical content.

2.4.9 *Negative stain transmission electron microscopy*

This work was done with the kind and expert help of Mrs Jackie Healy. Formvar-coated copper TEM grids (ProSciTech) were coated with protein and stained with a 2% uranyl acetate solution. Drops of 0.25 – 2.5 μM protein, uranyl acetate, and three drops of water were dispensed onto parafilm. The TEM grid was placed onto the protein drop for 60 s, then sequentially onto each of the three water drops for 20 s each. After the final water drop the grid was blotted dry and placed upon uranyl acetate for 60 s before a final blot to remove excess solution. TEM micrographs (89,000, 140, 000 or 180, 000 x magnification) were obtained on a Morgagni 268D TEM (FEI, Hillsboro, USA) operating at 80 kV fitted with a 40 μm objective aperture.

2.4.10 *Differential scanning fluorimetry*

This method is based on Henderson *et al*. (2013) and Niesen *et al.* (2007).[2,144]
Differential scanning fluorimetry (DSF) was used as a high throughput method for assessing the change in protein melting temperature as a function of nucleotide and protein concentration. The technique uses the dye Sypro Orange which fluoresces upon

exposure to the hydrophobic regions normally buried in folded proteins. The fluorescence was detected using a IQ5 Real-time PCR Detection System with iCycler (Biorad). The dye was excited at 490 nm and the emission was measured at 575 nm. Thin walled 96 well PCR plates were used for rapid heat exchange. Plates were spun to ensure the sample was at the bottom of the well after 5 min degassing. Generally 100 µL of sample was prepared consisting of 1 µL of Sypro Orange, x µL protein, x µL nucleotide and x µL $MgCl_2$ to the intended concentration, and BTP buffer to 100 µL. Concentrations used in each experiment are indicated in the relevant sections. To each well 25 µL of the solution was loaded, all measurements were taken in triplicate. Melting temperatures were determined as the point of maximum inflection using $-\Delta RFU/\Delta t$ and averaged across the replicates, where ΔRFU is the change in relative fluorescence units. Samples were heated from 20 to 70 °C in 0.2 °C increments with a 10 second dwell time at each temperature.

2.4.11 *Mass spectrometry*

This work was carried out by Dr Marie Squire (University of Canterbury). The high resolution accurate mass of purified proteins were analysed on a maXis 3G UHR-Qq-TOF mass spectrometer (Bruker Daltonik GmbH, Bremen, Germany) coupled to a Dionex Ultimate 3000 LC system (ThermoFisher, Waltham, USA). Proteins were first buffer exchanged into ultrapure water and run at a concentration of ~12 µM. Five microlitres of sample were injected and the data processed using Compass software (Bruker Daltonik GmbH, Bremen, Germany)

2.4.12 *Intrinsic fluorescence assay*

Protocols were developed based on Wang *et al*. (1993).[5] Intrinsic fluorescent assays were carried out in an Agilent Cary Eclipse fluorescent spectrophotometer. A low volume quartz cuvette with a path length of 5 mm was used. Previous studies had found that the emission maxima was 345 nm when excited at 296 nm. After replicating these results, these same wavelengths were used for all experiments presented here.

Briefly x μM Rubisco activase, x μM nucleotide and buffer were incubated at the spectrophotometer at 25 °C for 10 min prior to beginning the experiment. The concentration of variables is indicated in the appropriate results sections. Buffer was used as a blank. Each experiment was initiated by addition of 10 μL of 0.5 M $MgCl_2$ and recorded for 5 min.

Chapter Three: **Small oligomers of tobacco Rubisco activase are active**

3.1 Introduction

Proteins from the AAA+ ATPases typically form ring structures as the active oligomeric species, with some requiring ATP to trigger assembly into these active structures, as seen for ClpA and DnaA.[145,146] Rubisco activase from a number of species has previously been found to form a range of oligomeric states, with the distribution changing in response to protein concentration, temperature, and the presence of nucleotide.[5,11,103,105]

Differences between the β-isoforms from Solanaceae and non-Solanaceae plants have previously been found in their nucleotide response, while spinach Rubisco activase decreases in molecular weight in the presence of nucleotide, the tobacco enzyme appears unaffected.[11,110,147]

In this chapter I have sought to elucidate the range of oligomeric states present in a range of physiologically relevant conditions and propose an assembly pathway for high molecular weight Rubisco activase species. The changes in oligomeric state are related to Rubisco activase activities and a minimal oligomer for activity is suggested.

Binding affinities for different nucleotides are presented with the goal of gauging the ability of tobacco Rubisco activase to discern between them. Finally I will discuss the evidence gathered here and how it supports each of the two theories regarding the interaction of Rubisco and Rubisco activase.

3.2 Protomer concentration affects activity and oligomeric state

Previous studies have demonstrated the effect of protein concentration on oligomeric state. In this section I sought to first develop a detailed understanding of the oligomerisation of tobacco Rubisco activase and then relate this to its ATPase and Rubisco activation activities.

3.2.1 *Increased protein concentration increases the oligomeric state of tobacco Rubisco activase*

Initial studies were carried out using size exclusion chromatography static light scattering (SEC-SLS). Tobacco Rubisco activase was loaded at a range of protein concentrations from 18 – 142 μM onto a gel filtration column attached to inline detectors comprising low and right angle light scattering, refractive index, ultraviolet, and viscometry detectors. Due to the size of the proteins being measured the right angle light scattering detector was used as it is more accurate for proteins of the size I expected. As has been previously seen[5] the protein eluted as an asymmetric peak indicating the presence of a range of species in the sample (**Fig. 3.1A**). Using the light scattering detector I was able to measure the average eluting molecular weight continuously.

I found that at the highest loading protein concentration of 142 μM, the highest average molecular weight species was 450 kDa decreasing to150 kDa. At the lowest loading protein concentration, the average molecular weight was in the range of 160 to 80 kDa. The refractive index detector allows measurement of the concentration of the eluting protein, which combined with the light scattering detectors, allows calculation of the molecular weight over the whole elution profile. Smaller oligomeric species in the

leading edge of the trace suggests that the protein is in rapid equilibrium between oligomeric states (**Fig. 3.1A**), and the lack of discrete peaks indicates that the assembly of large species is likely to be continuous with no discrete intermediates. If there were stable intermediate species it would be expected that the elution profile would show these as discrete peaks.

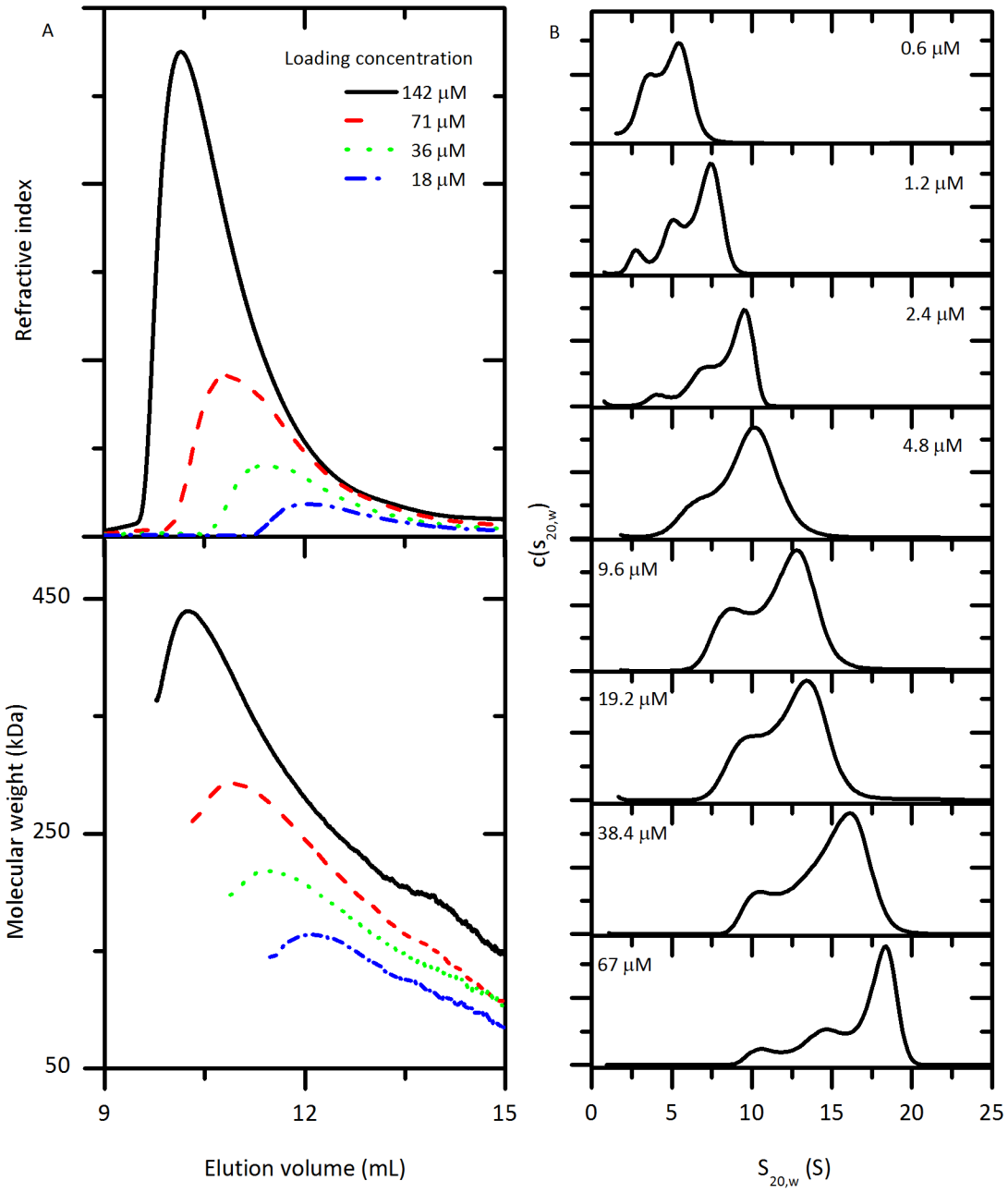

Figure 3.1. **Increased protein concentration gives rise to larger Rubisco activase oligomers.** A) SEC-LS traces showing an asymmetric elution profile of a range of loading protein concentrations. 200 µL of protein was loaded for each run at the indicated concentration. B) A c(s) analysis generated form AUC data shows the probability of a species at a given sedimentation coefficient being present. All samples were run in the absence of magnesium and nucleotide.

3.2.2 *Rubisco activase forms a dynamic range of oligomers*

To investigate the species distribution at a range of protein concentrations, analytical ultracentrifugation was carried out at protein concentration ranging from 0.6 to 67 μM (**Fig. 3.1B**). The results show that at all concentrations measured there was a range of species present, and that with increasing protein concentration both weight averaged and maximum species size increased. Without an accurate frictional ratio, which can only be obtained for a monodisperse non-interacting sample, I was unable to assign accurate molecular weights.

The continuous Svedberg distribution ($c(s)$) analysis requires little prior knowledge about the protein system.[148] The ideal c(s) equation relies on the species in solution being non-interacting over the time scale of the experiment. The Gilbert Jenkins theory states that for rapidly interacting species, such as Rubisco activase, sedimentation boundaries for individual species are not seen. Instead a reaction boundary representative of the distribution of species present in solution is seen.[148,149] This phenomena gives rise to the peaks seen in the data, and these can not necessarily be considered discrete, stable oligomeric species.

The relationship between S and molecular weight is not proportional, i.e. two proteins with the same S value may not have the same molecular weight. For an indication of the expected molecular weights from different Rubisco activase oligomers the program SOMO from the ULTRASCAN suite was used.[150] SOMO replaces the residues in an atomic structure with space filling spheres and calculates the theoretical $S_{20,w}$ for this model. Using the monomeric crystal structure (PDB 3T15) incremental oligomers were created and theoretical $S_{20,w}$ values generated (**Fig. 3.2**). Though the

crystal structure lacks a number of residues it can be used as an approximation of the theoretical S value of different oligomers.

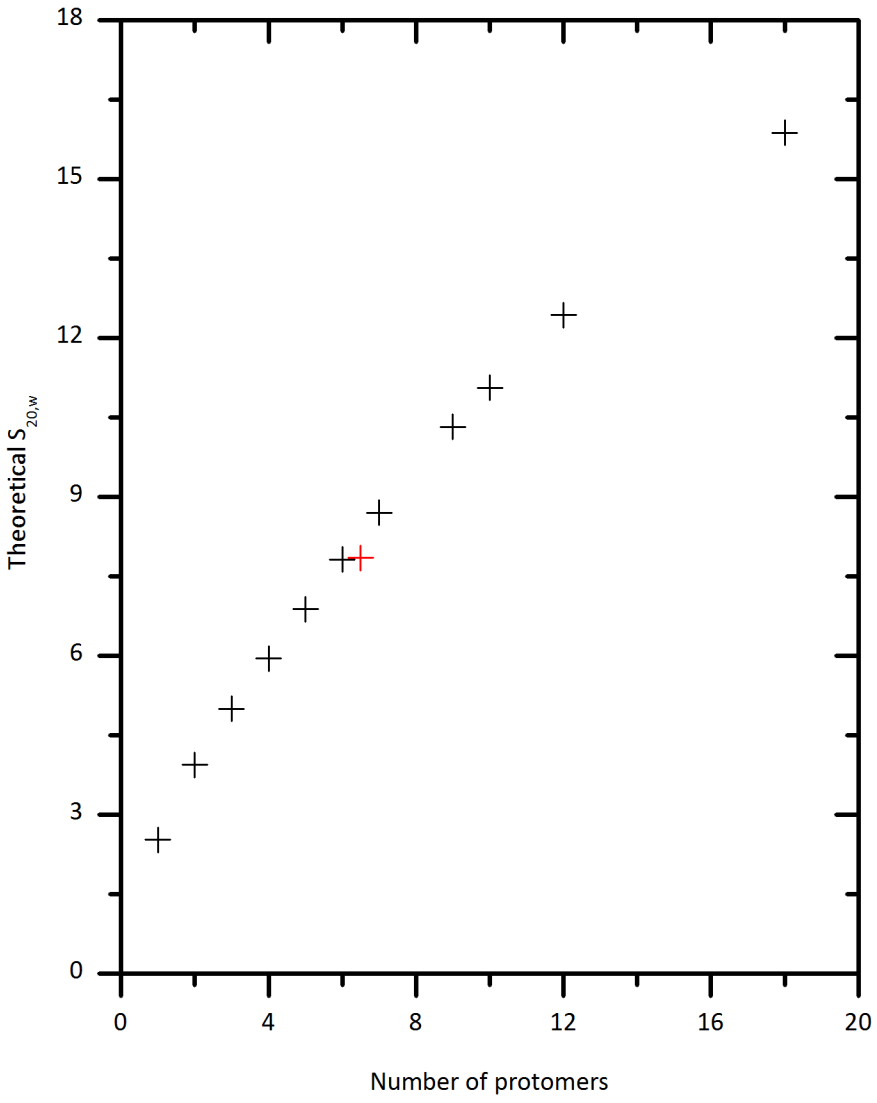

Figure 3.2. **SOMO can be used to approximate the theoretical S20,w from the spiralling Rubisco activase structure.** Theoretical $S_{20,w}$ values calculated using the spiralling crystal structure for a structure containing a given number of protomers. Red X indicates the position of a closed Rubisco activase hexamer (PDB 3ZW6).

At the lowest protein concentration it appears two species may be present at around 3 and 5 $S_{20,w}$. The SOMO approximations suggest 3 S corresponds to a monomer, while 5 $S_{20,w}$ is approximately dimeric. A previous study using fluorescence correlation spectroscopy (FCS) looked at the assembly process for the β-isoform of cotton Rubisco activase.[106] They found that at 0.6 μM, the lowest protein concentration for which data could be collected for AUC, Rubisco activase should be around 75% monomer and 25% dimer, this is in good agreement with the data presented here (**Fig. 3.1B**).[106] At a protein concentration of 0.3 μM they predicted that all protein will be monomeric.[106]

I sought to understand the oligomerisation steps by which tobacco Rubisco activase formed large species using sedimentation equilibrium AUC. SV and SE data were collected; however, an appropriate model for the assembly was not found. The data indicates that there are a series of species in solution. I propose that an isodesmic model, where a single protomer is added in sequential steps with equal affinity is a good approximation of the association. Isodesmic (addition of a single subunit) and two step isodesmic models (monomer going to dimer, dimers then associate) were fitted without success. It may be that too many oligomers are present in solution in a rapid equilibrium to find a single solution.

3.2.3 *The solution structure of tobacco Rubisco activase is increasingly elongated at higher protein concentrations*

To corroborate the SEC-SLS and AUC data, small angle X-ray scattering (SAXS) data was collected over a wide range of protein concentrations from 2.4 – 76.8 μM (**Fig. 3.3A**). A table of structural parameters including the radius of gyration, and an average molecular weight was calculated using I(0) (**Fig. 3.3C**). The calculated molecular weights agree well with molecular weights from the SEC-SLS data. CRYSOL was used to estimate the parameters for the monomeric and closed hexameric tobacco Rubisco activase crystal structures (**Fig. 3.3D**). These structures were of little use in discerning species present in the solution samples.

The raw scattering data from SAXS allows informed suggestions about the shape of the protein without any prior knowledge.[151] At the lowest protein concentrations the featureless curve suggests an oblate (elipse) shape, consistent with oligomers unlikely to be much larger than hexameric, though still containing a range of smaller oligomers (**Fig. 3.3A**). Higher concentrations suggest an increasingly prolate shaped protein. The combination of AUC and SAXS allows the assessment of the species which are present at each of these concentrations, creating a powerful set of data.

By transforming the scattering data from reciprocal to real space it is possible to create a distance distribution plot (P(r)). The P(r) plot is positively skewed at the highest protein concentrations which is strongly indicative of elongated species (**Fig. 3.3B**). At lower protein concentrations the P(r) is less skewed suggesting less elongated protein species.

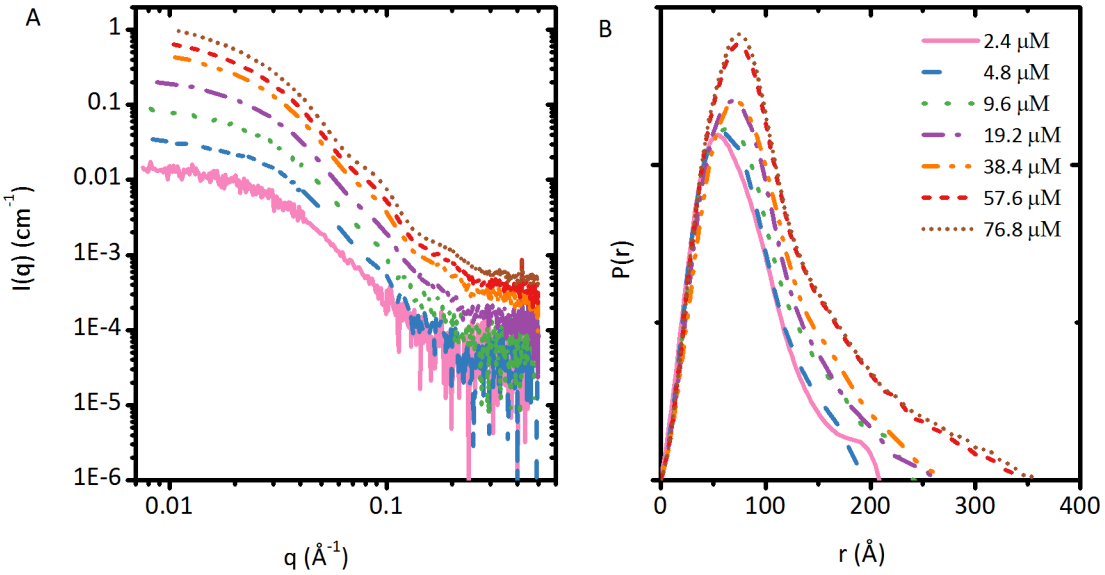

C

Concentration (µM)	Radius of gyration (Å)	I(0) (cm^{-1})	D_{max} (Å)	Porod volume ($Å^3$)	Molecular weight (kDa)
2.4	62.3	0.02	208	315,000	193
4.8	59.8	0.04	213	406,000	231
9.6	72.3	0.1	243	544,000	305
19.2	73.6	0.23	260	704,000	368
38.4	77.9	0.53	275	1,001,000	427
57.6	82.4	0.82	350	1,183,000	436
76.8	84.1	1.28	360	1,318,000	515

D

Construct	Radius of gyration (Å)	D_{max} (Å)	Porod volume ($Å^3$)	Calculated molecular weight (kDa)	Theoretical molecular weight (kDa)
Hexamer (3ZW6)	45.8	131	223,600	140	197
Monomer (3T15)	23.6	81	34,120	21	33

Figure 3.3. **Increasing protein concentration causes increases in both oligomeric state and protein elongation**. A) Scattering curves and B) real space distance distribution plots. C) Data table detailing parameters at a range of protein concentrations. D) Theoretical scattering of the monomeric and hexameric crystal structures. All data was collected in the absence of nucleotide and magnesium.

3.2.4 *Two to four Rubisco activase subunits are required for ATPase and Rubisco activation activity*

Once the changes in oligomeric state as a function of protein concentration were understood it was important to correlate this with the changes previously found in the specific activity.[5] To do this ATPase and Rubisco activation assays in the presence of a range of tobacco Rubisco activase protein concentrations were carried out. The specific ATPase and Rubisco activation activity increased up to a protein concentration up to ~1.5 μM protein, in good agreement with previously published data.[5,10,11,111]

Previous studies on spinach Rubisco activase have demonstrated the oligomeric state changes which occur in the presence of nucleotide[11] and magnesium.[5] One previous study using tobacco Rubisco activase showed that little change in oligomeric state was observed between Mg.ATP and Mg.ADP, I suggest that the conditions are essentially the same over the time scale of an SEC experiment where all ATP will be rapidly hydrolysed at the concentration used in this study. To assess any changes in oligomeric state caused by Mg, Mg.ADP or Mg.ATPγS SAXS was carried out at a range of protein concentrations and incorporating the additives as indicated. Contrary to the oligomeric state changes seen for spinach Rubisco activase, no combination of Mg and/or nucleotide caused an effect on the oligomeric state of tobacco Rubisco activase (**Fig. 3.4**).

By relating the specific ATPase and Rubisco activation activity to the oligomeric state it that prior to the average molecular weight being hexameric maximum specific activity is reached (**Fig. 3.4**). At the lowest protein concentration measured by AUC, 0.6 μM, only putative monomer and dimer are present (**Fig. 3.1B**), at this concentration 80% ATPase and 50% Rubisco activation activity remain. In this thesis $[P]_{0.5}$ will be used to

indicate the point at which half the ATPase or Rubisco activation is reached, with the value given in μM protein.

The $[P]_{0.5}$ for ATPase activity of 0.33 μM correlates to an average molecular weight of ~80 kDa, while the Rubisco activation $[P]_{0.5}$ of 0.58 μM is reached at an average molecular weight of ~120 kDa. By combining the data on oligomeric state from SEC-SLS, SAXS and AUC with the activity assays the data strongly suggests that a high level of specific activity is reached where no species larger than a tetramer are present.

It appears that a hexameric species is not required for either ATP hydrolysis or to power the removal of inhibitors form Rubisco. The data suggest that a small oligomer in the range of a dimer – tetramer is the minimally active species, and that this oligomer can fulfill all roles of tobacco Rubisco activase. Thus I present here, to my knowledge, the first AAA+ protein where the physiologically active species is not a closed ring, and instead suggest that for activity all that is required is small open oligomers.

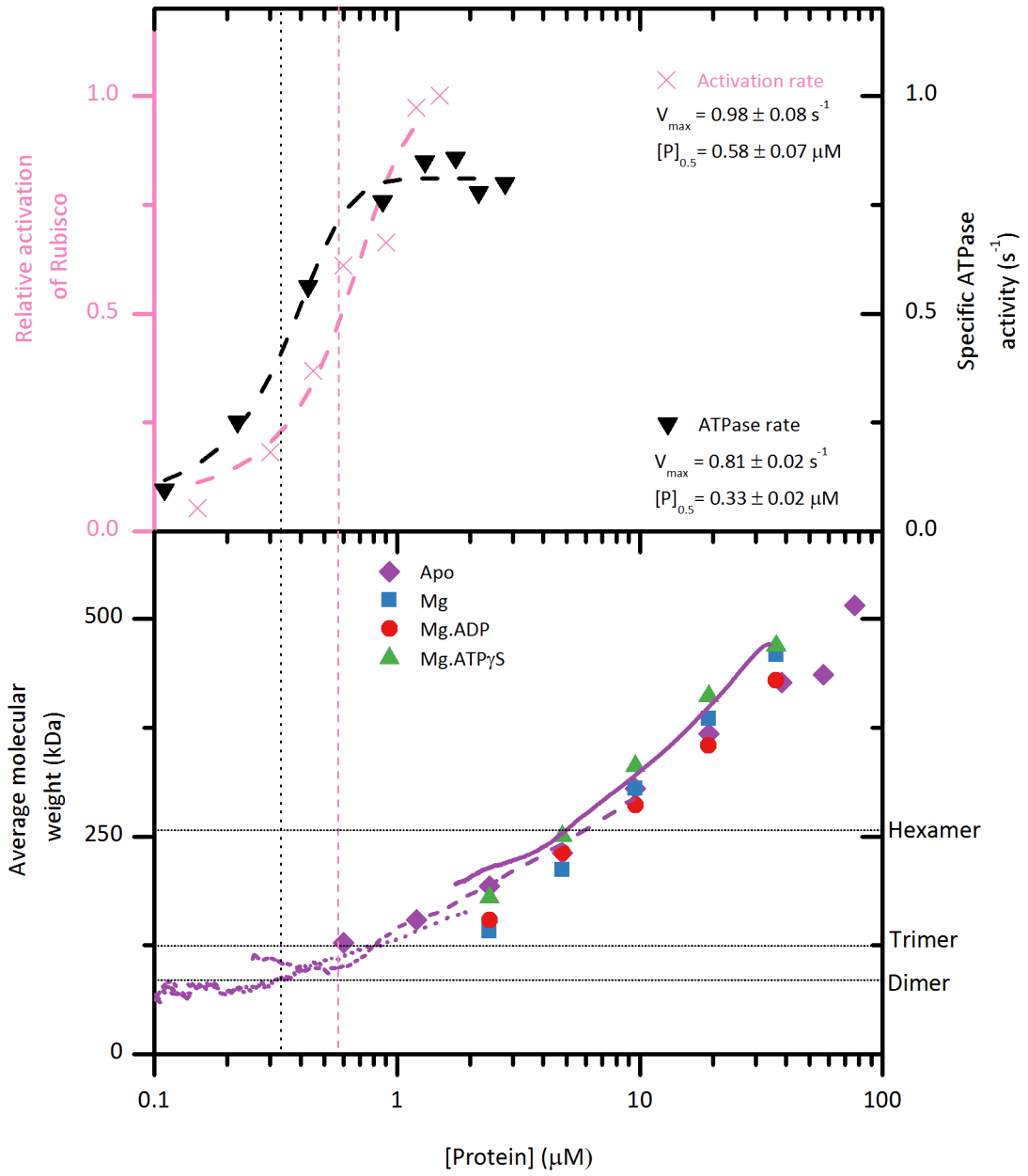

Figure 3.4. **Changes in specific activity correlate with oligomeric state**. The specific ATPase and relative activation of Rubisco activities, maximal rate for each is shown. Average molecular weights from SAXS (data points) and SEC-SLS (lines) are shown. 5 mM Mg and 0.2 mM nucleotide was added as indicated.

3.3 Changes in the stroma have little effect on tobacco Rubisco activase

3.3.1 *pH has little effect on oligomeric state*

In addition to nucleotide concentration, a number of other conditions change within the stroma during the diurnal cycle including magnesium concentration, redox potential and pH.[111,152-154] Redox potential will not be considered in this section as tobacco only produces the redox insensitive β-isoform.[92]

During the night the pH within the stroma drops from 8 to 7 and it is important to understand if this change causes a change in the oligomeric state or activity.[155] I found that in the presence of either Mg.ADP or Mg.ATPγS at either pH 7 or 8 little change in oligomeric state was seen (**Fig. 3.5A, B**). An increase in the specific ATPase activity of around 60% was seen upon decreasing the pH from 8 to 7 (**Fig. 3.5C**). It appears the change in activity is not due to the oligomeric state but perhaps a change in the nucleotide affinity.

3.3.2 *High concentrations of magnesium destabilise higher order oligomers*

Previous studies have noted that maximal changes to intrinsic fluorescence and ATPase specific activity required 2 mM Mg.[111] Additionally magnesium has been shown to cause a destabilisation of higher order oligomeric species[5] and decrease the thermal instability.[2] The free magnesium concentration in the chloroplast appears to change from 0.5 mM to 2 mM upon illumination.[154] However only free magnesium was measured, and large amounts of magnesium are complexed with nucleotides and RNA.[154] Owing to the large discrepancies in magnesium concentration in the literature I investigated the effect of a

wide range of concentrations, with the highest concentration measured 12.5 times the free magnesium in the stroma.

I found that a 5 fold increase from 2 mM, the point by which intrinsic fluorescence is saturated and maximal ATPase rate had been reached, to 10 mM caused a reduction in the integrated $S_{20,w}$ from 13.2 to 12.3 (**Fig. 3.5.D**). The further increase to 25 mM caused a decrease to an integrated $S_{20,w}$ of 10.7. Previously published data on the β-isoform from cotton Rubisco activase showed a 1 °C decrease in thermal stability with the addition of 5 mM $MgCl_2$.[2] Separately it was shown that incubation of the β-isoform from arabidopsis Rubisco activase with 5 mM $MgCl_2$ at 30 °C caused rapid aggregation.[105] Thus it appears that high concentrations of magnesium destabilise Rubisco activase; however, this does not appear to cause large changes in the oligomeric state of Rubisco activase.

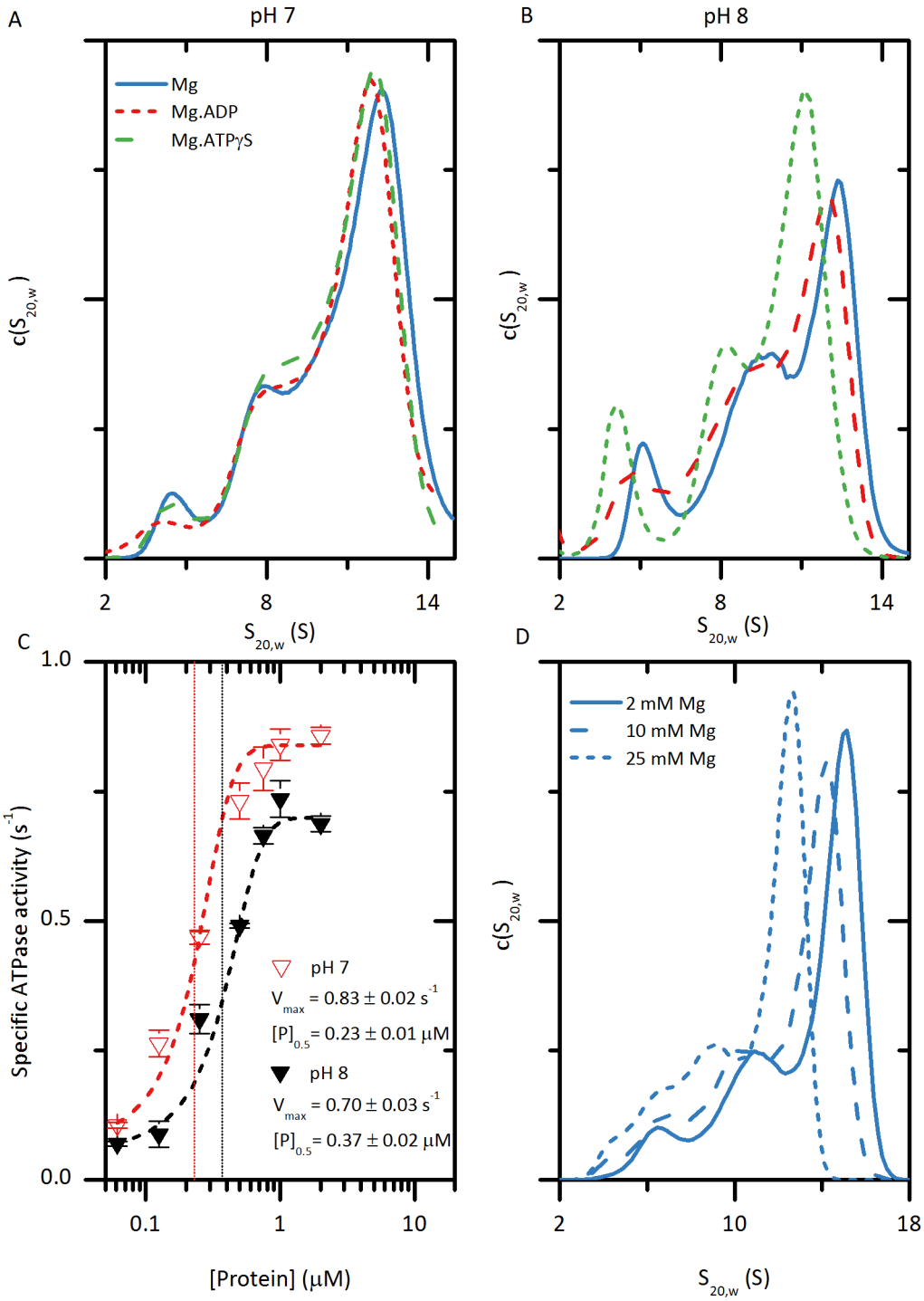

Figure 3.5. **The affect of changing conditions in the stroma on tobacco Rubisco activase**. A) 4.8 µM protein with 5 mM Mg, and 0.2 µM nucleotide at pH 7. B) 4.8 µM protein with 5 mM Mg, and 0.2 µM nucleotide at pH 8. C) ATPase assays carried out at pH 7 and 8, error bars display standard error. D) 9.6 µM protein supplemented with Mg as indicated.

3.3.3 *Increases in temperature cause slightly larger oligomer formation*

The thermal lability of Rubisco activase has been well documented both in the literature and in this thesis, thus it is important to understand the effect of temperature on the oligomeric state. An AUC study was carried out with a set protein concentration with Mg, Mg.ADP, and Mg.ATPγS added. Three temperatures, 4, 12, and 20 °C were tested. Attempts to collect data at higher temperatures were difficult due to the long experimental time and low thermal stability of the protein.

I found that an increase in temperature caused an increase in the oligomeric species present (**Fig. 3.6A**). In the presence of Mg.ADP at 4 °C tobacco Rubisco activase had an integrated $S_{20,w}$ of 10.5, at 12 °C this had increased to 11.2 $S_{20,w}$, and at 20 °C it had increased again to12 $S_{20,w}$ (**Fig. 3.6B**). Changes in oligomeric state have been seen previously for the AAA+ protein Vps4, with an increase in molecular weight of around 30% as the temperature increased from 4 to 20 °C.[156] For the tobacco plant this range of temperatures provides little physiological relevance, being grown in temperatures around 25 °C.

It may be that the oligomerisation process at higher temperatures favours large inactive soluble Rubisco activase species which have been reported in the literature.[105] As the leaf temperature increases and photosynthesis becomes less efficient, the 2 MDa species may act to sequester Rubisco activase protomers, allowing Rubisco to inactivate. A study by Rokka *et al.* (2001) suggested that at higher temperature Rubisco activase associated tightly with the thylakoid membrane and had a dual function where it protected thylakoid bound ribosomes during heat shock events.[157]

A

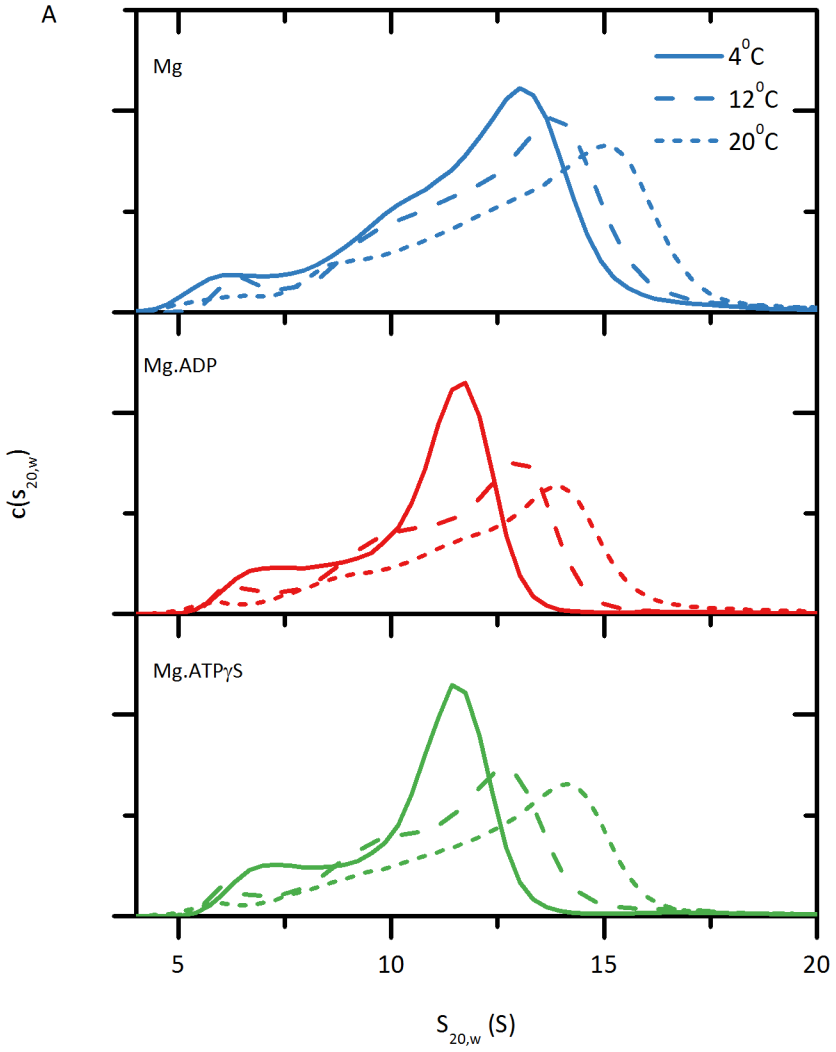

B

Integrated $S_{20,w}$

Additive	Temperature (°C)		
	4	12	20
Mg	11.18	11.72	12.6
Mg.ADP	10.46	11.15	12
Mg.ATPγS	10.46	11.04	12.1

Figure 3.6. **An increase in temperature causes an increase in the oligomeric state**. A) Tobacco Rubisco activase at 9.6 µM supplemented with 5 Mg and 0.2 mM ADP or ATPγS as indicated .B) Integrated $S_{20,w}$ values for each condition.

3.4 Tobacco Rubisco activase shows no specificity between ADP and ATP binding

Two techniques were used to determine the affinity of ADP, ATP, ATPγS, and AMP-PNP for tobacco Rubisco activase. Previously, changes in the intrinsic fluorescence were used to determine the affinity for ATP and ATPγS for spinach Rubisco activase, the binding of these nucleotides causes a conformational rearrangement, changing the environment of two tryptophan residues.[5,52,97]

The addition of ADP was found to cause no change in the intrinsic fluorescence and $MgCl_2$ must be included in the assay for a change in intrinsic fluorescence to be seen. The nucleotide affinities found by intrinsic fluorescence and 8-anilino-1-naphthlalenesulfonic acid (ANS) binding are comparable.[52] Differential scanning fluorimetry (DSF) has been used previously with the β-isoform of cotton Rubisco activase to screen the melting temperature under a range of conditions.[2]

Here I have used the point of half saturation ($S_{0.5}$), to compare the affinities of different nucleotides. For Intrinsic fluorescence this is the point at which the nucleotide concentration causes half the maximal intrinsic fluorescence. The thermofluor studies define $S_{0.5}$ as the nucleotide concentration at which half the maximal thermal stability is achieved.

3.4.1 *ATPγS causes changes in the intrinsic fluorescence*

The intrinsic fluorescence assays found Mg.ATPγS had a $S_{0.5}$ of 8.8 μM whereas Mg.ATP bound with an $S_{0.5}$ of 16.4 μM (**Fig. 3.7C**). The intrinsic fluorescence yield was used as a second point of comparison to indicate the hydrophobicity surrounding the tryptophan. The doubling in the fluorescence yield upon addition of ATPγS is thought to

be caused by the enzyme being trapped in an active conformation, unable to cleave the γ-phosphate (**Fig. 3.7C**).

3.4.2 *Addition of ADP and ATPγS causes an increase in thermal stability*

Thermal stability assays showed an increase of ~5 °C upon addition of 200 μM Mg.ADP or Mg.ATPγS, and both bound with a similar affinities of 24 and 22 μM, respectively (**Fig. 3.7A,C**). Mg.ATP was not included as during the time taken to run the experiment all ATP would be hydrolysed to ADP. A previous study used AMP-PNP, a non-hydrolysable ATP analogue, to compare the binding affinities with ADP, they found ADP bound more tightly.[13] However, the results indicate that AMP-PNP bound much less tightly than ATPγS (**Fig. 3.7A**). An AMP-PNP titration was trialed but failed to cause the change seen with ATPγS until the concentration was increased to 5 mM, 25 times higher than ATPγS. From this point AMP-PNP use was discontinued as the quantities required were limiting and such a high level of nucleotide could not be utilised for AUC experiments. Thus it appears a comparison of ADP vs. AMP-PNP is not an appropriate proxy measure of ADP vs. ATP binding.

3.4.3 *Nucleotide is bound with equal affinity at different protein concentrations*

I have shown that protein concentration affects oligomeric state, it is now important to understand if this change in oligomeric state affects nucleotide binding. The melting point of a range of protein concentrations, either in the absence or presence of Mg.ADP or Mg.ATPγS, was measured with DSF (**Fig. 3.7B**). To confirm it was the oligomeric state and not an effect of the dye used for DSF, a duplicate set of thermal melting

experiments were carried out using circular dichroism (CD). The study showed, independent of the inclusion of either nucleotide a 5 °C increase in stability was found as the protein concentration increased from 1 μM to 10 μM (**Fig. 3.7B**). A series of nucleotide titrations over the same range of protein concentrations showed very similar binding affinities across both protein concentrations and between Mg.ADP and Mg.ATPγS (**Fig. 3.7D**), indicating all oligomers bound nucleotide with similar affinities.

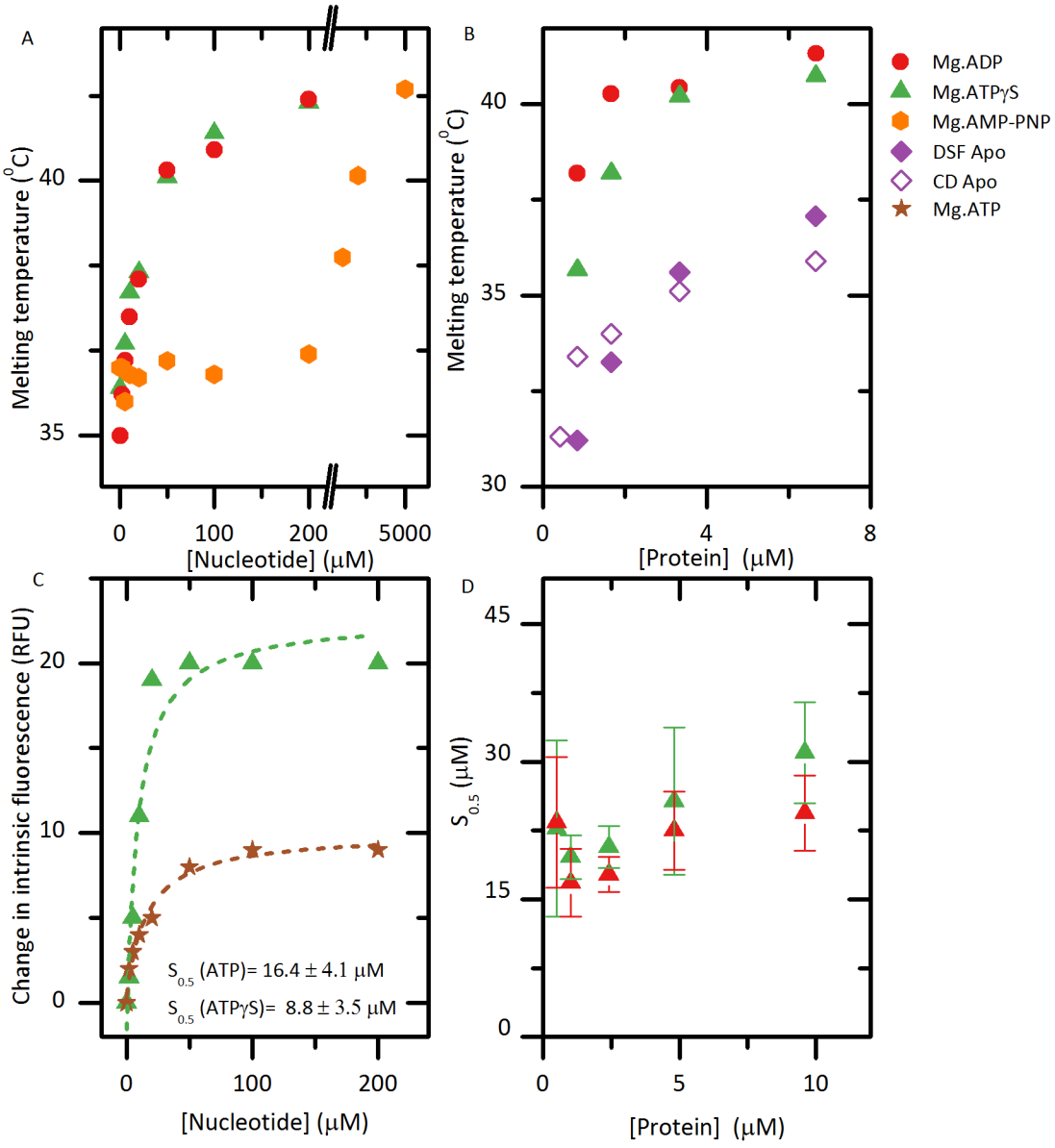

Figure 3.7. **Binding of nucleotide to tobacco Rubisco activase**. A) DSF assay with 9.6 μM protein, 5 mM $MgCl_2$ and nucleotide at the indicated concentration. B) DSF and CD of either apo or 5 mM $MgCl_2$ and 200 μM nucleotide at the indicated protein concentration. C) Intrinsic fluorescence assay carried out as per panel A. D) DSF nucleotide titration carried out at a range of protein concentrations as indicated in the presence of 5 mM $MgCl_2$.

3.5 Significance of these findings for Rubisco activase *in planta*

3.5.1 *Rubisco activase forms a range of active oligomers in solution*

Currently there are two proposed mechanisms for the interaction of Rubisco activase with Rubisco. Firstly the AAA+ hypothesis whereby a ring assembly, most likely a hexamer, forms from a pool of smaller oligomers and binds near the Rubisco active site, hydrolysing ATP to power a conformational change than results in the removal of the inhibitor.[3,43] The second theory is that a open Rubisco activase structure with no discrete oligomerisation steps is able to interact with Rubisco and remove the inhibitor, also through some form of conformational change powered by ATP hydrolysis.[121] The results suggest that tobacco Rubisco activase does not form distinct species and instead forms a range of oligomers which are in a rapid equilibrium.

SEC-SLS results show that the leading edge of protein eluting off the column is diluting, forming smaller species, strongly suggesting very rapid equilibrium between different oligomers. SAXS, AUC, and SEC-SLS all suggest a rapidly exchanging pool of oligomers, with larger oligomers present at higher protein concentration. I also showed that the presence of nucleotide or magnesium caused little change to oligomeric state, and that all oligomers showed similar nucleotide affinity. I furthered these findings by testing a range of changing stromal conditions including pH and temperature, finding that changes in these conditions caused little change on oligomeric state or ATPase activity. Thus I conclude that any changes in the stromal conditions do not cause large scale changes to the oligomeric state of tobacco Rubisco activase.

3.5.2 *Tobacco Rubisco activase forms elongated structures in solution*

Low resolution solution structural data suggest that as protein concentration is increased the resulting oligomer is not just larger but more elongated. The atomic resolution structure of the truncated tobacco Rubisco activase showed a spiraling structure in the crystal lattice.[3] Data presented here supports the theory that Rubisco activase forms an elongated spiralling structure in solution. The presence of a continuum of species, as seen at all protein concentrations with AUC, discounts the possibility of stacked hexamer formation.

While most AAA+ ATPases use discrete ring assemblies as their active oligomer, there are examples of spiral assemblies. The AAA+ ATPase protein 2C from the superfamily III helicase clade, forms a range of oligomeric species in solution.[107] The bacterial protein DnaA, from the initiator clade of AAA+ proteins, is able to bind helically around DNA.[145] The eukaryotic clamp loader protein from yeast, belonging to the clamp loader clade of AAA+ proteins, forms a 5 subunit helical assembly at the junction of primer and template in DNA replication.[158] Rubisco activase has been placed in the classical AAA+ clade; however, atomic resolution of the clade defining helix is still lacking.[3,145] It may be that though the activity of Rubisco activase resembles that of other AAA+ proteases, the structural arrangement in solution may not sit well within this paradigm.

3.5.3 *Small oligomers of tobacco Rubisco activase have activity*

Activity assays and sizing data suggest that at protein concentrations where the average molecular weight is dimeric almost 50% of the Rubisco activation activity is reached.

AUC confirms that not only is the average species approximately dimeric but also that it is highly unlikely that species larger than tetramers are present at these concentrations. This suggests that only a full catalytic site, produced by adjacent subunits, is required for activity. This is different to many other AAA+ ATPases, including the Rubisco activase from red algae[43], which function as hexamers.

Though it is uncommon for AAA+ proteins to be active at this small oligomeric state, others also function as dimers. Two proteins from the Helix 2 insert clade of AAA+ proteins, MCM and CoxD, are ATPase active dimeric AAA+ proteins.[159,160] The eukaryotic helicase proteins MCM2-7, is an evolutionarily conserved group of AAA+ protein subunits which come together to form an active hexameric structure.[159] Studies of subunit mixtures showed that some combinations form active dimeric species. CoxD, an enzyme important in the posttranslational incorporation of sulfur and copper into the active site of flavoproteins, is able to form both functional dimeric and hexamer structures capable of hydrolysing ATP.[160] Vps4, a member of the classical AAA+ clade, is a protein involved in disassembly processes. The F328A variant is dimeric, but maintains a full catalytic active site and ATPase activity.[156]

It is important to note that though all these examples are able to hydrolyse ATP, it is unknown whether any of these proteins can interact with their protein partners and carry out their physiological function. For Rubisco activase I have shown that at oligomeric states smaller than tetrameric, Rubisco can still be reactivated.

3.5.4 *Mechanism of interaction between Rubisco activase and Rubisco*

Many AAA+ proteins interact with the target protein through a series of residues located within the central pore of the active ring shaped oligomer.[63] The residues responsible for, at least, initial interaction with Rubisco are located on the outside of the spiral structure I propose.[113] The data suggest that oligomers comprising 2-4 subunits are able to reactivate Rubisco, this is in good agreement with another study which showed that trimeric Rubisco activase oligomers had ATPase activity.[3] This same study showed that small oligomers in the size range of 3-5 subunits had full Rubisco activation activity.[3] Thus I conclude that small oligomers have full biological function though the mechanism of interaction between these oligomers and Rubisco remains unknown.

Chapter Four: **Salt bridge variants of tobacco Rubisco activase**

4.1 Introduction

Many AAA+ proteins contain a conserved arginine residue within the sensor 2 motif which protrudes from an adjacent protomer into the active site where it binds directly with the β and γ phosphates of ATP.[73] This invariant residue is involved in ATP binding, ATP hydrolysis, and oligomerisation.[60,74,161-163] Members of the extended AAA ATPases group lack this arginine residue within the sensor 2 motif, instead containing an arginine four residues upstream.[73] In tobacco Rubisco activase this residue is R296, and mutation of this residue reduces ATPase activity to less than 10% of wild type.[11]

Located between R296 and the sensor 2 motif is a second arginine residue, R294, proposed to be involved in nucleotide or interface interactions.[11] Studies have found that mutation of R294 alters the affect nucleotides have on subunit assembly. The R294A/V variant protein forms stable hexameric oligomers in the presence of Mg.ATPγS.[3,11,13]

The atomic resolution model of tobacco Rubisco activase indicates a hydrogen bond network involving the side chain of R294 and the backbone carboxyl group of N99 (**Fig. 4.1**).[3] Mutation of R294 to alanine reduces ATP hydrolysis by 80%, while mutation to valine causes no change.[3,11] Currently is it is not apparent why there are such large differences in the activity of these two variant proteins.

In this chapter I used the R294A/V variant proteins and a novel variant N99A to probe the role of these intersubunit residues. Using existing atomic resolution data, models of the complete hexameric R294A/V oligomers were built to find the arrangement of the domain unresolved by existing structures.

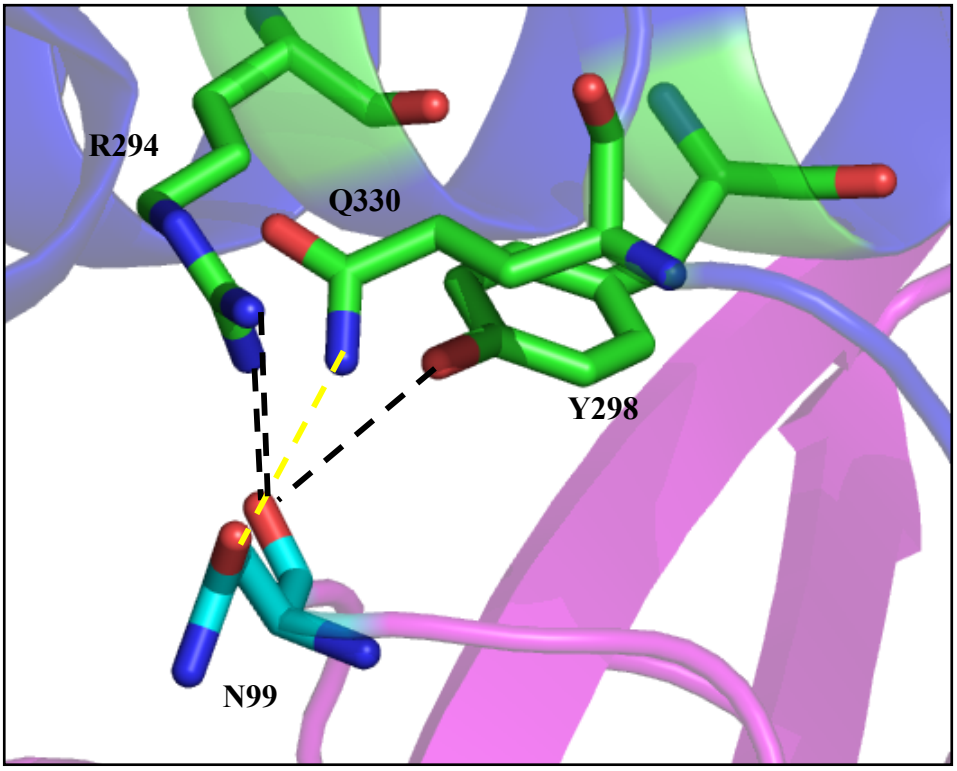

Figure 4.1. **R294 forms two hydrogen bonds with the backbone of N99**. Two adjacent tobacco Rubisco activase subunits are shown with the residues involved in the hydrogen bond network shown. R294 and Y298 interact with the backbone oxygen of N99 (black dashes). Glutamine 330 interacts with the side chain oxygen of N99 (yellow dashes).

4.2 Interface variants form a range of species with switchable oligomeric states

In this section I apply the same techniques as in chapter 3 to three variant proteins containing mutations of key residues in the hydrogen bonding network located at the intersubunit interface, R294A, R294V, and N99A.

4.2.1 *Mutation of the hydrogen bond network creates smaller oligomers*

In the absence of magnesium or nucleotide I found that all variants showed decreased molecular weights, compared to the wild-type enzyme (**Fig. 4.2A**). As was seen for wild-type Rubisco activase all variants eluted as asymmetric traces from SEC, indicating that a range of smaller oligomers are present in solution. Using the wild-type enzyme as a reference point, the N99A variant is next largest, with both arginine variants eluting later.

It appears that the higher order oligomer formation of the R294A/V variants, in the absence of nucleotide, is less stable than the N99A variant. My data suggest that the identity of the side chain at position 99 is much less important than the backbone oxygen for the formation of larger oligomers. No difference was seen in the absence of nucleotide or magnesium between R294A and R294V Rubisco activase variant enzymes.

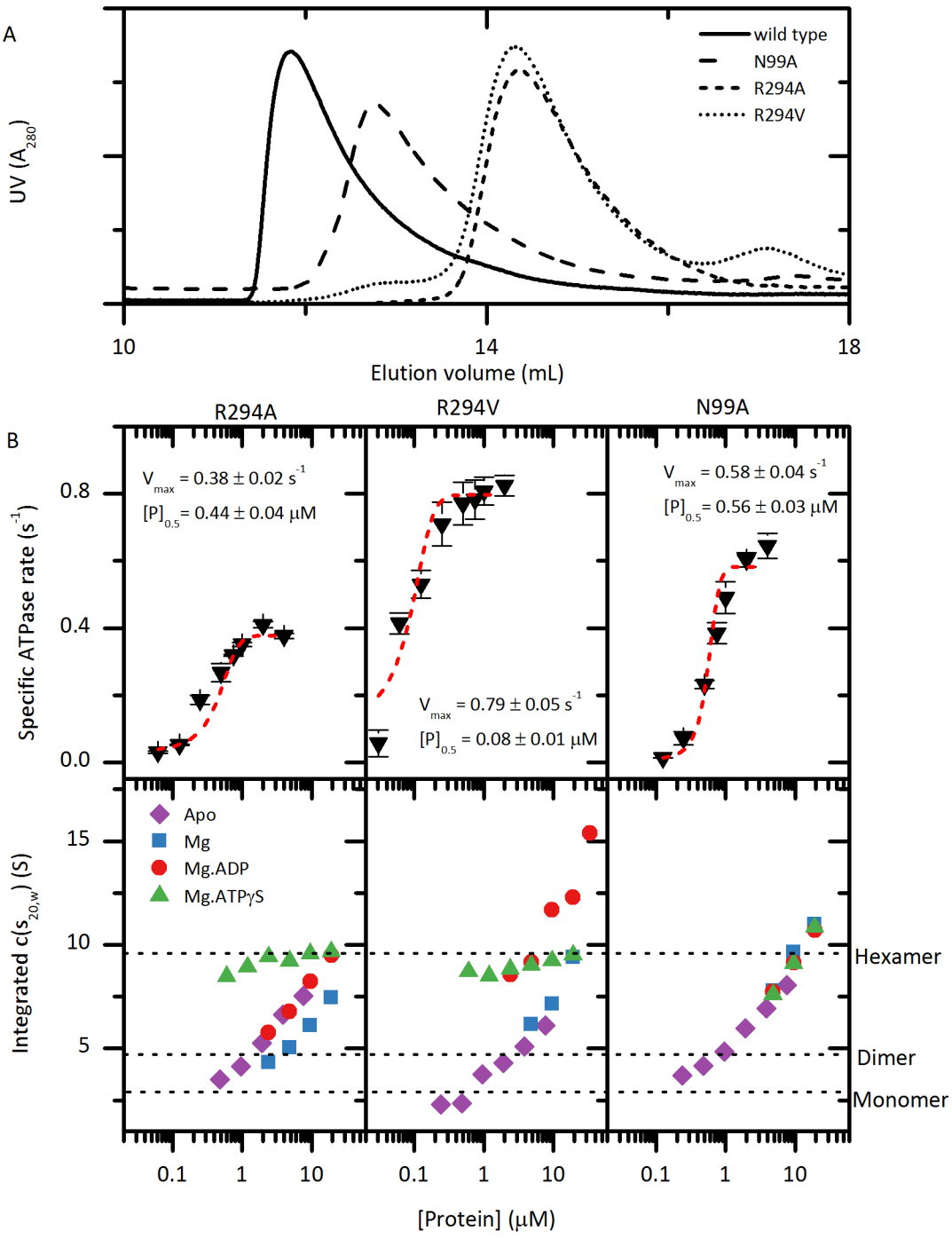

Figure 4.2.**Mutation at the interface change oligomeric state and activity.** A) 24 µM protein was loaded onto the SEC-SLS in the absence of additives. B) ATPase assays, where errors are standard errors of the mean. AUC experiments were run with nucleotide absent, or with 5 mM $MgCl_2$ and supplemented with 0.2 mM nucleotide as indicated. A Boltzmann equation was fitted to find V_{max} and $[P]_{0.5}$ values.

4.2.2 *R294A shows major differences to R294V with regards to activity and oligomeric states*

R294A shows a maximal specific ATPase rate of 0.38 s^{-1} compared to the wild-type enzyme which reached a maximum of 0.82 s^{-1} (**Fig. 4.2B**). The activity was dependent on protein concentration, and half the maximal specific activity was reached at a protein concentration of 0.44 μM. This [$P_{0.5}$] is higher than that of the wild-type enzyme at 0.33 μM and R294V. This may be caused by weaker hexamer formation under assay conditions.

The addition of 5 mM magnesium destabilises the enzymes oligomeric state, while Mg.ADP appears to have no effect (**Fig. 4.2B**). As seen with the wild-type enzyme, oligomeric state is still linked to protein concentration, with an increase in the $S_{20,w}$ from 5 at a protein concentration of 1 μM to 9.5 at 10 μM. This represents an approximate increase in the average oligomer from two subunits to six subunits. Addition of Mg.ATPγS causes the formation of a single stable oligomer at 9 $S_{20,w}$ across all measured protein concentrations.

R294V shows a similar maximal specific activity to the wild-type enzyme of 0.79 s^{-1}; however, it reaches [$P_{0.5}$] at a protein concentration of 0.08 μM, one quarter of the wild type value at 0.33 μM (**Fig. 4.2B**). The oligomer distribution appears unaffected by the presence of magnesium; however, 0.2 mM Mg.ADP makes R294V much larger, doubling the integrated $S_{20,w}$ (**Fig. 4.2B**). As is seen for R294A, R294V also forms stable monodisperse hexameric species with the addition of Mg.ATPγS.

For both arginine variants it is difficult to correlate the oligomeric state with the changes seen in the specific activity. Under assay conditions, it is difficult to know what

the distribution of oligomers is. To approximate conditions in the assay, where ATP is plentiful, the biophysical characterisation experiments include ATPγS to mimic the high concentration of ATP. At protein concentrations of below 0.6 μM I was unable to measure the oligomeric state by AUC due to the strong absorbance of the adenosine ring at wavelengths below 260 nm.[164]

4.2.3 *N99A forms catalytically active small oligomers*

The N99A variant has a maximal specific ATPase activity of 0.58 s^{-1}, which is approximately 70% of wild type (**Fig. 4.2B**). Half the maximal specific activity was reached at a protein concentration of 0.56 μM, approximately twice that of the wild-type enzyme. Unlike the R294 variants, the oligomeric state of N99A is unaffected by the addition of magnesium or nucleotide, with protein concentration being the determining factor of oligomeric state (**Fig. 4.2B**).

Because N99A forms smaller oligomers and doesn't change oligomeric state in the presence of nucleotide I was able to measure the oligomer distribution from no specific activity to full specific activity using AUC (**Fig. 4.2B**). At a protein concentration of 0.24 μM, N99A appears almost entirely monomeric and lacks ATPase activity (**Fig. 4.2B, 4.3**). When the protein concentration is increased to 0.48 μM the specific activity reaches 40% of maximal activity, while the sizing data suggest the presence of two species, most likely monomer-dimer. At a protein concentration of 0.96 μM the maximal specific ATPase activity is reached, and much larger species are now present in solution.

As previously mentioned because the AUC data is a reaction boundary, rather than a boundary representing a specific oligomer it is not possible to unambiguously assign oligomeric state to a given peak. Data which will be presented later in this thesis shows that monomeric tobacco Rubisco activase has an $S_{20,w}$ value of 3.1 and the dimer has an $S_{20,w}$ value of ~4.8. As the protein concentration increases and the abundance of larger oligomers increases, maximal specific ATPase activity is reached. In the previous chapter, examples of AAA+ ATPases which comprised catalytically active dimers were described.

The wild-type tobacco Rubisco activase data suggested small oligomers had ATPase activity, here I further refine that assertion and can show that at protein concentrations where no measureable amounts of species larger than trimer are present full maximal specific ATPase activity is reached.

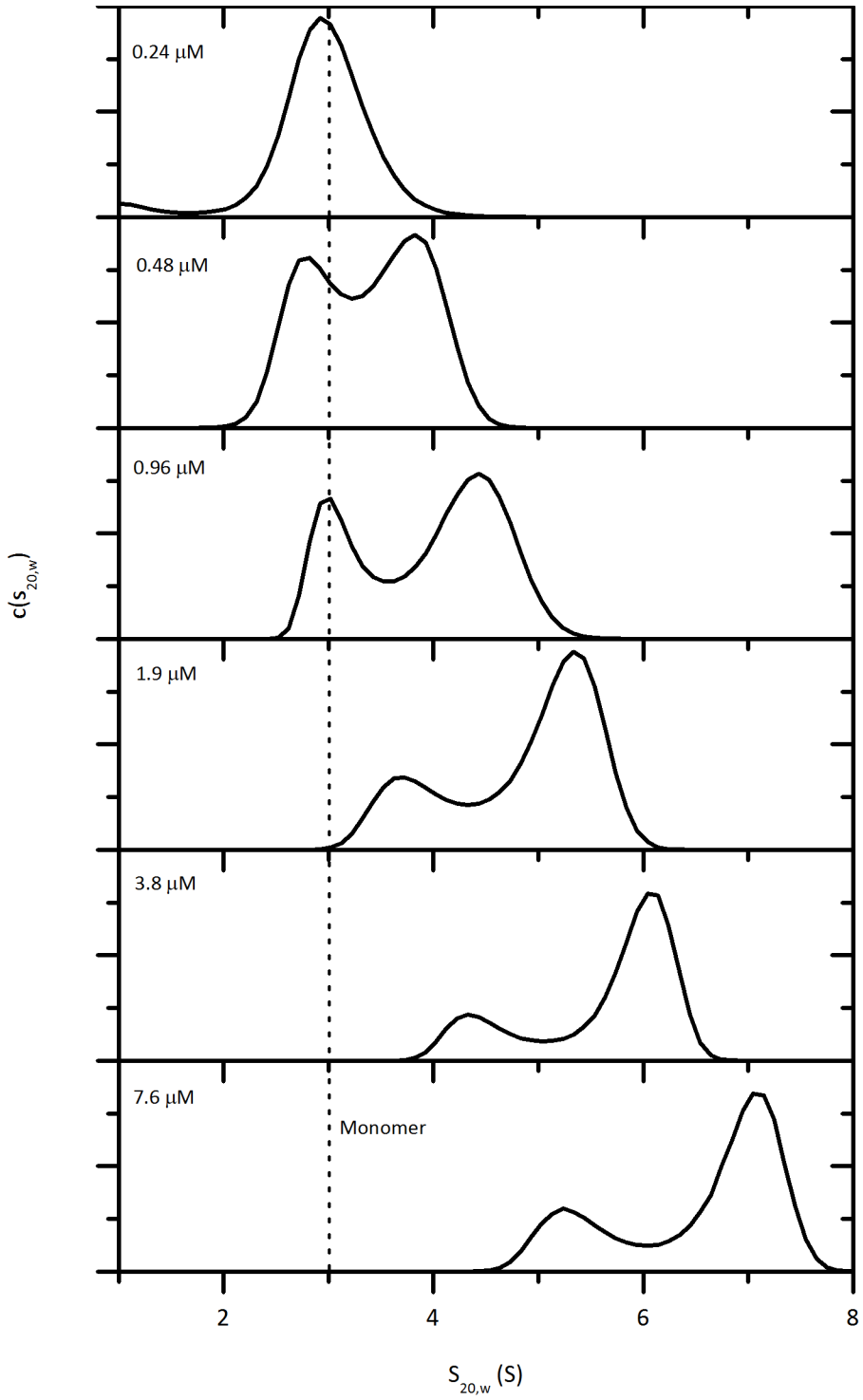

Figure 4.3. **N99A forms small oligomers at low protein concentrations.** AUC data was collected in the absence of nucleotide and magnesium on the N99A variant of tobacco Rubisco activase. The dotted line indicates the experimental $S_{20,w}$ for a monomeric Rubisco activase variant.

4.3 Stable hexameric species can form as shown by AUC

4.3.1 *Low concentrations of Mg.ATPγS cause hexamer formation for R294A*

A titration of ATPγS into a set concentration of R294A was carried out and the amount of nucleotide required to cause hexamer formation was measured, to assess the strength of the oligomerisation.

It was found that the change in particle distribution was dramatic and required a low concentration of ATPγS at a protein concentration of 4.8 μM (**Fig. 4.4A**). In the absence of nucleotide, species with an integrated $S_{20,w}$ of approximately 4 were seen (**Fig. 4.4B**). With an approximately equal stoichiometry of Mg.ATPγS and protein the distribution shifts to the right and larger species are present (**Fig. 4.4A)**. With the addition of 100 μM Mg.ATPγS the protein is almost completely hexameric, which is confirmed by molecular mass calculations from AUC (**Fig. 4.4B**).

In the c(s) and c(M) distributions a small species is present where a dimer is expected. The position of this peak suggests that the dimer may be the building block oligomer for larger species formation of the R294 variants.

By plotting the integrated $S_{20,w}$ against ATPγS concentration it is shown that ~15 μM ATPγS is the half point to trigger hexamer formation (**Fig. 4.4C**). The data recorded at this nucleotide concentration shows a wide range of species ranging from 3 – 9 $S_{20,w}$ (**Fig. 4.4A**). It should also be noted that though I was unable to attain highly pure ATPγS, the study shows with ADP contamination hexamer formation can still occur.

It appears that only a small excess of ATPγS is required for hexamer formation suggesting that *in planta* where the ATP levels are high, the R294A variant would most

likely form hexamers. This is in good agreement with the ATPase assays which suggest the hexameric oligomer is the minimal catalytic unit for the R294 variants.

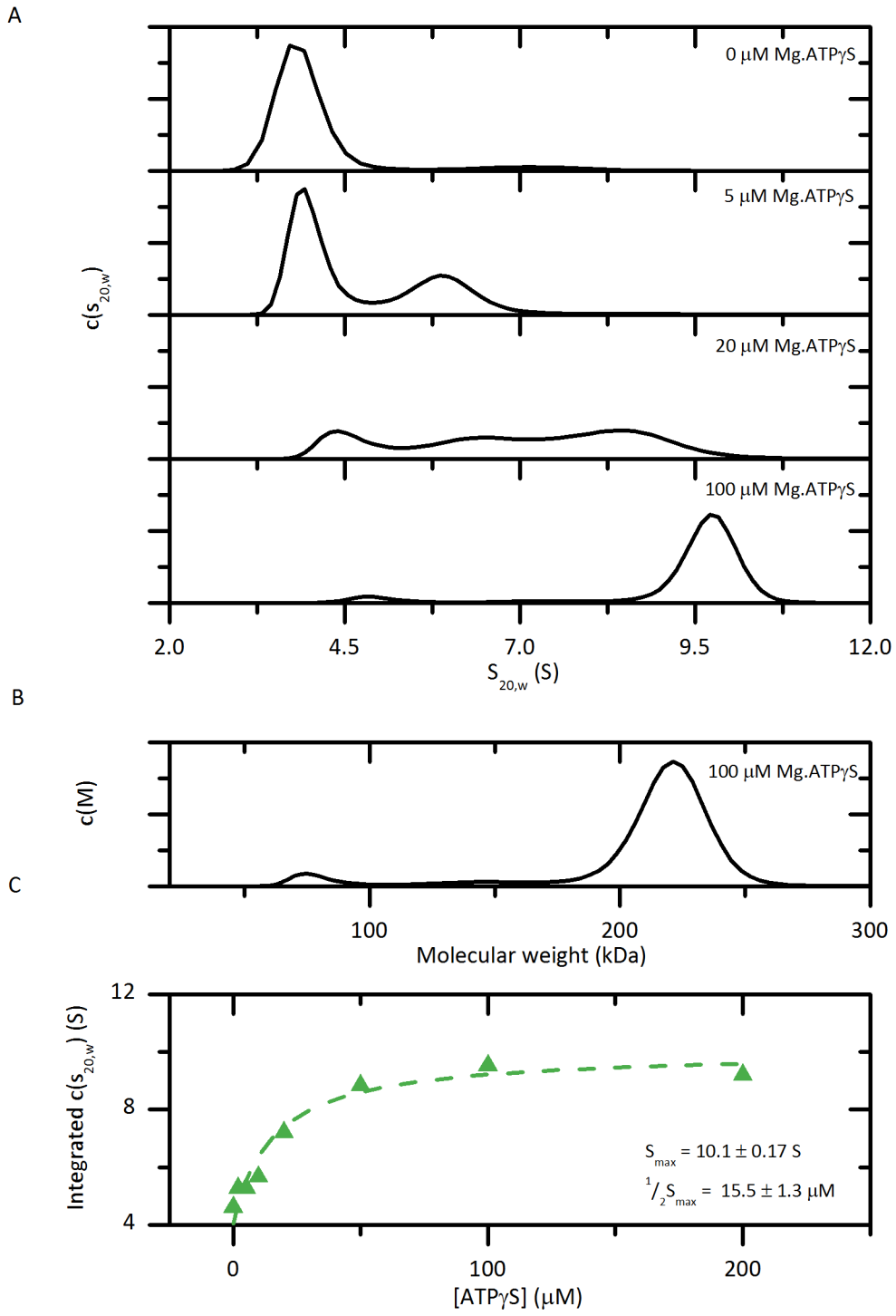

Figure 4.4. **50 μM ATPγS is required for R294A hexamer formation**. A) Particle distribution with increasing ATPγS concentration. B) Mass distribution for R294A. C) Integrated S versus ATPγS concentration. ATPγS at the indicated concentration was titrated into 4.8 μM R294A with 5 mM Mg.

4.4 Nucleotide binding and thermal stability

To investigate the effect of nucleotide on the R294 and N99 variants, intrinsic fluorescence and DSF assays were carried out. Binding affinities were calculated by fitting a hyperbolic curve, the point at which half the maximal change in intrinsic fluorescence or half the maximal increase in thermal stability has been reached is used as the point of comparison between different variants. For both techniques I refer to this value as $S_{0.5}$, the point of half saturation.

4.4.1 *R294 variants undergo structural rearrangement upon addition of ATPγS*

The intrinsic fluorescence change seen in Rubisco activase has been attributed to two tryptophan residues near the rossman fold whose environment changes upon the binding of ATP/ATPγS.[97] I have used this change in fluorescence to measure structural rearrangement upon ATP/ATPγS binding.

Both arginine variants show a doubling of the fluorescence yield with the addition of Mg.ATPγS over Mg.ATP, a similar level of change as to that which was seen for wild-type tobacco (**Fig. 4.5A**). However, the increase in intrinsic fluorescence of R294A is approximately double the fluorescence yield of wild type, while R294V has a threefold increase in fluorescence yield in response to Mg.ATPγS. A comparison of binding affinities shows that Mg.ATP binds with approximately half the affinity of Mg.ATPγS for all enzymes.

As measured by intrinsic fluorescence wild-type tobacco Rubisco activase binds Mg.ATPγS with an $S_{0.5}$ of 8.8 μM, R294V an $S_{0.5}$ of 3.6 μM, and R294A an $S_{0.5}$ of 1.2 μM (**Fig. 4.5C**). Previous studies using ANS binding, found that R294A bound ATP at

2.6 μM, whereas the wild-type tobacco enzyme bound at 4.3 μM.[11] This is in agreement with results showing that R294A binds ATP much more tightly than the wild-type enzyme. However, the previous study found different apparent binding affinities, presumably due to differences in the measurement technique.

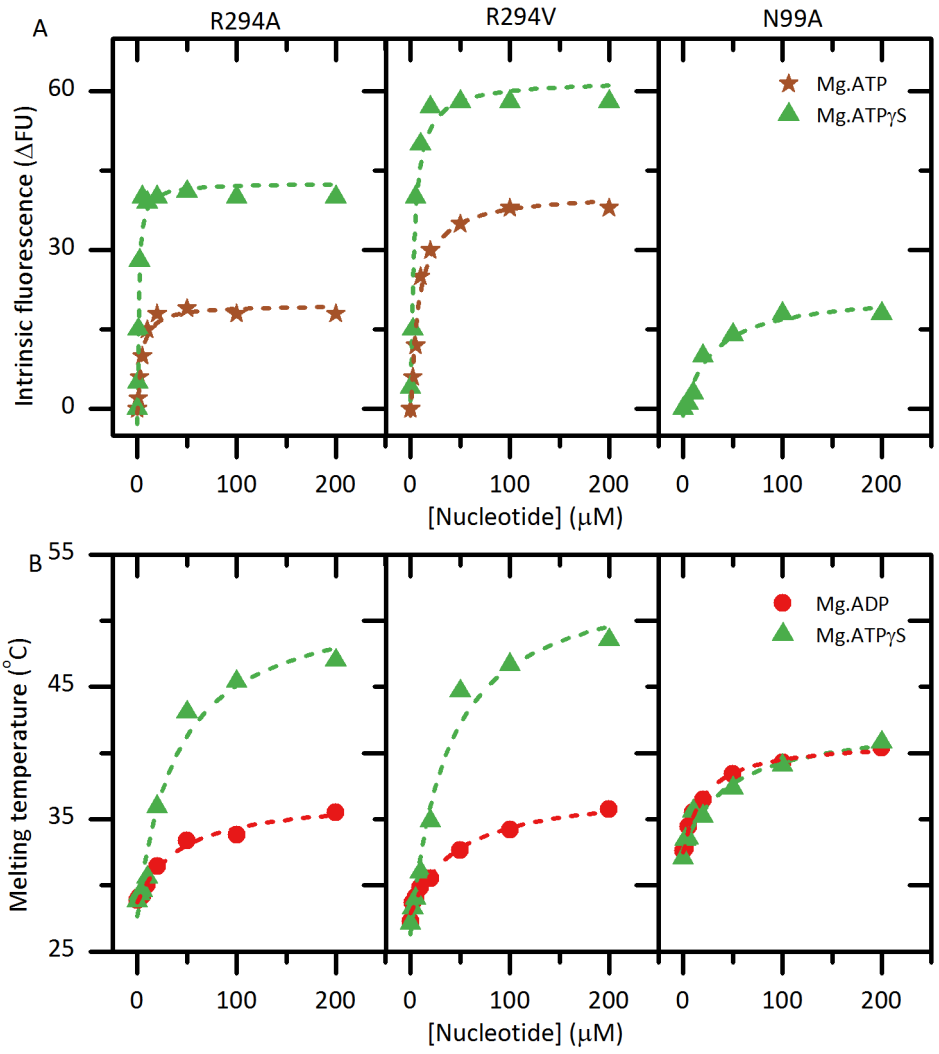

C

Additive	Method	$S_{0.5}$ (μM)			
		wild type	R294A	R294V	N99A
Mg.ATP	IF	16.4 ± 4.1	3.9 ± 0.9	8.0 ± 1.6	
Mg.ATPγS	IF	8.8 ± 3.5	1.2 ± 0.3	3.6 ± 1.1	28.1 ± 11
Mg.ADP	DSF	22.5 ± 7.1	42.4 ± 11.6	46.5 ± 12.5	20.6 ± 3.9
Mg.ATPγS	DSF	25.7 ± 8.0	38.9 ± 13.4	36.6 ± 11.3	47.8 ± 21.3

Figure 4.5.**Arginine mutants show a large increase in intrinsic fluorescence and thermal stability.** A) Intrinsic fluorescence, and B) DSF assays were carried out with nucleotide at the indicated concentration. C) Table of affinities for each mutant. Points of half saturation were calculated by fitting a hyperbola and the errors are standard errors. All experiments were carried out with 4.8 μM protein and 5 mM Mg.

4.4.2 *ATPγS causes large increase in thermal stability in arginine variants*

In the previous chapter, addition of nucleotide, either Mg.ADP or Mg.ATPγS was shown to cause an increase in the thermal stability of the wild-type tobacco enzyme.

In the absence of either nucleotide at the same protein concentration the Rubisco activase variants are much less stable than the wild-type enzyme, melting at approximately 28, 32, and 35 °C for the R294 variants, N99A, and wild type, respectively.

Previously studies by our group and others have shown that the addition of nucleotide increases the thermal stability of Rubisco activase.[2,51] In this thesis I have previously shown that wild-type tobacco Rubisco activase is stabilised by 7 °C upon addition of 0.2 mM of either Mg.ADP or Mg.ATP. The R294A/V variants had an increase in thermal stability of 7 °C with the addition of 0.2 mM Mg.ADP (**Fig. 4.5B**).

Addition of Mg.ATPγS, which triggers hexamer formation, increases the melting temperature by 20 °C, from 28 to 48 °C (**Fig. 4.5B**). It appears that the major increase in thermal stability and intrinsic fluorescence correlates with hexamer formation. Both nucleotides bind with equal affinities of 40 μM, approximately half the affinity of either nucleotide for the wild-type enzyme.

Previous studies have shown the presence of these highly stable Rubisco activase species for the α-isoform of spinach Rubisco activase in the presence of Mg.ATPγS, as measured by an increase in light scattering.[12,49,99] The recent results on the Rubisco activase α-isoform from spinach suggests that these hexameric species show a similar level of thermal stability to the R294 variants.

4.4.3 *N99A has a similar nucleotide response to the wild-type enzyme*

Intrinsic fluorescence assays with Mg.ATPγS showed a similar maximal change to the wild-type enzyme; however, the binding affinity was reduced to 28 μM compared to the wild-type value of 8.8 μM. As was also seen for wild type, the addition of 0.2 μM Mg.ADP or Mg.ATPγS caused an increase in the melting temperature of ~7 °C (**Fig. 4.5B**). However, the protein is destabalised by 2 °C in the presence or absence of either nucleotide compared to wild-type Rubisco activase.

4.5 Solution structure of the Rubisco activase hexamer

4.5.1 *Arginine variants show a differential response to ATP*

In order to expand the results showing hexamer formation with an ATP analogue, the native substrate was used for biophysical studies.

An experiment was designed using SAXS where the protein would be exposed to a high concentration of Mg.ATP in an SEC running buffer. As the protein moved through the column more quickly than the small ADP molecule the protein would constantly be exposed to fresh Mg.ATP. It was theorised that constant exposure to Mg.ATP would drive the protein to form the hexameric species. This experiment was also attempted using SEC-SLS; however, due to the long time frame the experiment was not successful as the Mg.ATP was completely hydrolysed, and the protein eluted as an asymmetric peak.

For R294A it appears that the reduced rate of ATP hydrolysis trapped an average state which is more similar to the protein with ATPγS bound, presumably this state has a higher prevalence of hexamer. The differences in the scattering curves seem small, with both curves flattening at the low q angles suggesting a monodisperse system (**Fig. 4.6A**). This is reflected in similar maximum particle dimension in the P(r) plot (**Fig. 4.6C**). The ATPγS bound structure has a larger number of shorter distances indicating that it is possibly a more tightly packed structure, as would be expected from a closed hexamer.

Unlike R294A, R294V shows fewer similarities between the Mg.ATP and Mg.ATPγS solution structures. The scattering curves show an upward inflection at the low q angles, indicating an oligomerisation process is occurring (**Fig. 4.6B**). The

maximum particle distance is also increased in the ATP bound structure (243 Å) compared with the ATPγS structure (178 Å) (**Fig. 4.6E**).

There is a large difference in the distribution of intraparticle distances where the ATP bound structure has many more long distances, strongly indicating an elongated structure (**Fig. 4.6D**). I propose that the R294V structure I see in the presence of Mg.ATP is most likely predominantly ADP bound, having previously shown that the ATPase rate of R294V is more rapid that R294A (**Fig. 4.2B).** With all necessary components for the reaction present I suggest that ATP is hydrolysed too quickly for data collection on the stable ring form. I have shown by AUC that the addition of Mg.ADP to R294V causes large increases in the oligomeric state, whereas little change is seen for R294A. From the current data it is difficult to determine whether structure is forming stable hexameric species in the presence of Mg.ATP for either variant. Future experiments utilising a transition state ATP analogue such as BeF_3 or AlF_3 may be more able to trap the stable hexamer.

Why the arginine variants are able to form stable hexamers is currently unknown; however, an adjacent patch of hydrophobic residues may be important. The crystal structure of tobacco Rubisco activase shows highly hydrophobic residues L97 and I100 from an adjacent protomer may be able to form interactions with the variant alanine and valine residues. This interaction may be able to stabilise the intersubunit interface trapping the hexameric oligomer. Whether or not these residues are still able to interact with each other after nucleotide binding is not currently known.

The reason for the increase in oligomeric state seen with the addition of Mg.ADP in the valine variant but not the alanine variant remains unknown. It may be that valine

with its higher hydrophobicity and increased size is able to form stronger interactions with neighbouring hydrophobic residues.[165] Without atomic detail of a nucleotide-bound structure, unravelling the mechanism is difficult.

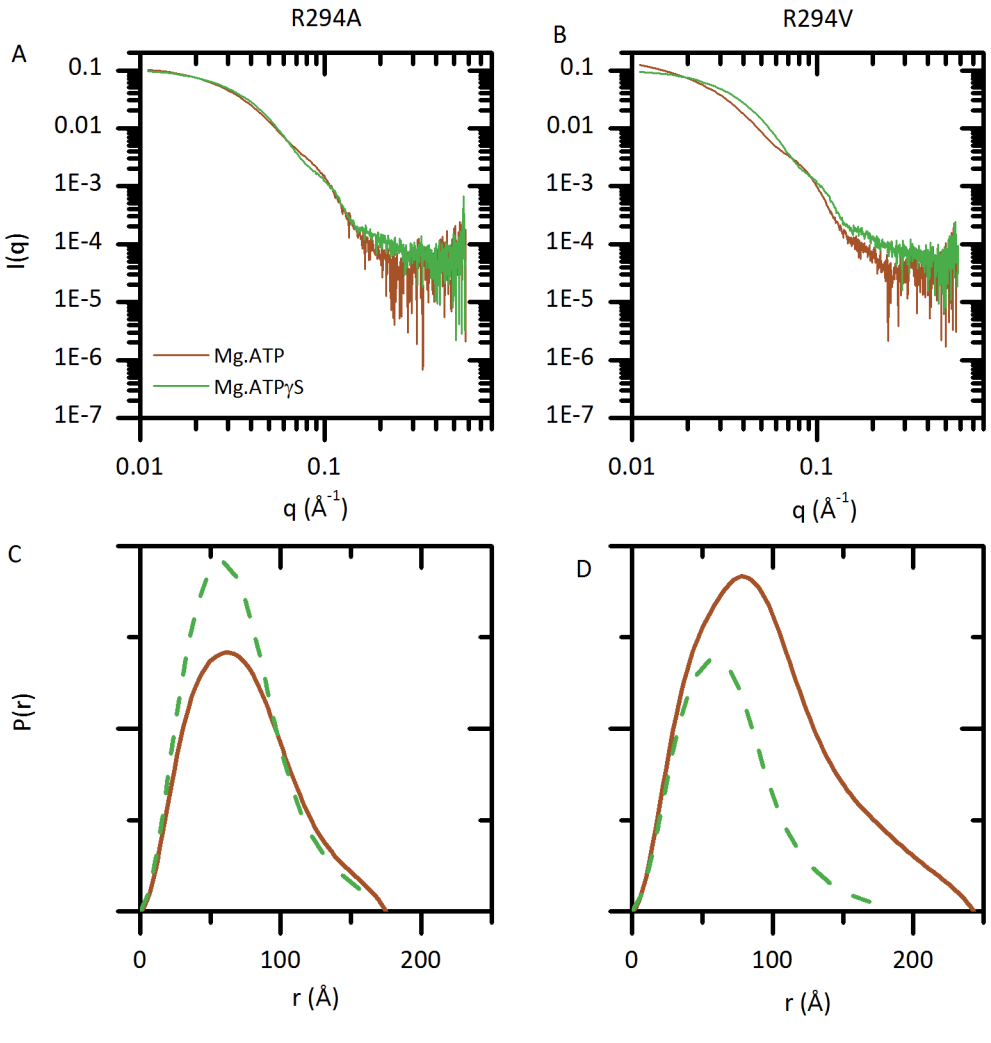

E

Variant	Additive	Radius of gyration (Å)	I(0) (cm^{-1})	D_{max} (Å)	Porod volume ($Å^3$)
R294A	Mg.ATP	56.9	0.113	175	572,760
	Mg.ATPγS	52.6	0.13	171	547,498
R294V	Mg.ATP	75.4	0.255	243	1,006,460
	Mg.ATPγS	53.1	0.16	178	569,303

Figure 4.6. **R294V shows a large difference between ATP and ATPγS while R294A does not.** A, B) Intensity curves for each sample. C, D) Plots of the real space particle distance distribution for each sample. E) Table of parameters for each sample. Each variant was loaded at 144 µM in the presence of 5 mM Mg and either 0.2 mM ATPγS (green) or 2 mM ATP (brown). Frames showing maximum intensity were averaged and used for further analysis. All samples were collected post SEC.

4.5.2 *R294 variants have a similar solution structure in the presence of Mg.ATPγS*

With a suitably stable hexamer system characterised using AUC and SAXS it was now possible to test how the crystal structure compared to the solution structure.

The R294A and R294V hexamers generated very similar scattering profiles (**Fig. 4.7A**). The radius of gyration, D_{max}, Porod volume, and pair wise distance distribution plot were all very similar (**Fig. 4.6E, 4.7B**). Further data analysis was carried out using the R294A data set.

A comparison of R294A and the two proposed hexameric models created from the crystal structure of tobacco Rubisco activase was carried out. The "closed" hexamer model was created from the crystal lattice fitted to a negative stain-EM envelope (PDB 3ZW6). Twisting a crystal structure from a spiraling arrangement to a flat hexamer will possibly affect its theoretical scattering, due to changes in the D_{max} and the protein volume. The second structure I compared was that of an "open" hexamer ($P6_5$) with spiral arrangement of subunits still present (PDB 3T15). It should be reiterated here that both arrangements of wild-type tobacco Rubisco activase lack 68 N-terminal and 23 C-terminal residues. Additionally four small loop regions were not resolved in the crystal structure.[3] In total, approximately 25% of the residues present in the full length structure are missing from the crystal structure. A comparison of the theoretical scattering of the two wild type crystal arrangements with either R294 variant hexamer show large differences in the scattering profile (**Fig. 4.7C**). This is not unexpected due to the large number of absent residues. I replicated the EM results previously published[3] with the R294V variant showing ring assemblies of approximately 15 nm, the expected size of the Rubisco activase hexamer (**Fig. 4.7D**).

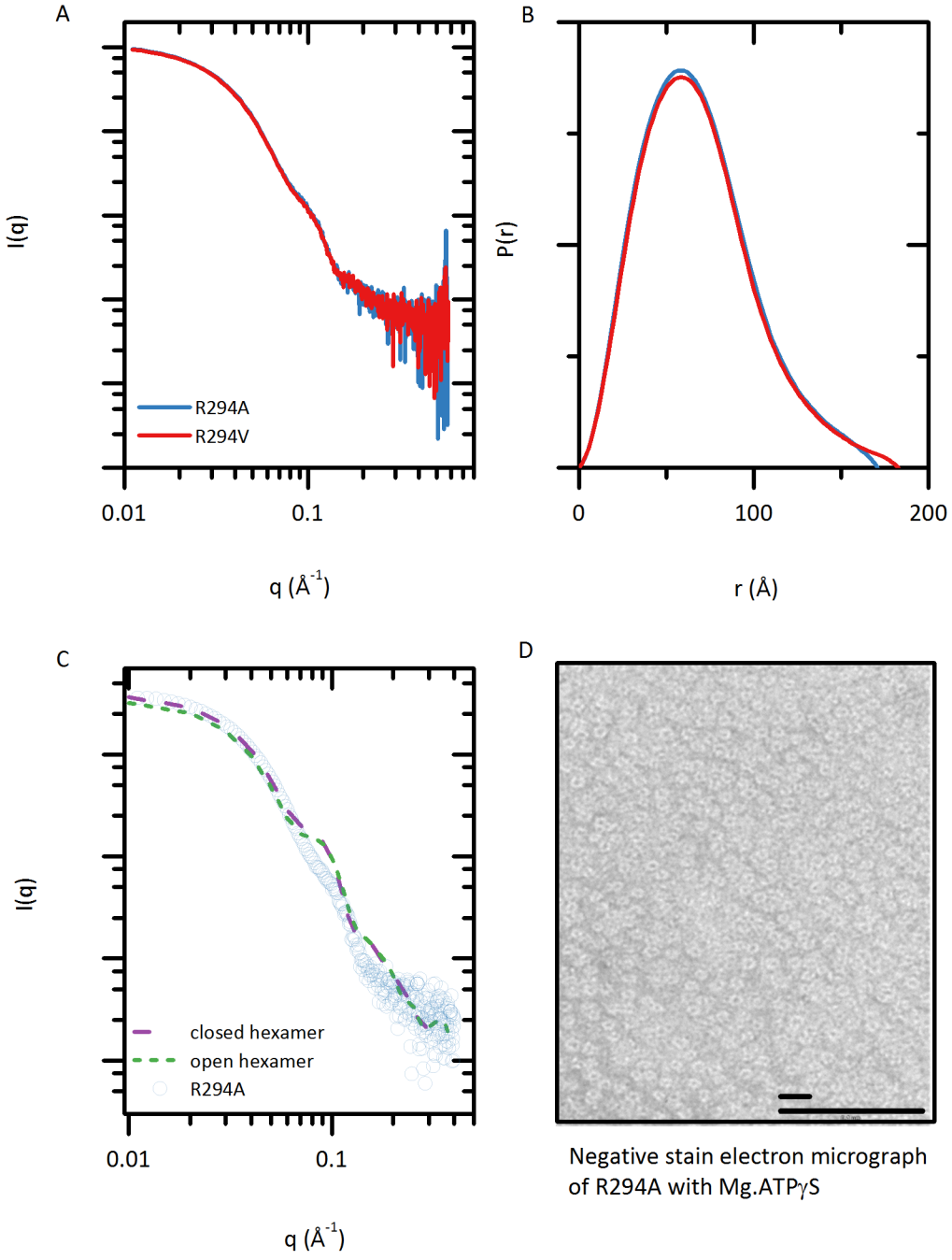

Figure 4.7. **The hexameric arginine variants are highly similar**. A, B) Intensities and P(r) for R294 variants supplemented with Mg.ATPγS. C) Theoretical scattering of the closed (P6) and open spiralling ($P6_5$) tobacco crystal structure hexameric R294A. D) Negative stain EM showing R294A hexamer in the presence of 0.2 mM Mg.ATPγS. The scale bars are 0.1 and 0.5 µm.

4.5.3 *SAXS can be used to model missing crystal structure residues*

Advances in SAXS data analysis has been led by the creation of programmes created to model residues which are missing from a crystal structure. Two types of modelling can be carried out with SAXS data. The first type, *ab initio* modelling, assumes little prior knowledge requiring only the number of residues in the asymmetric unit. If a known symmetry exists then this can be used as a constraint. A selection of dummy atoms is then created and iteratively rearranged until the theoretical scattering of the residues matches the supplied data.

The second type, rigid-body modelling, requires more prior knowledge. In the context of the modelling carried out here, symmetry operators, atomic resolution models, and the lengths of missing residues were all used as constraints in model development. Both modelling strategies have strengths and weaknesses, but rigid-body modelling is generally considered more accurate providing any data used as a constraint is validated using complimentary methods. I will describe the use of CORAL to model in the residues which are missing from the wild-type crystal structure to gain a sense of the position of these residues.

CORAL uses a library of random length dummy atom chains to model in missing fragments of a crystal structure.[140] Upon placement of a dummy atom chain the scattering of the new structure is calculated and compared to the experimental scattering. If the scattering is in better agreement than the previous theoretical loop arrangement then the new arrangement is accepted, this procedure is then iterated. CORAL uses simulated annealing to measure optimal positions of the linkers.

For the modelling carried out here the position of all crystal structure elements is fixed, as this represented the most accurate representation of the experimental data. The length of missing linker regions and missing terminal regions was specified. The position of the following residues were modelled, 67 residues at the N-termini, 14 residues missing between residues 176 to 191, 11 residues missing between residues 207 to 219, and 23 residues at the C-termini. Two small loop regions were not modelled as CORAL will not model linkers smaller than five residues. No symmetry operations were applied. CORAL was run four times and the model presented here is representative.

I found that the loop regions were located in the central pore of the hexamer (**Fig. 4.8**). This was anticipated as the short linkers have a known start and end point within the crystal structure. The large 68 N-terminal domain was extended away from the core helix, with all domains showing different arrangements (**Fig. 4.8**). The importance of the result for the N-terminal domain is that it demonstrates the high level of flexibility of this domain. CD spectroscopy of this domain suggests no α-helices and a low content of β-sheet.[109] I was also able to place the C-terminus into missing density on the top face of the previously generated negative stain-EM model (**Fig. 4.8**). The negative stain EM single particle reconstruction lacked resolution of the N-terminal domain.

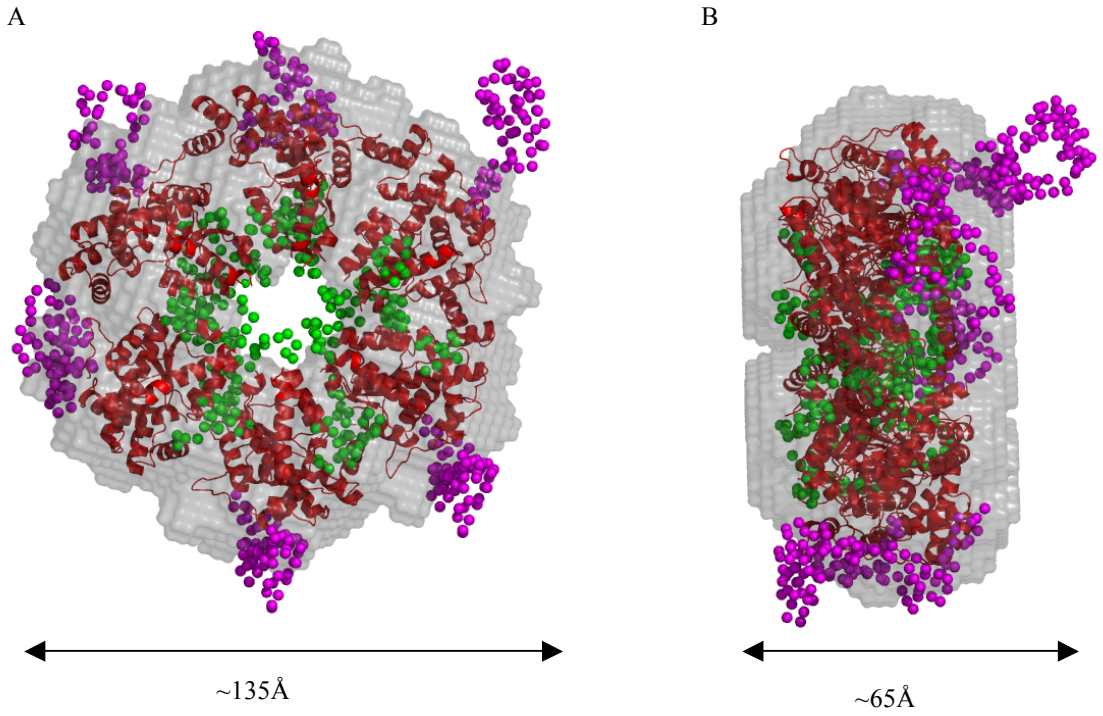

Figure 4.8. **SAXS modelling reveals the extended nature of the N-terminal domain**. A) Front view of the Rubisco activase hexamer. B) 90° rotation of the front view. The crystal structure (PDB 3ZW6) is shown in red. Dummy atom bead model generated from the negative stain EM envelope is shown in grey. Rigid body modelling of residues are shown as sphere with the N-terminal residues shown in purple, with the loop and C-terminal residues shown in green.

4.6 Understanding the mechanism of Rubisco activase oligomerisation

4.6.1 *Interface mutations destabilise Rubisco activase*

The two residues that were mutated, R294 and N99, are involved in a large hydrogen bond network through the side chain amide groups of the arginine residue and the backbone oxygen of the asparagine (**Fig. 4.1**). I sought to understand the importance of these residues at the intersubunit interface.

I found that mutation of the highly charged arginine residue to hydrophobic residues caused a large level of destabilisation in the oligomer, decreasing both oligomeric state and thermal stability (**Fig. 4.2B, 4.4B**). Mutation of N99, a polar uncharged residue, to a weakly hydrophobic alanine caused oligomer destabilisation but to a lesser extent than mutation did to either of the R294 variants (**Fig. 4.2A**). N99A exhibited larger oligomeric states and higher thermal stabilities in the absence of nucleotide than either of the arginine variants (**Fig. 4.2B, 4.4B**). This is presumably as mutation of the side chain retains the R294-A99 backbone hydrogen bond. However, a hydrogen bond between glutamine 330 and the side chain of the asparagine residue is lost, causing oligomer destabilisation.

N99A has similar kinetic parameters to wild-type but requires higher protein concentrations to achieve similar oligomeric states and activities. This is useful in determining the minimal oligomeric state as it is now possible to measure the oligomeric state across the range of specific ATPase activities. Previous studies using variants which allow oligomerisation on only one interface showed that ATPase activity required three subunits.[3]

I found that at the lowest protein concentration where there was nominal ATPase activity the protein was predominantly monomeric (**Fig. 4.2B**). Dimeric species were present when the specific ATPase activity was at approximately 40%. Once the protein concentration increased above 1 μM no changes were seen in the specific activity as all protomers were incorporated into higher order oligomers (**Fig. 4.2B**). This corroborates well with the wild-type enzyme which showed 50% specific ATPase activity when an average molecular weight of a dimer was reached. Here I can assess the distribution of particles and found that dimers or trimers appear to be the minimal ATPase catalytic unit.

Both R294 variants form hexamers under conditions which simulate the condition within the ATPase assay, namely a high concentration of ATP/ATPγS. At all protein concentrations which the activity was measured the variants were almost completely hexameric. (**Fig. 4.2B**). Technical limitations preclude measurement of the oligomeric state at very low protein concentrations in the presence of nucleotide. Thus the results indicate there may be active open and closed oligomers.

4.6.2 *Closed hexameric oligomers have different characteristics to spiraling oligomers*

It has been established that the arginine 294 variants both form stable hexamers in the presence of Mg.ATPγS. It is now important to discuss the differences between the closed hexamer and open oligomers. Open oligomers such as the wild-type tobacco or N99A variant enzyme are both examples of Rubisco activases which appear to form open spiralling oligomers. Both enzymes have similar responses to Mg.ADP and Mg.ATPγS, increasing the thermal stability by around 7 °C while not affecting the oligomeric state.

The closed variants R294A and R294V; however, are affected by the presence of nucleotide. Addition of 0.2 mM Mg.ATPγS increased thermal stability by ~20 °C and caused the protein to undergo a change in oligomeric state to form a hexamer (**Fig. 4.4B, 4.5A**). Without an atomic resolution nucleotide bound structure, a detailed mechanism for nucleotide binding and hydrolysis cannot be proposed. However, a general mechanism can be proposed.

When ATPγS binds in the active site, it induces a rearrangement of the nucleotide binding α/β subdomain, locking the protein in a prehydrolysis hexameric conformation. The intrinsic fluorescence experiments with Mg.ATPγS have shown that nucleotide binding causes a rearrangement in the Rossman fold; however, no hydrolysis occurs. This has been shown by a change in the intrinsic fluorescence previously attributed to W109 and W250, residues both located in the α/β sub domain.[97] However, the same experiments carried out with Mg.ATP show increased intrinsic fluorescence which diminishes as the nucleotide is hydrolysed. Additionally the more ordered locked ring conformation requires more energy to be broken, resulting in a greatly increased thermal stability.

4.6.3 *Solution structures suggest a role of the N-terminus in Rubisco recognition*

Current atomic models of Rubisco activase lack residues from both the N- and C-termini. A comparison of electron microscopy envelopes and the truncated crystal atomic resolution structure show an area of empty density on the one face of the hexamer. The authors of this paper suggested that this could accommodate some or all missing residues from the N-terminus.[3] I have used SAXS to generate solution structures of a hexameric

variant, R294A. These results suggest that the N-terminus if very flexible and tends to protrude away from the core of the hexamer. It is proposed that the empty density could be filled by the missing C-terminal residues.

Studies implicate the N-terminal domain being strongly involved in the interaction with Rubisco, as mutation of W16 or removal of the first 68 residues from Rubisco activase maintains ATPase activity but obliterates any Rubisco activation activity.[3,82] It may be that the largely unstructured N-terminal domain, which mediates protein-protein interactions, adopts a more folded state upon binding to Rubisco making the process energetically favourable.

Chapter Five: **Salt bridge variant proteins have novel oligomeric states**

5.1 Introduction

In chapter four I demonstrated how mutation of residues located in the intersubunit hydrogen bond network affected oligomeric state, activity and nucleotide response. In this chapter I look at another important interface interaction between Lys-92 and Asp-299 (**Fig. 5.1A**). Analysis of the interface showed that a salt bridge (electrostatic interaction) and hydrogen bond is formed between these two residues.[3] Both the open and closed oligomers allow formation of this bond between these residues.

Charge switching of the lysine and aspartic acid residues has been shown to form putative monomers (**Fig. 5.1B**).[109] This study found no change in molecular weight with the addition of either ADP or ATP.[109] The double mutation K92D/D299K was also monomeric.[109] All monomeric proteins have no ATPase or Rubisco activation activities[3], this is most likely because the active site of Rubisco activase requires residues form an adjacent protomer.[3]

In this chapter I first confirm the oligomeric state of the three variants K92D, D299K and the double mutant K92D/D299K. Mixing of the single mutation variants was then carried out and found to have a novel oligomeric state. The solution structures of these oligomers were then characterised using SAXS and models were built. Finally the nucleotide binding affinities and activity of the different variants were assessed.

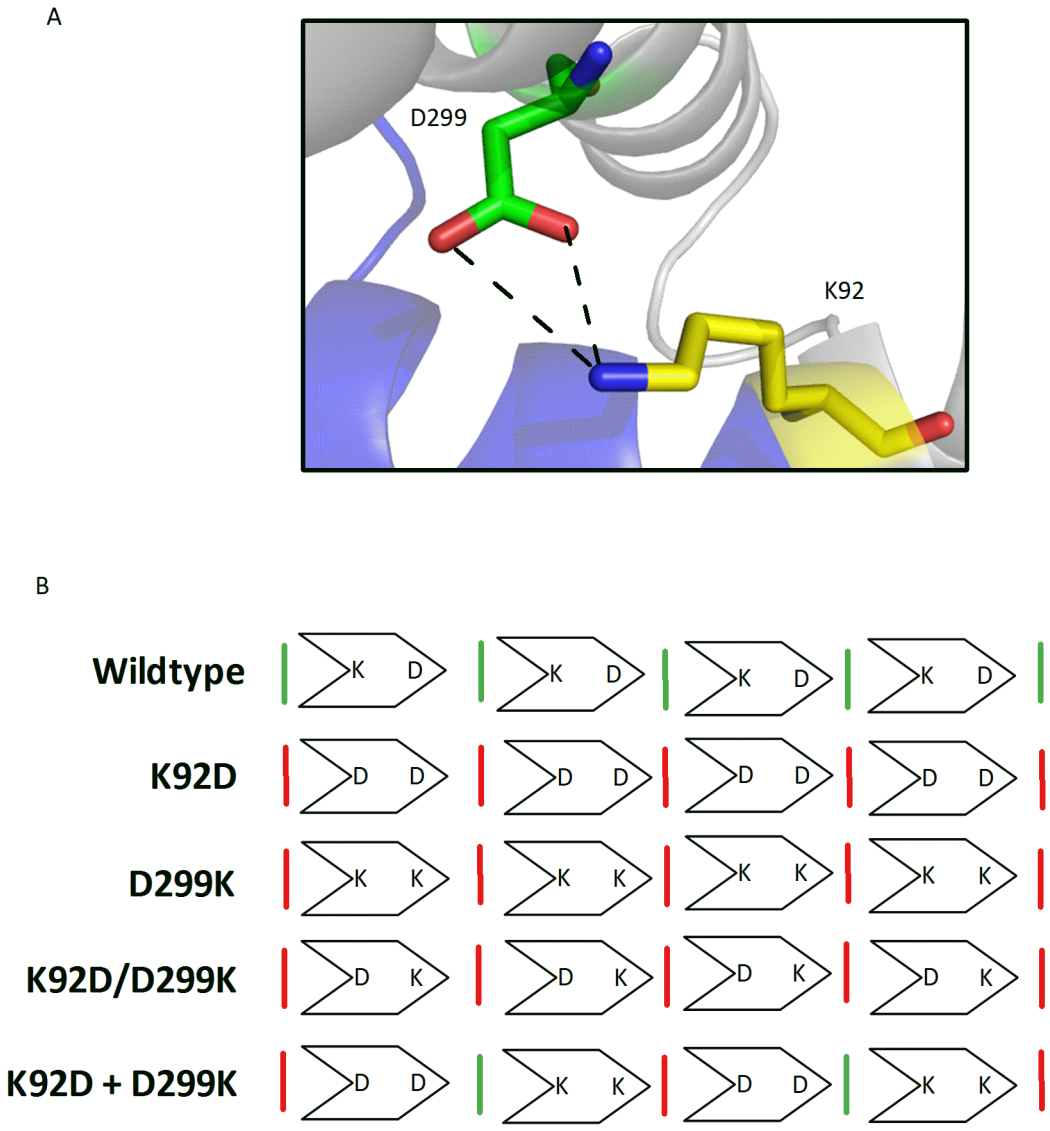

Figure 5.1. **A salt bridge is formed between K92 and D299**. A) The salt bridge between lysine 92 and aspartic acid 299. B) Schematic representation of possible interactions for the wild type and variant proteins. Green bars indicate an interaction is possible while a red bar indicates it is not.

5.2 Switching of the salt bridge effects oligomeric state

5.2.1 *All salt bridge variants are monomeric*

The oligomeric state of the two single and one double mutation variants was previously investigated using analytical SEC; however the measured molecular weight was not sufficiently accurate to assess the oligomeric state, giving a molecular weight of ~70 kDa.[109] Here SEC-SLS and AUC were used to accurately measure the molecular weight of the variant proteins.

All variants eluted as single peaks by SEC-SLS and had constant molecular weights across the entire peak, unlike the wild-type enzyme (**Fig. 5.2A**). Mg.ADP was necessary as it increased the thermal stability of the enzymes, which was required due to the length of time the experiment took at room temperature. Data without nucleotide could not be collected due to the low thermal stability of the enzyme.

The proteins had measured molecular weights of 44.2, 43.3 and 46.7 kDa for K92D, D299K, and K92D/D299K, respectively. This is in good agreement with the expected molecular weight of monomeric tobacco Rubisco activase of 42.7 kDa. AUC also showed a single species was present in solution with each protein having the molecular weight expected of a monomer and a $S_{20,w}$ of 3.1 (**Fig. 5.2B, C**).

From the data I confirm that the salt bridge between K92 and D299 is vital for the formation of higher order oligomers. While in the previous chapter mutation of the intersubunit hydrogen bond network destabilised larger oligomer formation, mutation of the salt bridge stopped formation of any higher order species.

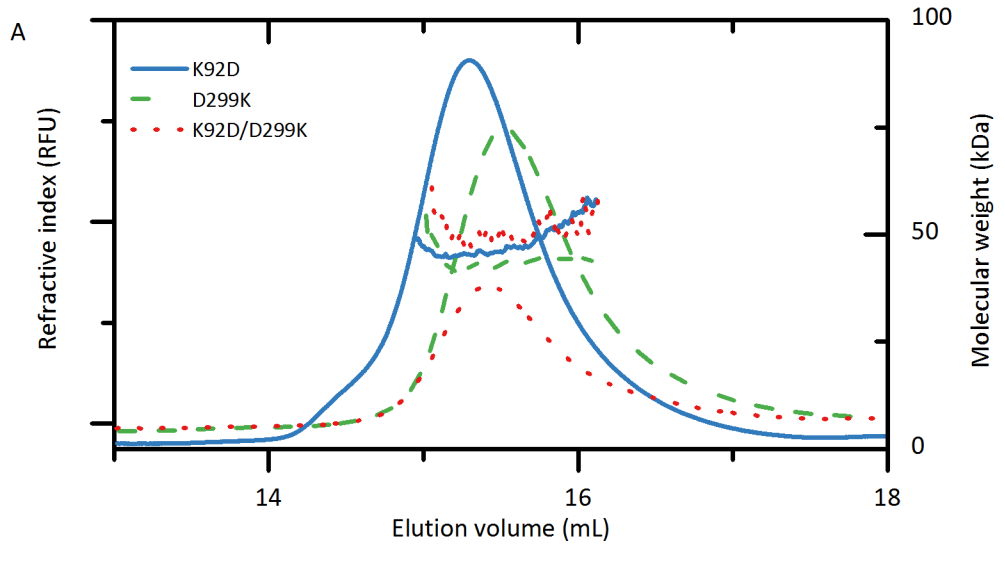

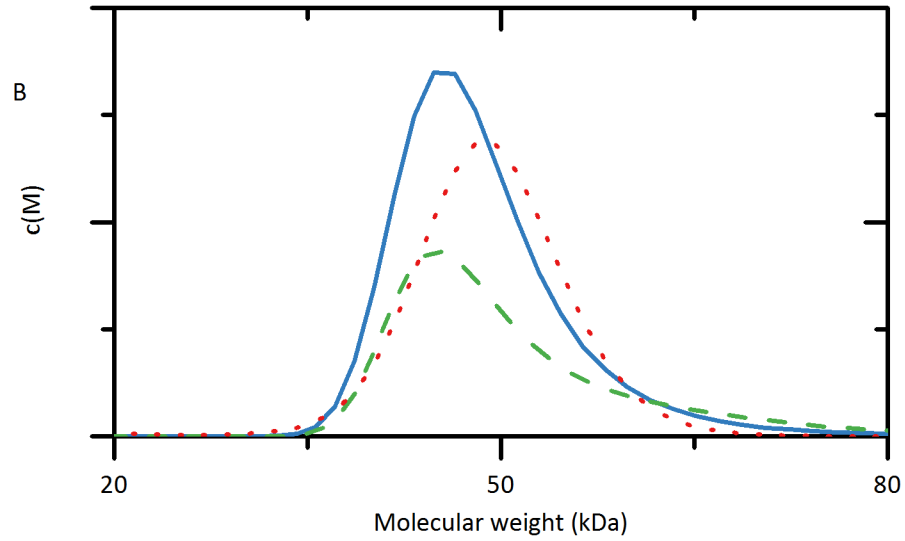

C

Variant	Frictional ratio	Integrated molecular weight (kDa)	Integrated c($s_{20,w}$)
K92D	1.49	46.6	3.07
D299K	1.39	42.8	3.14
K92D/D299K	1.47	47	3.14

Figure 5.2. **Charge switching of the interface salt bridge causes monomer formation**. A) SEC-SLS experiments were carried out in the presence of 0.5 mM ADP, with 24 µM protein at 28 °C B) c(M) analysis for AUC data of each variant protein, the protein concentration was 10 µM. C) Table of AUC parameters for each variant protein. Data was collected at 12 °C.

5.3 Mixing charged switched variant proteins

5.3.1 *Mixing of K92D and D299K results in dimer formation*

Since the two charge switched variants, K92D and D299K, maintained an original interface, mixing of the two proteins would allow formation of a dimeric species (**Fig. 5.1B**).

AUC was carried out using 20 μM of mixed protein and the c(s) profile analysed. This showed that while each variant individually had an distribution centred around 3.1 $S_{20,w}$, the mixed protein had a distribution of species with a maximum $S_{20,w}$ of ~5 (**Fig. 5.3A**). Thus it appeared mixing the two proteins caused dimer formation.

In order to determine the association constant of the complex, the oligomeric state of a range of protein concentrations were measured and the integrated c($S_{20,w}$) was plotted (**Fig. 5.3B**). Fitting a hyperbolic function gave an association constant of 3.3 μM . The data agrees well with a study previously carried out by Chakraborty *et al.* (2012) who found that for the Rubisco activase β-isoform from cotton had a monomer-dimer dissociation constant of ~4 μM. [106] This study was carried out in the presence of Mg.ADP but it is not believed that this will cause a change in the equilibrium position. Evidence presented later in chapter 7 of this thesis suggests Mg.ADP does not affect the oligomeric state of the Rubisco activase β-isoform from cotton.

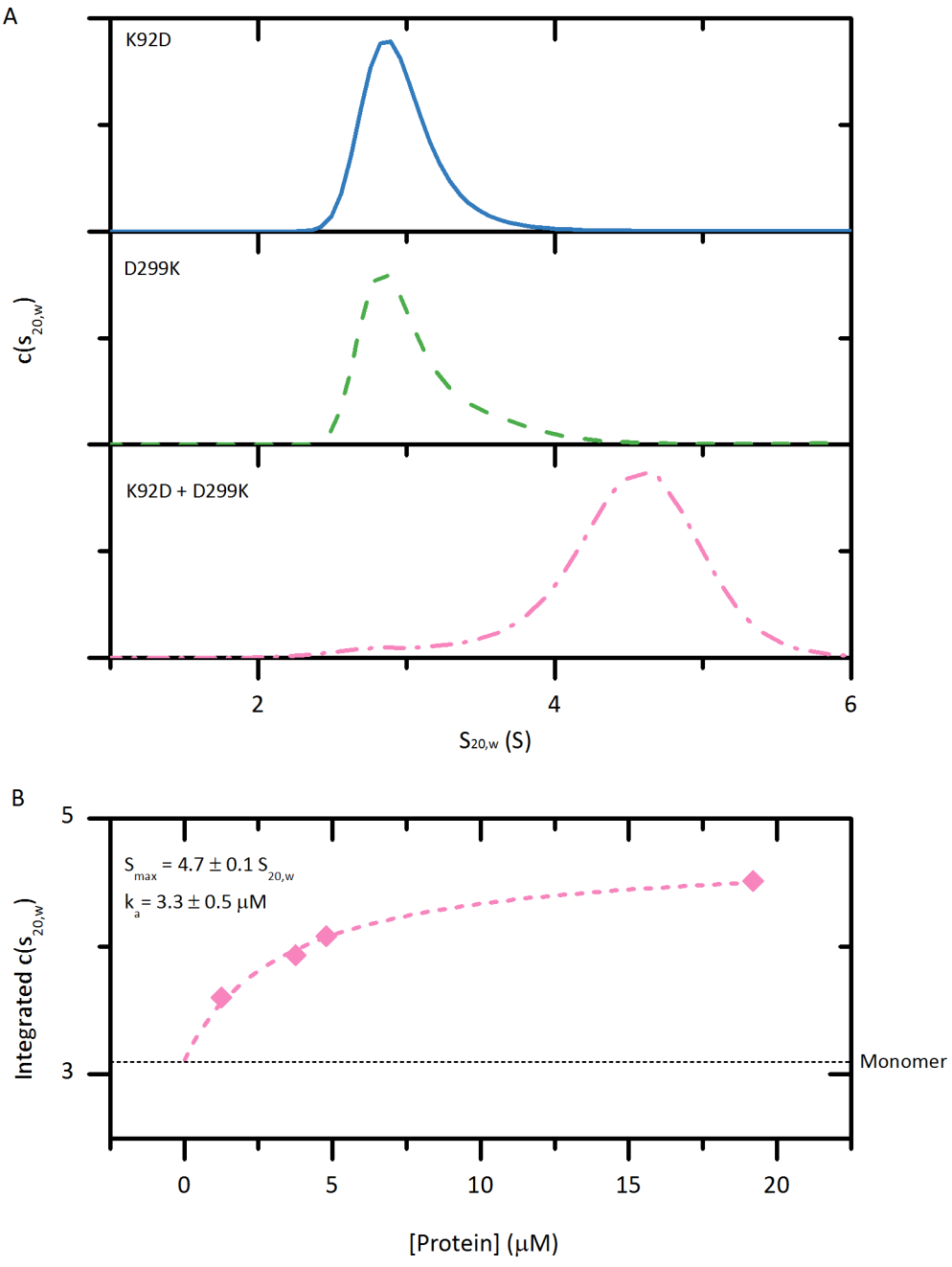

Figure 5.3. **Mixing K92D and D299K causes formation of a dimer**. A) c(s) analysis of AUC data collected on K92D, D299K and K92D + D299K. K92D and D299K were loaded at 10 µM. K92D + D299K was loaded at 19.2 µM. C) Integrated $S_{20,w}$ versus the concentration of K92D + D299K. A hyperbola was fitted and a k_a of 3.3 was found. The integrated $S_{20,w}$ of monomeric Rubisco activase is indicated. No nucleotide or magnesium was included.

5.3.2 *The monomer dimer dissociation constant is in the low micromolar range*

To accurately define the association constant for the monomer – dimer equilibrium I used sedimentation equilibrium AUC. Three protein concentrations, centred on the k_a found by the sedimentation velocity experiments (**Fig. 5.3B**), were chosen. The wavelength of 249 nm was chosen so the highest protein concentration had an absorbance of ~0.3.

For accurate measurement of the dissociation coefficient (k_d) it is important to have a protein concentration above, below, and close to the k_a. The curvature of the protein concentration gradient is a function of the rotor speed and molecular weight of the species. The use of different protein concentrations means that as the speed is increased the abundance of higher order species changes and the protein moves further towards the bottom of the cell. Programs like SEDPHAT[166] and HETEROANALYSIS[133] are able to analyse the changes at the different loading concentrations and apply a global fit to the data. From this fit it is possible to measure accurate average molecular weights and association constants.

In this section I used SEDPHAT and fitted a monomer-dimer self association. Though not a self association, as two different monomers are forming the dimeric species, to reduce the complexity of the modelling it was assumed that these species were the same and could only oligomerise through a single interface. The theoretical mass was that of wild-type tobacco Rubisco activase at 42,727 Da. Mass conservation was used as a constraint. The experiment was carried out at 12 °C to ensure the protein did not aggregate over the time period of the experiment.

To choose appropriate rotor speeds the reduced molecular weights (σ) at each speed for each protein concentration were calculated.[167] Four speeds were chosen so that

the σ at the lowest protein concentration ranged from 0.65 to 2.6 as the speed increased from 10,000 to 20,000 rpm. The highest protein concentration had σ from 0.89 at 10, 000 rpm which increased to 3.57 at 20,000 rpm.

To assess the quality of the fit, errors were calculated using the chi-square error surface projections method.[166,168] Once the best fit for the data is found, the critical chi-square value is calculated, a confidence interval of 68% was used. A new value for the k_a, around 0.1 higher than the best fit value is input and fixed while all other parameters are floated. If the new value is higher than the critical chi-square then the new k_a is outside the error interval. In this case a new k_a, closer to the best fit, is tried until a chi-square is found just above the critical chi-square. This is an iterative process and the original best fit is reloaded prior to a new k_a being input. This process allows the determination of the error range.

The results show that the dissociation constant of K92D and D299K to form K92D + D299K is not higher than 3.5 μM (**Fig. 4.4**). The calculated k_d was 2.8 μM with an upper limit of 3.5 μM, while the lower error limit could not be determined due to the high level of noise in the lowest protein concentration. For this reason it is not possible to specifically define the k_d for this interaction from the data. This value is in good agreement with both the own k_a found by sedimentation velocity experiments and the previous study on the β-isoform from cotton Rubisco activase.[106]

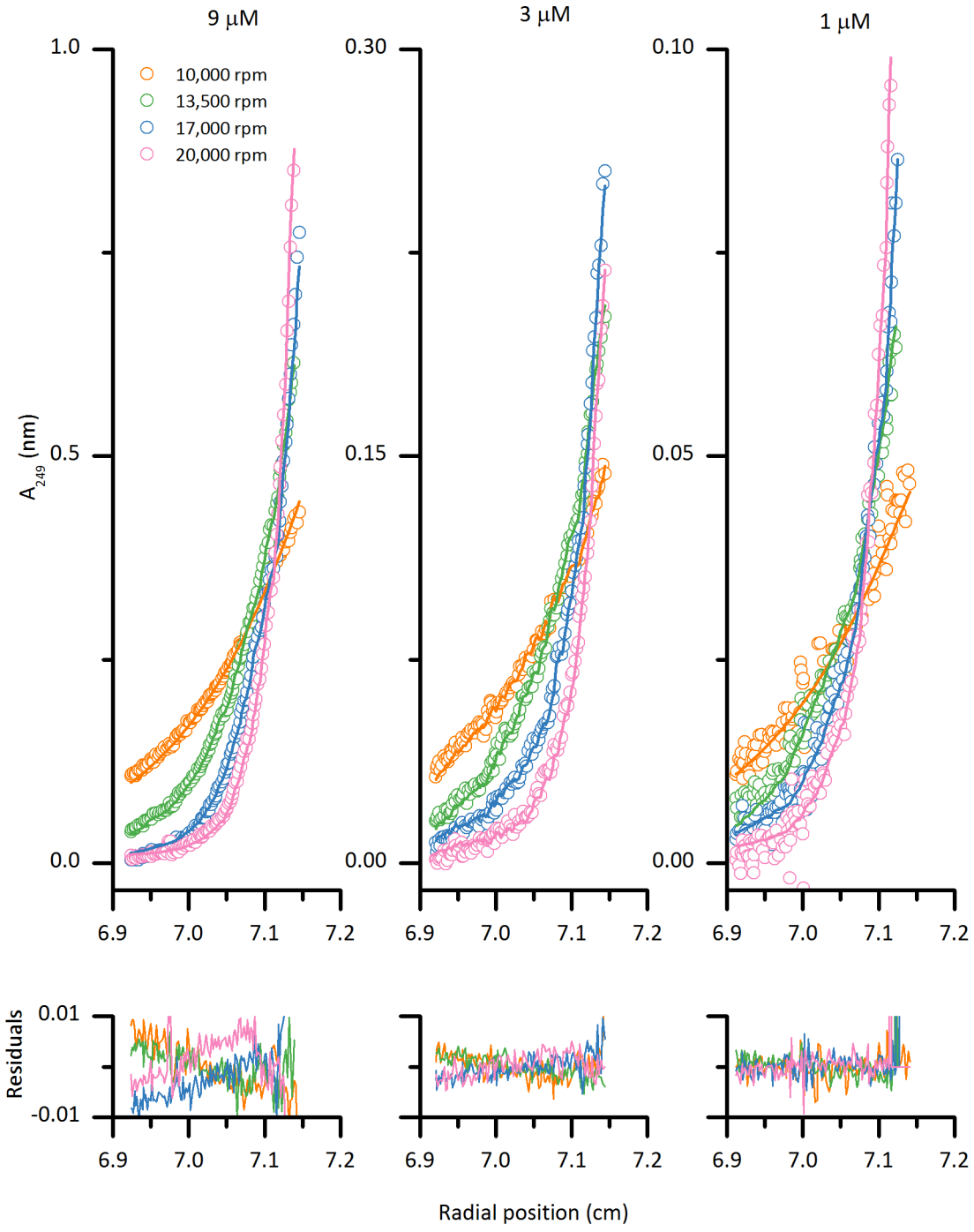

Figure 5.4. **The monomer dimer equilibrium is in the low micromolar range**. An equimolar mixture K92D and D299K were loaded at a protein concentration of 9, 3, and 1 μM. Raw data (circles), the fit (lines), and residuals are shown. Data was recorded at a wavelength of 249 nM at 12 °C.

5.4 Solution structure of monomeric and dimeric Rubisco activase

5.4.1 *SAXS suggests small oligomers are highly flexible*

In order to determine the solution structure of the small Rubisco activase oligomers, SAXS was carried out on D299K and K92D + D299K. K92D was prone to aggregation and yielded low quality data. In an effort to increase enzyme stability, data were collected in the presence of 0.5 mM Mg.ADP, which later in this chapter will be shown to stabilise the protein. High quality, aggregate free, scattering data were collected by running the samples through the inline SEC column to eliminate aggregated protein. The Guinier region of each data set was checked closely for signs of aggregation.

The scattering for both the monomeric and dimeric enzymes showed an elongated structure (**Fig. 5.5A, B**). Comparisons to the truncated monomeric and dimeric atomic resolution structures indicate similarities between the solution structures and the truncated atomic structure. By transforming the data from reciprocal to real space in the p(r) it can be seen that D299K appears elongated, while K92D + D299K is more globular as indicated by the centering of the Rg within the D_{max} (**Fig. 5.5C**). This increased maximum dimension may be caused by the double mutations affecting protein flexibility or folding.

The normalised Kratky plot, indicative of the flexibility of a protein, indicated that the monomeric D299K is more flexible than the dimeric K92D + D299K (**Fig. 5.5D**). The normalisation was carried out using BIOISIS.[169] Rubisco activase comprises two nucleotide binding subdomains, linked only by flexible loop regions. In higher order structures these domains will be constrained in their movement by neighbouring

protomers. However, in the small oligomeric variants presented here these subdomains will be much more flexible.

There is little difference in the radius of gyration or D_{max} between the monomer and dimer; however, the Porod volume is almost double for the dimeric mixture (**Fig. 5.5E**). Molecular weight approximations using the Porod volume for D299K and K92D + D299K were 45.9 and 76.8 kDa, in good agreement with the expected values for a monomer and dimer, respectively.

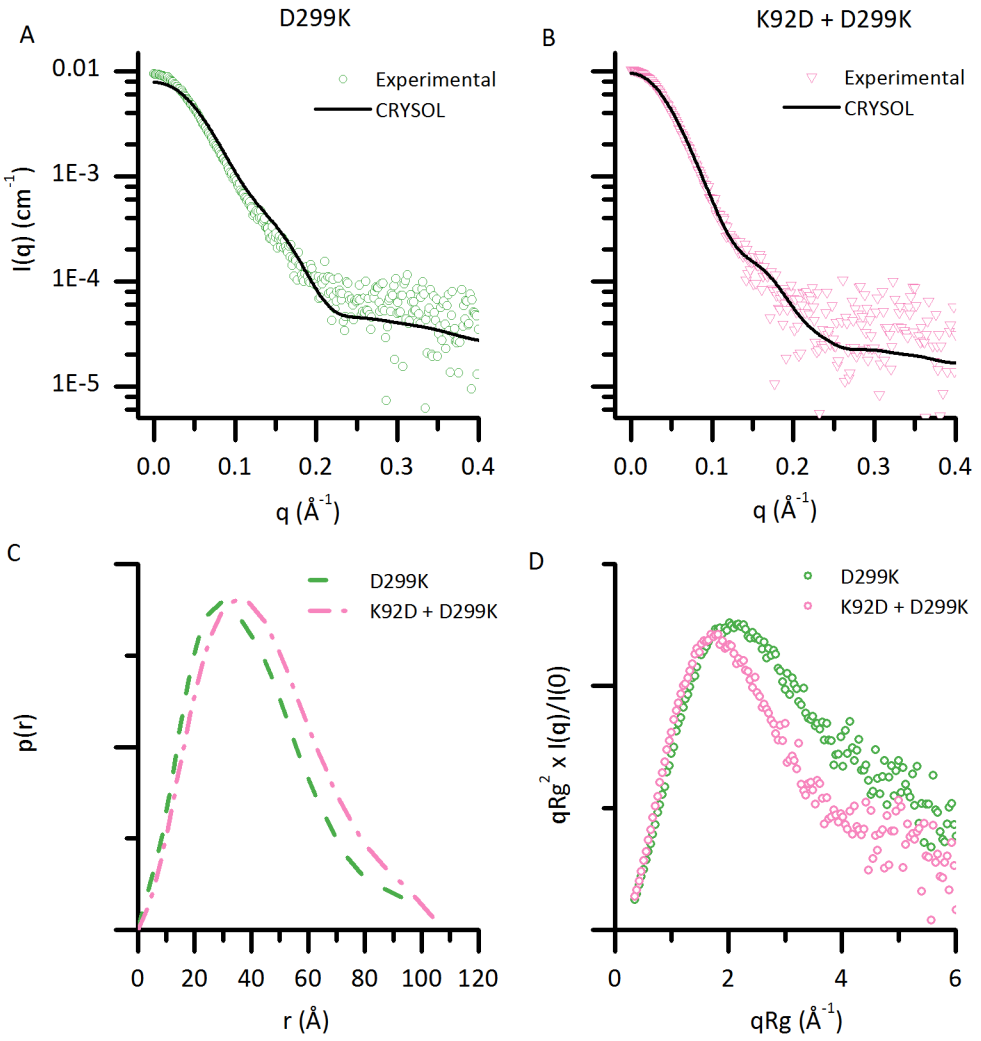

E

Construct	Radius of gyration (Å)	I(0) (cm^{-1})	D_{max} (Å)	Porod volume ($Å^3$)	Molecular weight (kDa)
D299K	31.5	0.1	103	73,473	45.9
K92D + D299K	34.7	0.1	108	122,238	76.8
Monomer (3T15)	23.6	N/A	81	34,120	N/A
Two adjacent 3T15 protomers	29.1	N/A	115	68,200	N/A

Figure 5.5. **SAXS shows differences between monomeric and dimeric oligomers**. A, B) Experimental and theoretical scattering D299K and K92D + D299K. C) Pair distance distribution plot. D) Normalised Kratky plot. E) Calculated table of values. All samples loaded at 168 µM and run in buffer containing 0.5 mM Mg.ADP. CRYSOL was used to generate theoretical scattering profiles.

5.5 Ab initio and rigid body modelling indicates possible solution conformations of monomeric and dimeric tobacco Rubisco activase

In this section I sought to use the existing atomic resolution structure of the α/β domain of the β-isoform from tobacco Rubisco activase as a template to model the entire protein in solution.

In order to determine the position of the missing residues in the existing crystal structure , the program BUNCH was used to model in the missing residues.[140] In a similar manner to CORAL, which was utilised in the previous chapter, BUNCH places loops representing missing residues and calculates the optimal position of the loops to match the experimental scattering. The model indicates that the N-termini on average in solution forms a separate discrete domain and does not interact with the α/β nucleotide binding domain (**Fig. 5.6A**). Previous studies have shown that the N-terminal domain is largely unstructured and does not participate in ATP hydrolysis.[3,109]

To assess the range of possible structures in solution the modelling program EOM was used.[139] In EOM a large pool of random structures which match the provided experimental scattering are produced. High resolution data is used as a template where available, otherwise dummy atoms are added as required. After the large pool of structures has been generated a small subset of these structures are found which, combined, represent the experimental scattering. If all structures generated in the large pool are highly similar then only a small number of structures will be needed to represent the experimental data. Thus EOM allows me to understand the number of possible conformations which may be present in solution. The results showed that four dummy atom arrangements were needed to accurately describe the experimental scatter (**Fig.**

5.6B). When no crystal structure was supplied a pool of ten conformations were found, nine of which showed conformations so highly extended they are not physiologically possible.

Two of the conformations from the rigid body approach have the N-terminus positioned close to the nucleotide-binding domain, a similar location to the BUNCH model. The other two configurations show a much extended N-terminus similar to that seen for the hexameric variants seen in the previous chapter. The C-terminus and loop regions were in similar positions in all arrangements, indicating that their position is not highly variable.

Dimeric Rubisco activase was modelled using *ab initio* and rigid body approaches using GASBOR[138] and CORAL, respectively.[139] GASBOR creates a dummy atom for each residue present in the protein and assembles them so that the theoretical scattering of the assembly matches that of the experimental data.

Rigid body modelling suggests a similar location for the N-terminal domain as has been for the other oligomers, extended away from the central α/β-domain (**Fig. 5.6C**). The *ab initio* bead model showed a much less elongated protein. This is not unexpected as GASBOR is highly unlikely to create a extended single strand of dummy atom residues as this is a highly unlikely conformation in most globular proteins.

In summary the modelling suggest the monomeric tobacco Rubisco activase variant D299K adopts an extended and highly flexible conformation in solution, quite possibly the reason for the difficulties in crystallising it. The C-terminus and loop regions appear to be similarly placed regardless of the oligomer used to model them, consistently being modelled on what would be the internal face of the oligomer. The N-terminal

domain adopts two conformations, one which is much extended and one which is much closer to the nucleotide binding domain. The reason for the extended conformation of the N-terminal domain may be so that the protein can interact with Rubisco more easily.

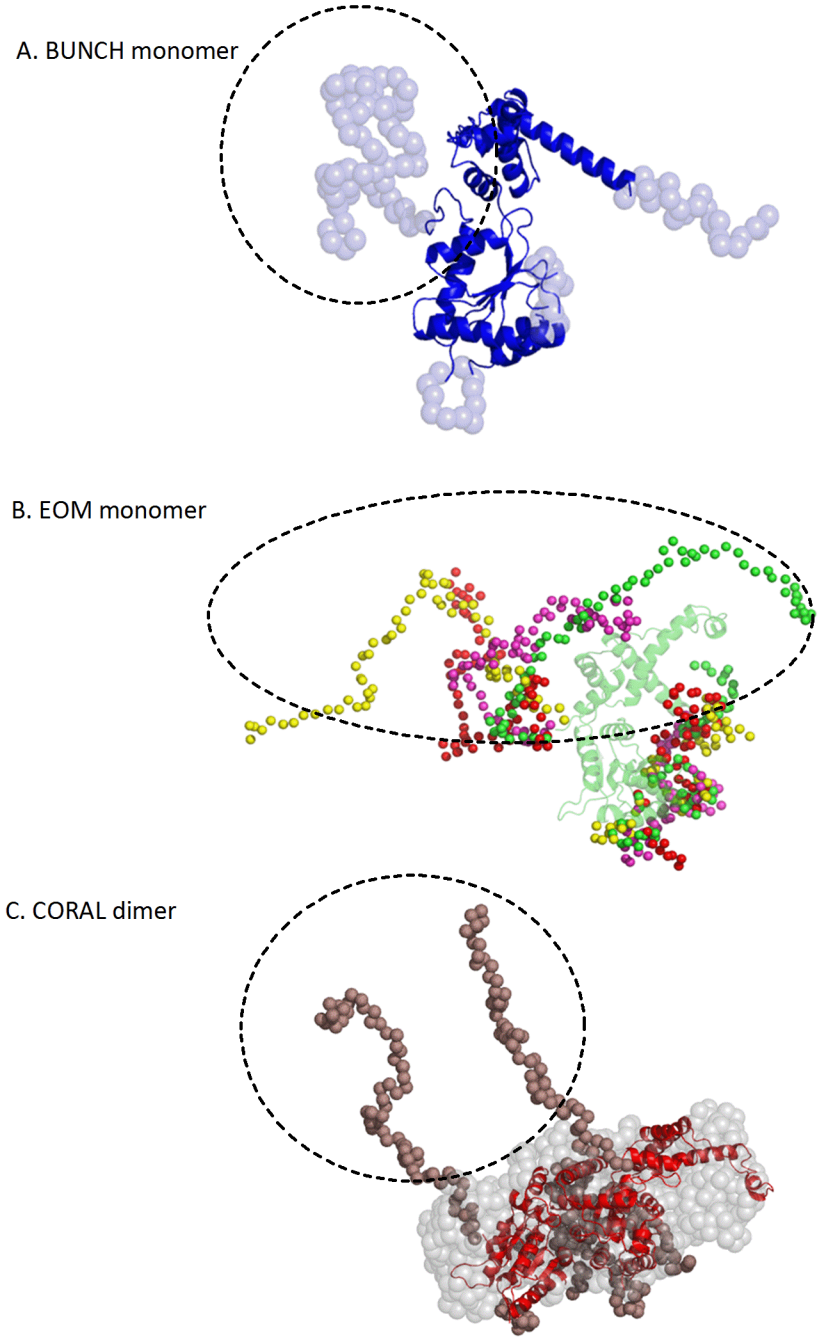

Figure 5.6. **SAXS modelling gives insights into the solution structure of small Rubisco activase oligomers**. A) BUNCH was used to model in the residues missing from the crystal structure (PDB 3T15). B) EOM modelling of missing crystal structure resides showing the four conformations. C) CORAL dummy atoms (brown), and the atomic structure (red) used as a scaffold. GASBOR dummy atom model (grey) of dimeric Rubisco activase. Dotted circles indicate the possible position of the N-terminal domain.

5.6 Nucleotide binding of monomeric and dimer variants

5.6.1 *Small Rubisco activase oligomers can bind nucleotide*

To test whether monomeric Rubisco activase variants are able to still bind nucleotide, though they lack a complete active site, thermal stability assays were carried out. K92D showed an increase of 8 °C from 30 to 38 °C in the presence 500 μM of either Mg.ADP or Mg.ATPγS (**Fig. 5.7A**). D299K showed a 9 °C stability increase with the addition of Mg.ADP, while Mg.ATPγS increased stability from 31 to 39 °C (**Fig. 5.7B**). The double mutant K92D/D299K showed a 9 and 7 °C increase with Mg.ADP and Mg.ATPγS, respectively (**Fig. 5.7C**). The mixture, K92D + D299K, showed a near identical nucleotide response for Mg.ADP and Mg.ATPγS with a 10 °C increase from 30 to 40 °C upon addition of 500 μM nucleotide (**Fig. 5.7D**). These mutants were much less stable than the wild-type enzyme in the absence of nucleotide melting at around 30 °C.

Only K92D showed a difference between the two nucleotides tested, binding Mg.ADP 70% more tightly than Mg.ATPγS (**Fig. 5.7E**). D299K had similar affinities for Mg.ADP and Mg.ATPγS of approximately 50 μM. The double mutant K92D/D299K showed a slightly increased affinity for nucleotide compared with D299K or K92D + D299K. All mutants for either nucleotide, apart from K92D with Mg.ADP, showed binding affinities at least half as strong as the wild-type enzyme which had a binding affinity for either nucleotide of ~20 μM. Thus all variants bind nucleotide independent of whether adjacent protomers, and a full catalytic active site, are present.

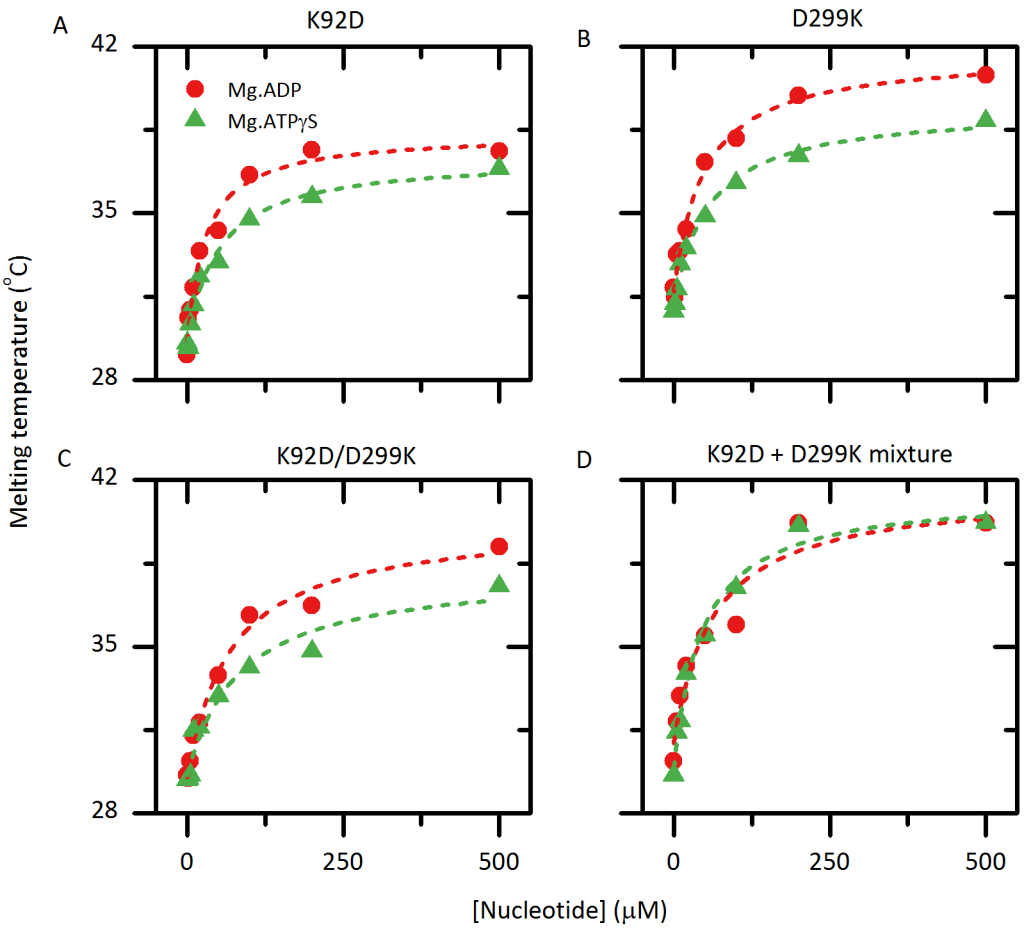

E

Variant	$S_{0.5}$ (μM)	
	Mg.ADP	Mg.ATPγS
K92D	29 ± 5.3	48 ± 12
D299K	48 ± 8.3	55 ± 8.7
K92D/D299K	70 ± 9.7	84 ± 20
K92D + D299K mixture	63 ± 17	45 ± 10

Figure 5.7. **Nucleotide can bind to monomeric and dimeric Rubisco activase**. A-D) 9.6 μM protein with 5 mM $MgCl_2$ and nucleotide at the indicated concentration was subjected to DSF. Hyperbolic functions were fitted to find the $S_{0.5}$.E) Table of nucleotide binding affinities for each variant protein with Mg.ADP and Mg.ATPγS. Errors are standard errors of the mean.

5.6.2 *Dimeric Rubisco activase can hydrolyse ATP*

The K92D + D299K dimer has a full catalytic active site with residues contributed to the active site from the adjacent protomer. Here the ATPase and Rubisco activation activities of the dimeric Rubisco activase oligomer were tested.

ATPase assays were carried out over a range of protein concentrations from 1 – 12 μM with a stoichiometric mixture of K92D and D299K. For this dimeric enzyme the number of active sites is n/2, where n is the number of subunits. For wild type and variant proteins which form larger oligomers the number of possible active sites is n-1, where n is the number of protomers. In these oligomers an additional protomer will add a catalytically competent active site. Both equations assume all subunits are in oligomers.

The activity of 12 μM Rubisco activase dimer was measured and the enzyme found to have a low level of activity (**Fig. 5.8A**). In contrast to all other ATPase assay data presented in this thesis where a sigmoidal response of the specific ATPase activity to protein concentration has been seen, for the K92D + D299K mixture a hyperbola curve was fitted.

This protein concentration (12 μM) was chosen as it was far above the k_d for monomer – dimer association of 3 μM, thus the protein will be predominantly dimeric. The ATP hydrolysis activity was found to be low, so a number of control experiments were carried out to measure the background NADH oxidation and ADP carryover rate. Firstly the assay was run in the absence of Rubisco activase and NADH oxidation was measured, this was repeated in triplicate and the rate then subtracted from the measured rate with Rubisco activase present. The background rate was less than 5% of the ATP hydrolysis rate of Rubisco activase at 12 μM protein (**Fig. 5.8A**).

Previous studies have shown the propensity of Rubisco activase to carry ADP through purification [13], as can be seen with an increased A_{260}/A_{280} ratio. Assays were carried out in the absence of ATP, thus any ADP present in the reactions is from endogenous sources. ADP is a substrate of the first coupling enzyme, pyruvate kinase. This experiment showed that the enzyme did have endogenous ADP, demonstrated by a burst of the NADH oxidation at the beginning of the assay (**Fig. 5.8A**). The ADP appeared to be consumed after around 300 s, thus the measured rate was taken for all further studies from 350 – 400 s. This endogenous ADP is only important because of the low activities measured here, and is insignificant at the rates measured for the wild type and hydrogen bond variant proteins. A further control of monomeric K92D or D299K alone showed no ATPase activity (data not shown).

Measuring the changes in specific activity showed the specific activity decreased as the protein concentration decreased below 3 μM, the concentration where I expect a decrease in prevalence of the dimeric oligomer (**Fig. 5.8B**). The point at which half maximal specific activity was reached was 0.9 μM, lower than expected though this may be caused by the inability to measure many low protein concentration data points due to the lack of absolute activity. The lack of low concentration data points detrimentally affects my ability to fit a function to the data. Rubisco activation by the dimer was undetectable over the range of protein concentrations at which the ATPase assay was measure. Though the dimer is ATPase active, it is essentially a dead enzyme when considered in a biological context with a specific ATPase activity 0.125% of the wild-type enzyme, and thus was not expected to activate Rubisco.

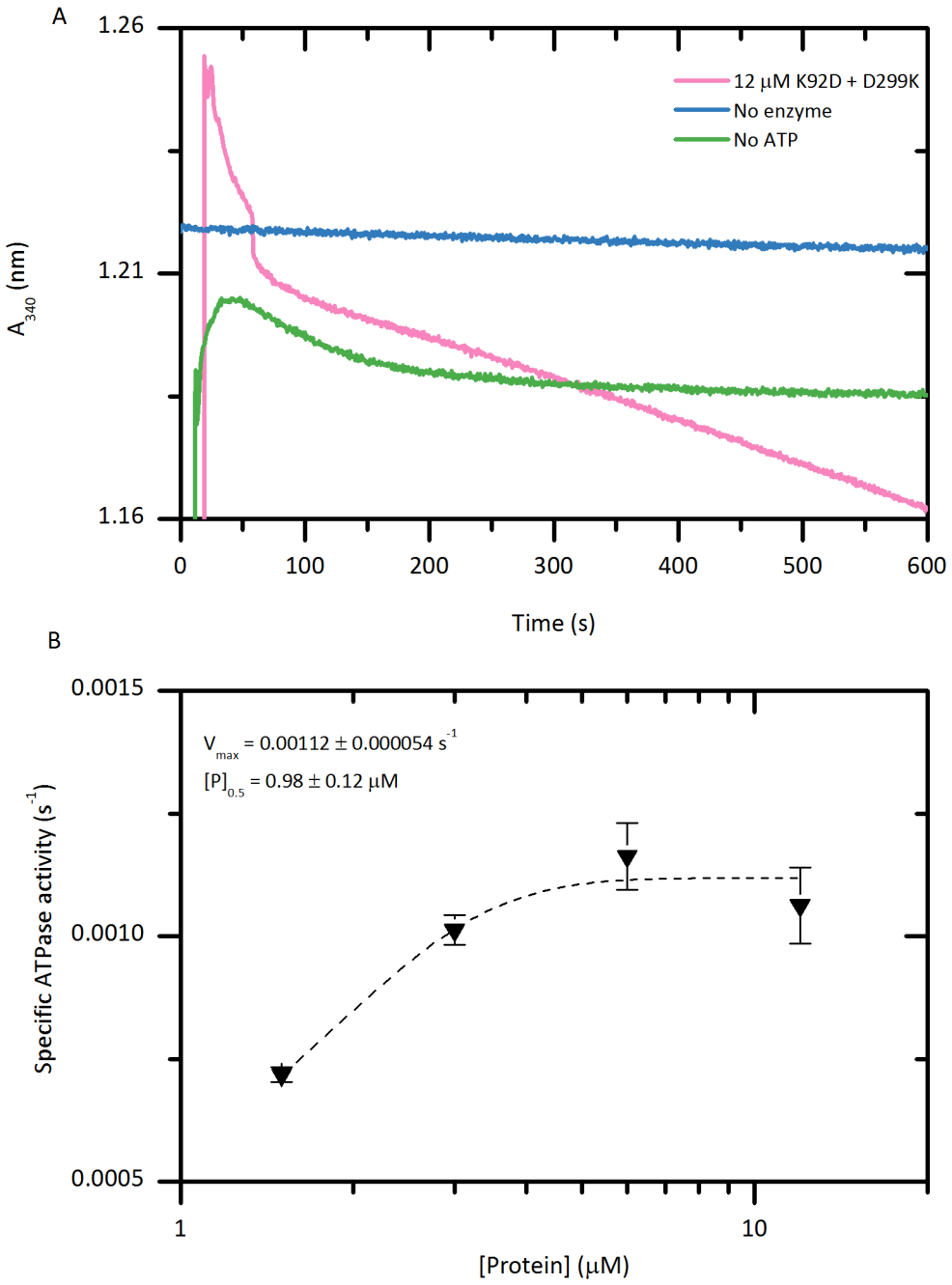

Figure 5.8. **K92D + D299K can hydrolyse ATP**. A) Rate of NADH oxidation, in the presence of Rubisco activase dimer and with control experiments. B) Specific ATPase activity as a function of protein concentration. Errors are standard errors of the mean. A hyperbolic function was fitted to find V_{max} and $[P]_{0.5}$.

5.7 What these variants reveal about wild-type Rubisco activase

5.7.1 *The intersubunit salt bridge destabilises higher order oligomer formation*

I have shown in this chapter that not only does mutation of the interface salt bridge, K92D – D299K, affect the oligomeric state, (**Fig. 5.2**) but also the thermal stability (**Fig. 5.7**). The variant proteins are all monomeric, suggesting that the contribution of the salt bridge to higher oligomer formation is vital for oligomerisation. In the absence of nucleotide the proteins have melting temperatures of approximately ~30 °C (**Fig. 5.7**), versus ~35 °C for the wild-type enzyme.

Mixing stoichiometric amounts of the charge switched variants K92D and D299K caused formation of a stable population of dimeric Rubisco activase (**Fig. 5.3**). I found the association constant of the monomer - dimer equilibrium is in the low micromolar range (**Fig. 5.3B, 5.4**). This dimeric species can bind nucleotide, as demonstrated by an increase in the thermal stability with the addition of either Mg.ADP or Mg.ATPγS (**Fig. 5.7D**). That the protein is ATPase active suggests that the dimer is the minimal catalytically active oligomer; however, with such a low ATPase rate it will be unable to effectively reactivate Rubisco. It should be emphasised that the maximal specific activity is only 0.125% of wild-type.

These variant proteins suggest an order for the binding and hydrolysis of ATP in the wild-type tobacco enzyme. When ATP binds to a catalytically active oligomer, the enzyme undergoes a conformational change prior to hydrolysis. I can trap this prehydrolysis step using the non-hydrolysable substrate analogue ATPγS, as evidenced by a prolonged increase in the intrinsic fluorescence. Hydrolysis then occurs, and with ADP now bound the Rossman fold reverts back into the low intrinsic fluorescence state.

5.7.2 *The solution structure of small Rubisco activase oligomers*

SAXS has been widely used in this chapter to provide theoretical solution structures of monomeric and dimeric Rubisco activase oligomers. By using the ensemble optimisation method, and *ab initio* and rigid body modelling I have been able to generate a range of models to help understand how Rubisco activase behaves *in situ*.

I found that the monomer was highly flexible in solution and this flexibility probably came from the large unstructured N-terminal domain and the two subdomains from the AAA+ domain moving relative to each other (**Fig. 5.5D, 5.6A, B**). Modelling of the dimeric enzyme showed similar results with a very flexible N-terminal domain (**Fig. 5.6C**). I propose that the extended N-terminal domain is mostly unstructured; however, upon contact with the target Rubisco it becomes more structured.

Chapter Six: **Characterisation of the α- and β- isoforms of Rubisco activase**

6.1 Introduction

The α- and β- isoforms of cotton Rubisco activase are produced by different genes, not by alternate splicing as is the case for many other Rubisco activase isoforms and they are present in equal amount in plants.[12] The α-isoform has a C-terminal domain which is extended by 39 residues and contains two cysteines. When oxidised these cysteines form a disulfide bond and possibly contribute to the increased stability of the α-isoform relative to the β-isoform.[12]

Cotton Rubisco activase, like plant species, has an increased thermal stability upon the addition of nucleotide.[2] Incubation of the β-isoform with either ADP or ATP has been reported to increase the aggregation of the protein.[2] Both isoforms have similar nucleotide binding affinities and levels of thermal stability.[12] A twofold greater ATPase rate was found for the α-isoform over the β-isoform.[12]

Previous studies of Rubisco activase have predominantly focused on the β-isoform in isolation or a mixture of both α- and β- isoforms. In chapter six I will compare the oligomeric state, activity, and thermal stability of the cotton Rubisco activase α- and β-isoforms separately then combined at relevant *in planta* stoichiometries. A recent study by the Pearce lab presented the first biophysical study of an isolated α-isoform Rubisco activase from spinach.[110] This study represents the second such study on the isolated α-isoform from cotton.

6.2 Changes in oligomeric state between isoforms and a 1:1 mixture

6.2.1 *The α-isoform forms larger oligomeric species than the β isoform*

Previously in this thesis I have presented data illustrating that protein concentration is a major force driving the change in oligomeric state. Here I sought to test whether the results for tobacco Rubisco activase, namely that increases in protein concentration increased the oligomeric state, would hold true for the cotton isoforms.

It was found the β-isoform of cotton Rubisco activase formed small oligomers over a wide range of protein concentrations increasing from an integrated $S_{20,w}$ of 3.4 at 0.6 μM to ~5.8 $S_{20,w}$ at a protein concentration of 9.6 μM (**Fig. 6.1**). The addition of Mg.ATPγS caused no change in the oligomeric state of the β-isoform (**Fig. 6.2**). The α-isoform formed much larger species with an increase in $S_{20,w}$ from ~5 to ~12 $S_{20,w}$ over a similar range of protein concentrations. The addition of Mg.ATPγS caused a small decrease in oligomeric state; however, a wide distribution of species was still seen at all protein concentrations. I found no stable hexamer oligomer, as was recently reported for the Rubisco activase α-isoform from spinach.[110]

Mixing of the two isoforms at a 1:1 ratio produced species at an intermediate size between the isoforms individually. Over a similar range of concentrations to the other isoforms the $S_{20,w}$ increased from ~4.5 to ~7. No change in oligomeric state was seen with the addition of either ADP or ATPγS. Previously in this thesis I have shown that tobacco Rubisco activase β-isoform showed an increase in the $S_{20,w}$ from 4.6 to 11.5 over a similar range of protein concentrations discussed here.[147] Nucleotide had no effect on the oligomeric state. Thus it appears that the β-isoform from cotton is much smaller than the tobacco enzyme, which is similarly sized to the cotton α-isoform.

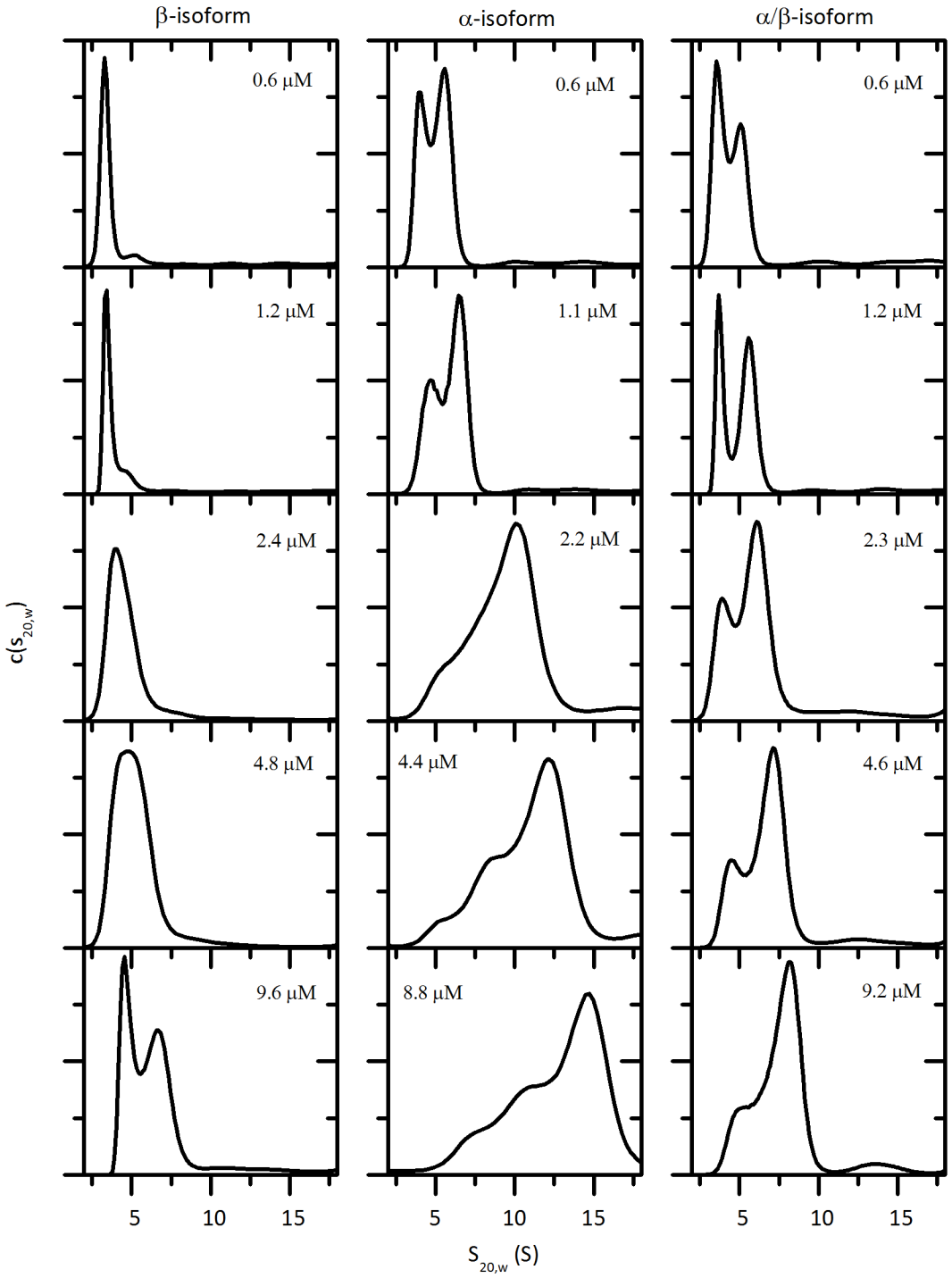

Figure 6.1. **Protein concentration drives changes in the oligomeric state of cotton Rubisco activase**. Cotton isoforms separately and a 1:1 mixture were loaded at the indicated protein concentration. Magnesium was included at 5 mM for all samples.

6.3 Oligomeric state correlates with ATPase activity

In chapter three I found that tobacco Rubisco activase, which produces only the β-isoform, had ATPase and Rubisco activation activities with oligomers comprising two to four protomers. Here I sought to understand whether the same minimal oligomer for the cotton α-, β- and α/β- isoforms was active.

6.3.1 *Small cotton Rubisco activase oligomers have ATPase activity*

ATPase assays showed that the α-isoform had a 40% greater specific activity than the β-isoform (**Fig. 6.2A**). Mixing the isoforms at a 1:1 ratio decreased the V_{max} to 0.13 s^{-1}, less than either isoform alone (**Fig. 6.2B**). However, the [$P_{0.5}$], at 1.43 μM, was approximately in the middle of the two isoforms separately (**Fig. 6.2B**). These values are in good agreement with a previous study which showed that the cotton α-isoform was more active than the β-isoform.[12]

Using average molecular weights from SAXS data I can relate oligomeric state to the specific ATPase activity. The β-isoform reaches half its maximal specific activity at 2.3 μM, at this protein concentration the average molecular weight is ~80 kDa (**Fig. 6.2A**). The average molecular weight at the [$P_{0.5}$] of 0.9 μM for the long isoform was below the measured range. However, it could be extrapolated from the other data points that the molecular weight would be in the range of 80 to 100 kDa. The same is true for the α/β mixture, where data was not collected at sufficiently low concentrations with SAXS, again extrapolation suggests the average molecular weight would be equivalent to a dimer at the [$P_{0.5}$]. Combined, these results suggest, as was the case for tobacco, that the

α, β, and the α/β mixture all have a similar minimal active oligomeric state of two to four subunits.

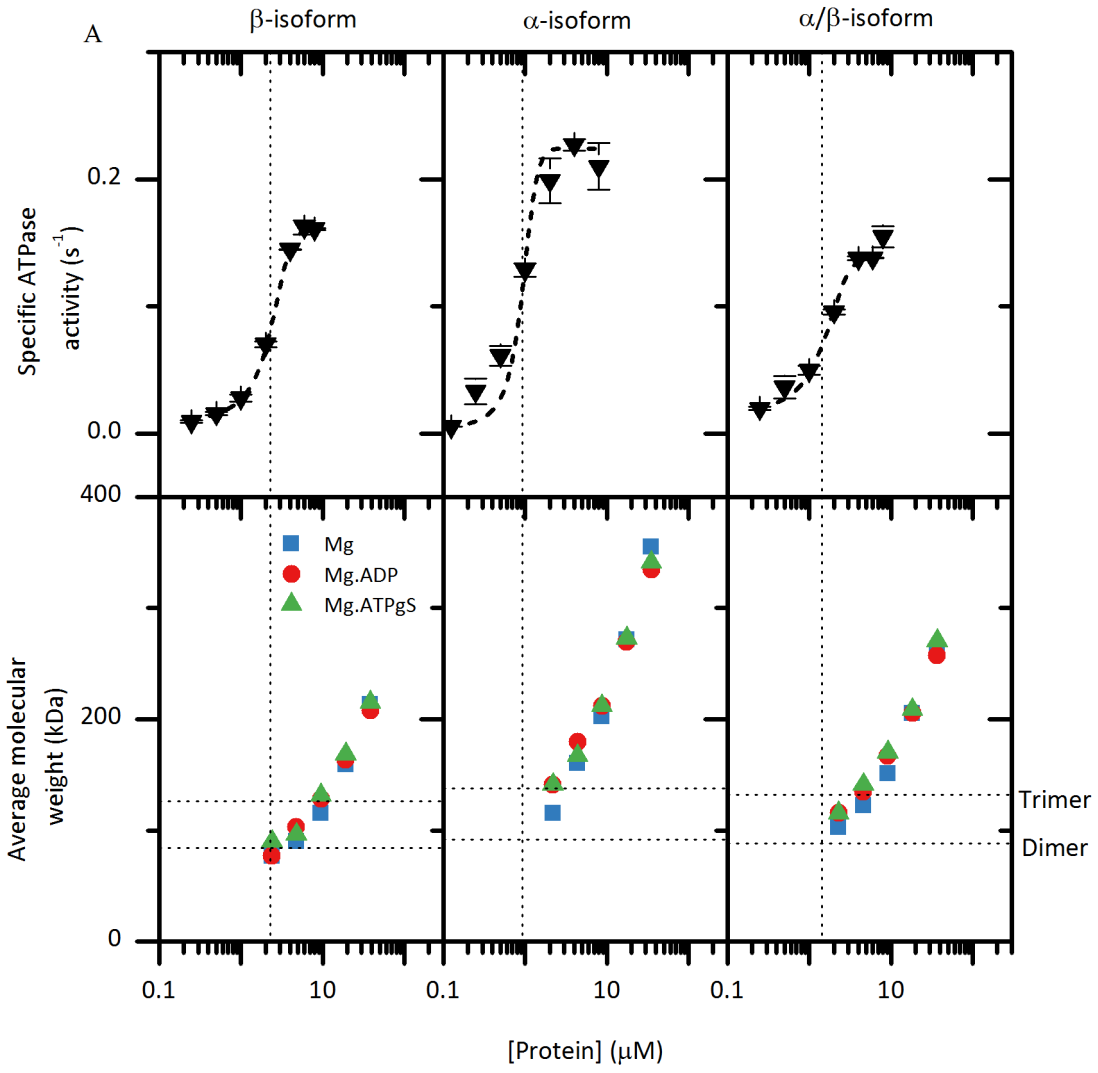

B

Isoform	V_{max} (s^{-1})	$[P_{0.5}]$ (μM)
β	0.16 ± 0.009	2.3 ± 0.04
α	0.22 ± 0.01	0.92 ± 0.06
α/β	0.13 ± 0.0005	1.43 ± 0.04

Figure 6.2. **Small oligomers of spinach Rubisco activase have ATPase activity**. A) ATPase assays and Molecular weights from SAXS data recorded at a range of protein concentrations. The magnesium concentration was 5 mM and nucleotide concentration was 0.2 mM. B) Kinetic parameters were found by fitting a sigmoidal function. Errors are standard errors from replicate experiments.

6.4 Nucleotide binding

To assess nucleotide affinity of the different isoforms DSF assays were carried out with varying nucleotide concentrations at a single protein concentration.

6.4.1 *The α-isoform binds nucleotide twice as tightly as the β-isoform*

Nucleotide titrations were carried out in the presence of either Mg.ADP or Mg.ATPγS (**Fig. 6.3A**). Addition of 0.2 mM Mg.ADP caused an increase in the thermal stability of 10 °C, Mg.ATPγS at the same concentration caused a 12 °C increase for either isoform in isolation (**Fig. 6.3B**). When the isoforms were mixed addition of 0.2 mM Mg.ADP or Mg.ATPγS caused an increase of 9 °C.

The α-isoform, which forms larger oligomers than the β-isoform, was ~3 °C more stable that the β-isoform in the absence of nucleotide (**Fig. 6.3A**). This is in good agreement with the tobacco Rubisco activase which showed larger oligomers were more thermally stable. The mixture which formed oligomers of an intermediate size between the α- and β-isoforms in the absence of nucleotide was ~1.5 °C more stable than the β-isoform.

I found no difference in the binding affinity of ADP or ATPγS with either of the isoforms or the mixture (**Fig. 6.3B**). The α-isoform bound either nucleotide with an affinity of ~20 μM, while the β-isoform bound with an affinity of ~50 μM. The large difference in binding is presumably caused by the highly extended C-terminus which increases the affinity for nucleotide. The biologically relevant mixture, a 1:1 mixture of each isoform, bound with an intermediate affinity of ~30 μM. Thus it appears the inclusion of the β-isoform reduces nucleotide binding affinity.

A

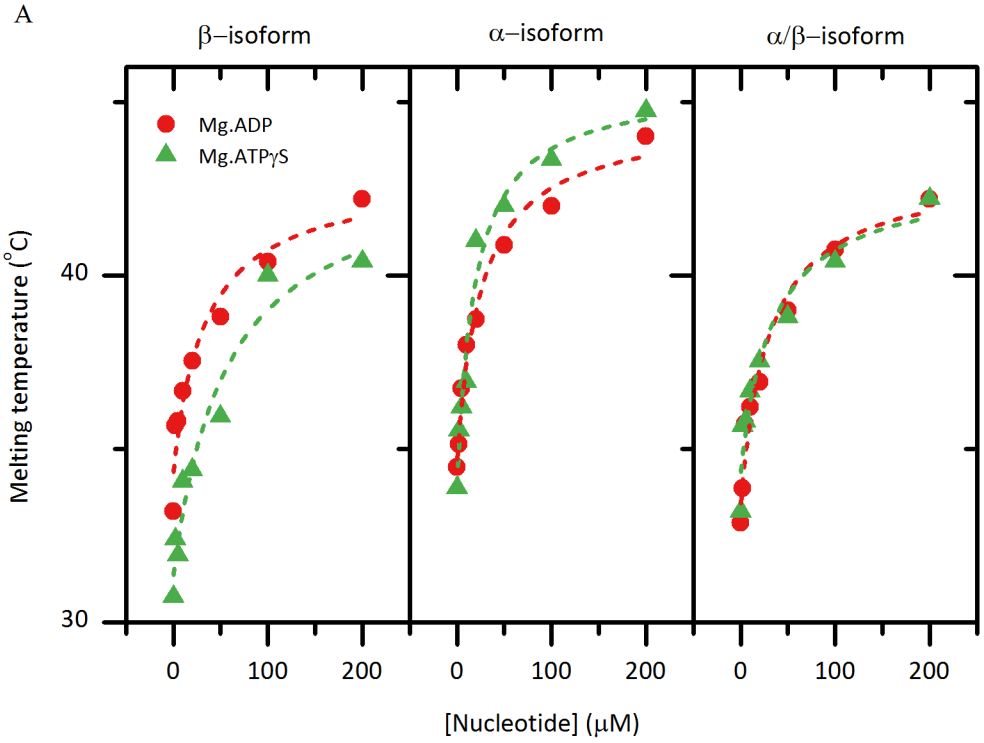

B

Isoform	Nucleotide	ΔT_{max} (s^{-1})	$S_{0.5}$ (μM)
β	ADP	10.0 ± 0.73	46.3 ± 12
	ATPγS	12.0 ± 1.4	56.7 ± 21
α	ADP	9.85 ± 0.4	26.2 ± 4.4
	ATPγS	11.5 ± 0.4	19.4 ± 3.1
α/β	ADP	9.09 ± 0.4	30.4 ± 5.4
	ATPγS	8.57 ± 0.6	33.8 ± 8.7

Figure 6.3. **Small differences exist between the isoforms and their nucleotide affinity**. A) DSF was used to measure the change in thermal stability as a function of ADP and ATPγS concentration in the presence of 5 mM $MgCl_2$. Hyperbolic functions have been fitted to measure the $S_{0.5}$ for ADP and ATPγS. B) Table of DSF parameters. Errors are the standard error. Protein was loaded at 9.6 μM.

6.5 Comparison of Rubisco activase from different species

6.5.1 *The cotton α-isoform and tobacco β-isoform have many similarities*

In this chapter I have presented the first biophysical data on the cotton Rubisco activase α-isoform in isolation. I found many similarities between this isoform and the β-isoform from tobacco with regards to the oligomeric state, activity, and nucleotide affinity.

I have shown that they form similarly sized oligomers which increase in size as the protein concentration is increased, and that this increase in oligomeric state correlates with an increase in specific activity. A similar increase in thermal stability with the addition of nucleotide is seen for both proteins. Both enzymes also have similar Mg.ADP and Mg.ATPγS affinities of ~20 μM, and show little discrimination between the two nucleotides. A study comparing the α- and β-isoforms form arabidopsis found that the affinity for ADP was the same for both isoforms, even when the α-isoform was reduced. The β- and reduced α-isoform had similar ATPγS affinities; however, the oxidised α-isoform bound ATPγS with half the affinity.[113] It may be that no change in the nucleotide binding parameters will be seen for the cotton enzyme when carried out on the reduced enzyme, though this experiment should be carried out in future.

The additional C-terminal residues present in the α-isoform have been shown to change the relative affinity of the α-isoform for ADP and ATP, with truncation increasing the rate of ATP hydrolysis.[92,93,170,171] An arabidopsis α-isoform variant lacking the C-terminus showed no inhibition of ATP hydrolysis by ADP.[95,171] Transgenic plants lacking the α-isoform showed unchanged activity; however, these plants were unable to regulate Rubisco activase activity in response to changes in the cellular redox state.[172] When the cysteines in the C-terminal domain are oxidised ADP binds preferentially; however, upon

reduction of the cysteines ATP and ADP bind equally, effectively causing an increase in activity.[92]

This allows Rubisco activase to sense changes in the cellular redox state in response to the light/dark cycle.[92] To reduce the cysteines both a reducing agent and thioredoxin F are required, neither of which have been used in this thesis.[92,113] By not reducing the α-isoform it may be that I am not accurately representing the most active state. To accurately measure changes in oligomeric state it would be best to characterise the α-isoform under both reducing and non-reducing conditions to replicate changes in the physiological environment.

6.5.2 *Cotton and tobacco Rubisco activase use the same mechanism to activate Rubisco*

Previously in this thesis I have presented evidence that the β-isoform of tobacco Rubisco activase requires only two to four subunits for activity. For both the cotton isoforms and the mixture I have found that oligomers with between two and four subunits are able hydrolyse ATP (**Fig. 6.2A**). An oligomerisation pathway for the β-isoform from cotton has previously been proposed with dimer, tetramer, closed hexamer and then four stacked hexamers.[106] The SAXS and AUC data both suggest that no discrete species are formed as part of the oligomerisation pathway under the conditions presented here. This suggests a mechanism of interaction where, contrary to other AAA+ proteins, small non-hexameric oligomers are able to effectively interact with Rubisco and power removal of active site inhibitors. It appears that mixing the two isoforms at a physiological ratio produces oligomers which have the oligomeric state, ATPase activity and nucleotide binding properties between the individual isoforms.

6.5.3 *Differences between spinach and cotton Rubisco activase*

The data collected on the two cotton Rubisco activase isoforms suggested that they behaved in a similar manner to the β-isoform of the tobacco enzyme. A recent study from the Pearce lab suggests a second oligomerisation pathway is present in spinach.[110]

Keown and Pearce (2014) showed that the α-isoform of spinach Rubisco activase was able to form stable ring conformations, similar to those seen for the tobacco R294 variant proteins.[110] The spinach α-isoform in isolation was able to form thermally stable hexamers in the presence of Mg.ATPγS and it maintained ATPase and Rubisco activation activities at low protein concentration. The β-isoform was unable to form hexamers and behaved similarly to the tobacco and cotton β-isoforms.

A mixture of the α-and β- isoforms was also able to form stable hexamers, suggesting that the α-isoform was able to act as a scaffold for the stable oligomer formation. This suggests under physiological conditions that Rubisco activase is likely to be hexameric in spinach. It was suggested that the ability of the spinach α-isoform to form hexamers was due to the C-terminal extension; however, cotton which has a similar extension is unable to form stable hexameric oligomers. Currently the reason spinach but not cotton can form these oligomers is unknown.

Chapter Seven: **Discussion**

The reactivation of Rubisco by Rubisco activase in higher plants is required for photosynthesis to continue when the active site of Rubisco becomes inhibited. Previous studies have shown that Rubisco activase has a low thermal stability[2]; this low stability is thought to be a limit on photosynthesis at temperatures above 30°C.[44] As climate change intensifies it is thought that the ability of Rubisco activase to maintain the activity of Rubisco may diminish as temperatures increase.

In this thesis I have characterised the activity, stability and oligomeric state of tobacco Rubisco activase β-isoform, and the Rubisco activase α- and β- isoforms from cotton. A range of physiological conditions were trialed and found to have a small affect on the oligomeric state; however, changes in protein concentration caused large changes in the molecular weight.

Currently in the literature there exist two theories about the active oligomeric state of Rubisco. Some studies suggest that the active state is a hexameric ring oligomer similar to that which is found for many other AAA+ proteins.[3,43] The other theory, and that which is supported by the data presented in this thesis, suggests that small oligomers are able to be the active oligomeric complex.[147] Mutation of Arg 294 allowed the formation of closed hexamers, suggesting a possible role for this closed species in Rubisco activation. Wild type and variant protein constructs suggested small oligomers were all that was necessary for activity.

In this section I will compare the results for tobacco and cotton Rubisco activase enzymes with other studies carried out on Rubisco activase from spinach and Antarctic

hairgrass (*Deschampsia antarctica*). Possible mechanisms of interactions between Rubisco and its chaperone will then be discussed, and finally the implication mutation of Rubisco activase may have on crop yields in changing climate conditions.

7.1 The species dependent oligomeric state of Rubisco activase

A number of studies have investigated the biological arrangement of Rubisco activase; however, these studies have utilised Rubisco activase from a small number of species. The most common species studied is tobacco[3,5,11,13], followed by the β-isoform from spinach[11], with a small number of more recent studies using the cotton[2] and arabidopsis β-isoforms.[105]

For future studies it will be important to consider the diversity of plant species surveyed as currently there have been biophysical studies on a small number of Rubisco activase species (**Fig. 7.1**). The two well characterised enzymes, tobacco and spinach β-isoforms, appear very close together on a phylogenetic analysis of all plants which have sequenced genomes. It will also be important to further understand how the α-isoform affects biological activity.

To begin addressing this gap in the literature the Pearce lab has investigated the oligomeric state of a Rubisco activase α- and β- isoforms from a range of plant species and a green alga. In this section I will discuss work carried out in the Pearce lab, investigating whether the stable hexameric species found for the α-isoform of spinach Rubisco activase[110] and the tobacco R294 variant proteins[13] are found in other species of Rubisco activase.

.

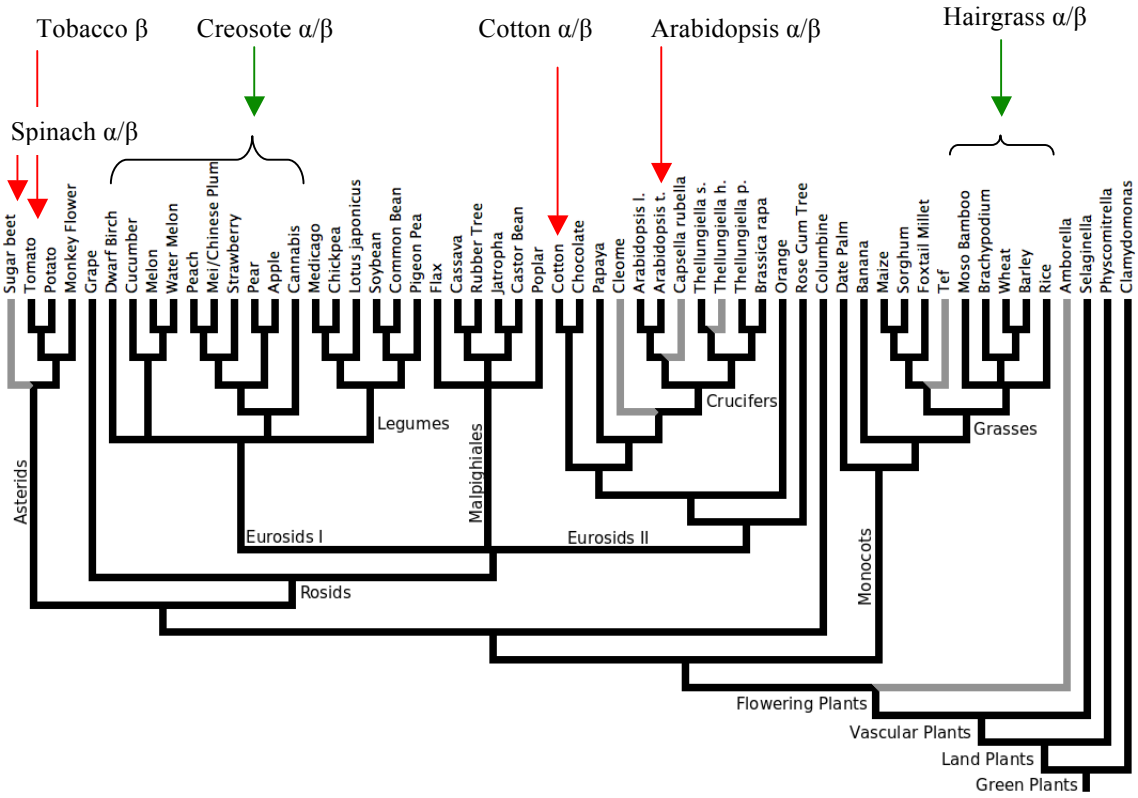

Figure 7.1. **A phylogenetic tree showing all full plant genomes which have been sequenced**. The phylogenetic tree shows plants which have complete genomes available. Indicated in red are species or related species which have been studied with biophysical techniques in the literature and our lab. Species indicated in green have only been studied in our lab. No α-isoforms from any species have been studied biophysically outside of our lab. Image from Genome Evolution (2012).

The Rubisco activase β-isoform from spinach follows a similar oligomerisation pathway to other Rubisco activase β-isoforms from tobacco or cotton presented in this thesis, forming a range of oligomers which increase in size with increasing protein concentration and are insensitive to the addition of nucleotide (**Fig. 7.2a**). The α-isoform; however, forms stable hexameric species upon the addition of Mg.ATPγS (**Fig. 7.2b**). These hexamers are similarly stable to R294A/V in the presence of Mg.ATPγS. Additionally the addition of Mg.ADP causes a large increase in the oligomeric state. This nucleotide sensitivity is similar to that seen for the R294V variant discussed in Chapter four of this thesis.

The spinach isoforms *in planta* are found in equimolar amounts.[173] By mixing stoichiometric quantities of the isoforms it was shown that a stable hexameric species was present, however as the protein concentration decreased the hexameric species was lost (**Fig. 7.1c**). It appears at least in spinach the hexameric form is physiologically relevant. I propose in species containing both isoforms the α-isoform is able to act as a scaffold promoting hexameric oligomer formation. The hexameric species show a similar level of thermal stability to the highly thermally stable arginine variants of the tobacco enzyme.

Preliminary data from the creosote and arabidopsis α- and β- isoforms suggest that both are insensitive to the nucleotide conditions, with no change in the apparent molecular weight (F. G. Pearce, personal communication). Protein concentration is again the main driver of oligomeric state change.

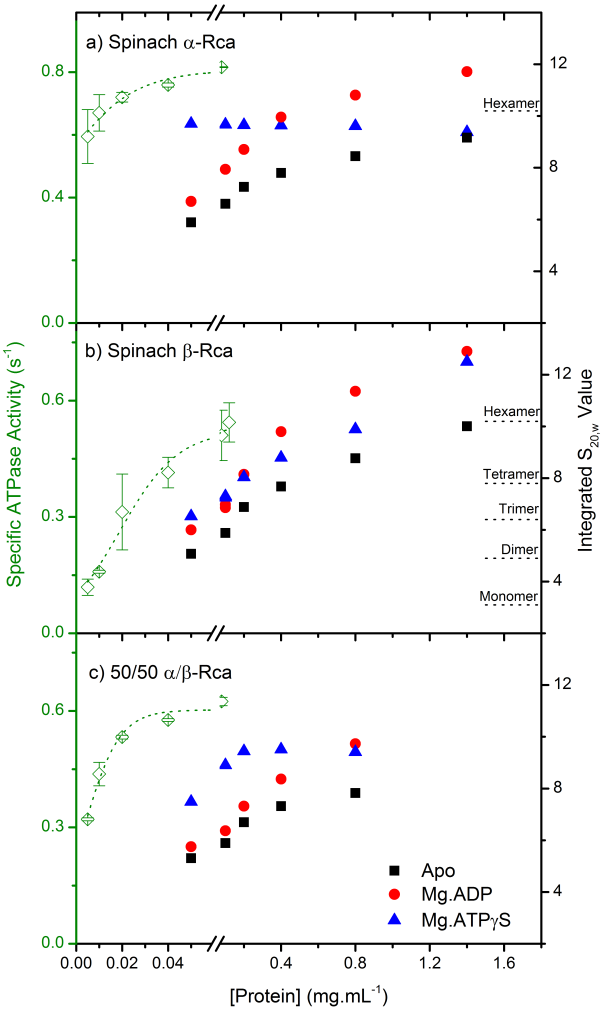

Figure 7.2 **The spinach Rubisco activase α-isoform forms stable hexameric species**. ATPase activity of the α-, β-, and a 50/50 mixture of the two isoforms was measured (green diamonds). The oligomeric state was measured using sedimentation velocity AUC in the presence of no additive (black squares), 0.2 mM Mg.ADP (red circles), or 0.2 mM Mg.ATPγS (blue triangles). Adapted from Keown and Pearce (2014).[110]

Preliminary studies investigating the oligomeric state of the Antarctic hair grass Rubisco activase isoforms using AUC suggests a range of species are present whose size is not dependent on protein concentration (**Fig. 7.3**). Initial studies suggest that over the concentration range measured there are a number of stable intermediate species and that the addition of Mg.ATPγS does not trigger stable hexamer formation. As mentioned previously, due to the polydispersity of the system, I was unable to assign molecular weights or oligomeric species to these peaks.

This is currently the only example of a Rubisco activase enzyme from monocotyledon plants which has been studied using biophysical methods. Currently I do not know whether this result is indicative of the plant grouping or not.

Future experiments plan to survey a wide range of genes annotated as Rubisco activase. High throughput screening using the DSF assay, AUC and ATPase assays should allow the development of a better understanding of changes in Rubisco activase protein structure across a range of plant and algal families. The data may hopefully be used to understand the evolutionary background of the Rubisco activase protein.

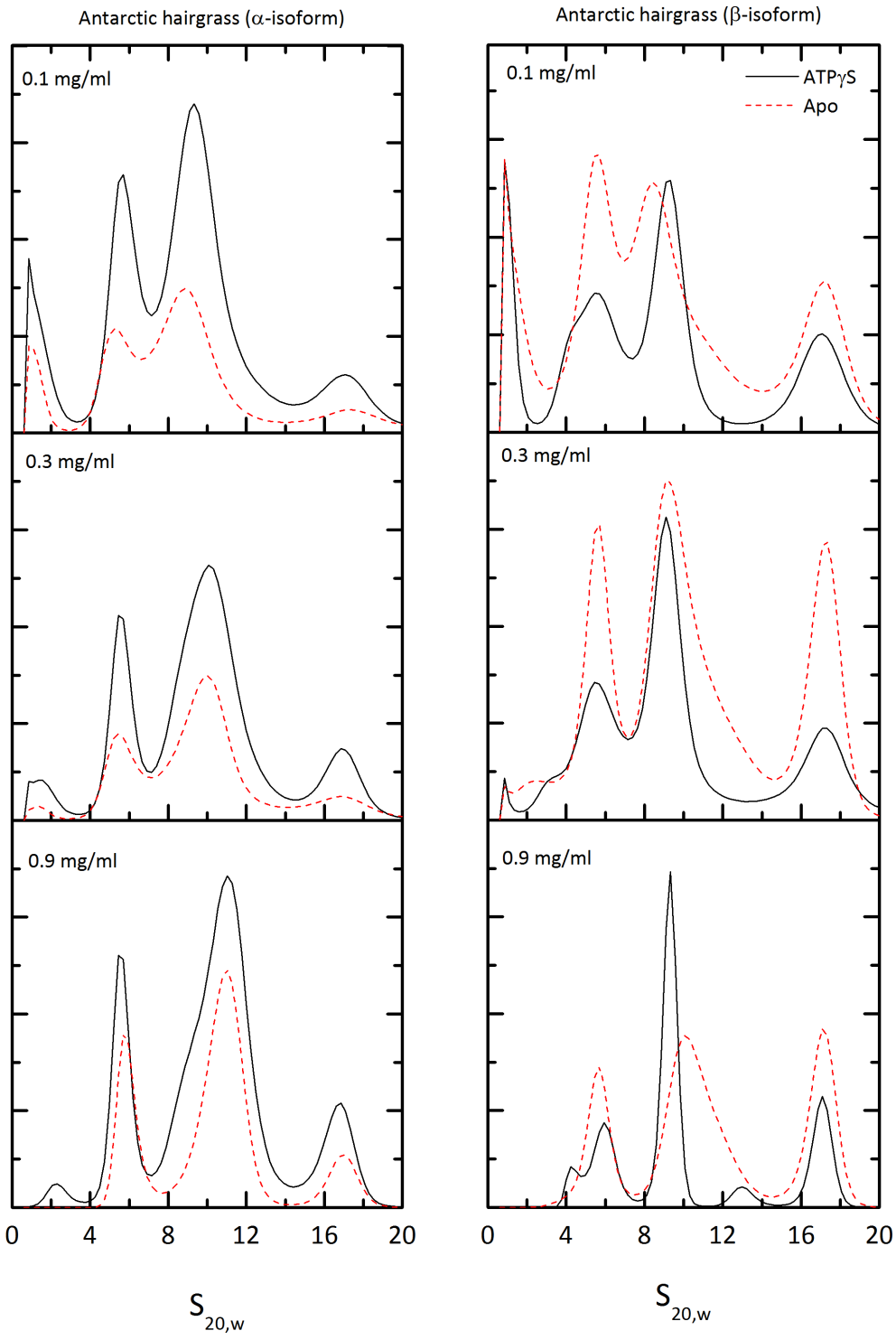

Figure 7.3. **Antarctic hair grass does not change oligomeric state changes in response to protein concentration**. The α- and β- isoforms of Rubisco activase from Antarctic hairgrass were analysed using AUC in the presence (red dashes) and absence (black line) of 0.2 mM Mg.ATPγS. F. G. Pearce, personal communication.

7.2 The interaction between Rubisco activase and Rubisco

Rubisco activase is a member of the AAA+ protein family whose active oligomeric state is most commonly a closed hexameric ring.[59] The mechanism of action for these proteins commonly involves the binding of a flexible termini to a target protein followed by hydrolysis of ATP. The energy released by this hydrolysis is used to power the movement of one subunit relative to the adjacent subunit unravelling the termini. These ring assemblies pull the termini through the central pore of the oligomer allowing constant contact with the termini and enabling efficient protein unfolding.

It is thought the reactivation of Rubisco by Rubisco activase proceeds via the same general mechanism; however, currently molecular detail is lacking. The inhibited active site of Rubisco is covered by N-terminal loop 6 of the large subunit of Rubisco[174], this must be relocated prior to inhibitor release. In red algal Rubisco it has been demonstrated that the CbbX hexamer is capable of binding and unravelling the N-terminal domain reactivating the Rubisco.[43] It may be that green type Rubisco activase may reactivate Rubisco by a similar mechanism.

Tobacco Rubisco activase has been shown to form a continuous range of oligomeric species in solution with no discrete species being seen. Mutational studies have shown that the residues required for interaction with Rubisco are located on the outside of the oligomer.[113] The location of these residues appears to suggest the Rubisco activase may interact side on with Rubisco. However, mutation of residues in the central pore drastically reduces or stops Rubisco activation.[3] This suggests that the site of interaction and recognition with Rubisco is structurally separate from the site of activation. The absence of detectable ring oligomers for tobacco and cotton Rubisco

activase suggests that either these ring assemblies are highly transient or a closed oligomer is not required in these plant species for reactivation.

A key finding of this thesis was the discovery of a highly thermally stable hexameric variant tobacco Rubisco activase. The R294A/V variant tobacco proteins and the α-isoform of spinach Rubisco activase are both able to form a stable hexameric species in the presence of Mg.ATPγS. It has been suggested that the R294A/V mutation and extended C-terminal domain of the spinach α-isoform acts to stabilise the hexameric conformation.[110] Modelling of the C-terminal domain from the spinach isoform suggests the C domain will localise at the interface between two subunits. The mechanistic detail of how this may proceed will require an ATP/ATPγS bound crystal structure and a crystal structure of a Rubisco activase α-isoform.

7.3 Increased thermal stability of Rubisco activase as a method for increasing global photosynthetic capacity

It is widely accepted that climate change is occurring at a increasingly rapid pace and that the yield of crop plants, particularly grain plants, will be reduced in the coming decades.[45,175,176] It has been shown that Rubisco activase activity is the rate limiting component of photosynthesis at temperatures above 30°C.[44] I have shown that mutation of an interface arginine reside can promote the formation of thermally stable hexameric oligomers, and it appears that similar hexamers are present *in situ* within spinach. An increased understanding of how the oligomeric state changes affect thermal stability of Rubisco activase may suggest was to improve carbon fixation. Genetic engineering of a highly stable Rubisco activase, such as the hexameric R294 variants in tobacco or the α-

isoform from spinach, may maintain Rubisco activity when it would otherwise be inactivated. These plants would be able to maintain photosynthetic activity to higher temperatures and may even have an increased yield in the presence of higher atmospheric CO_2 concentrations.

Thermally stable hexameric Rubisco activase may represent a new way in which plants can be given resistance against warmer temperatures, and may produce opportunities for increased plant growth under higher temperatures or climate change conditions.

References

1 Pearce, F. G. & Andrews, T. J. The relationship between side reactions and slow inhibition of ribulose-bisphosphate carboxylase revealed by a loop 6 mutant of the tobacco enzyme. *Journal of Biological Chemistry* **278**, 32526-32536 (2003).

2 Henderson, J. N., Hazra, S., Dunkle, A. M., Salvucci, M. E. & Wachter, R. M. Biophysical characterization of higher plant Rubisco activase. *Biochimica Et Biophysica Acta-Proteins and Proteomics* **1834**, 87-97 (2013).

3 Stotz, M., Mueller-Cajar, O., Ciniawsky, S., Wendler, P., Hartl, F. U., Bracher, A. & Hayer-Hartl, M. Structure of green-type Rubisco activase from tobacco. *Nature Structural & Molecular Biology* **18**, 1366-U1378 (2011).

4 Henderson, J. N., Kuriata, A. M., Fromme, R., Salvucci, M. E. & Wachter, R. M. Atomic resolution X-ray structure of the substrate recognition domain of higher plant Ribulose-bisphosphate Carboxylase/Oxygenase (Rubisco) activase. *Journal of Biological Chemistry* **286**, 35683-35688 (2011).

5 Wang, Z. Y., Ramage, R. T. & Portis, A. R. Mg^{2+} and ATP or adenosine 5'-gamma-thio-triphosphate (ATP-gamma-S) enhances intrinsic fluorescence and induces aggregation which increases the activity of spinach Rubisco activase. *Biochimica Et Biophysica Acta* **1202**, 47-55 (1993).

6 Somerville, C. R., Portis, A. R. & Ogren, W. L. A mutant of arabidopsis-thaliana which lacks activation of RUBP carboxylase invivo. *Plant Physiology* **70**, 381-387 (1982).

7 Portis, A. R. & Salvucci, M. E. The discovery of Rubisco activase - yet another story of serendipity. *Photosynthesis Research* **73**, 257-264 (2002).

8 Salvucci, M. E., Portis, A. R. & Ogren, W. L. A soluable chloroplast protein catalyzes Ribulose bisphosphate carboxylate oxygenase activation invivo. *Photosynthesis Research* **7**, 193-201 (1985).

9 Robinson, S. P. & Portis, A. R. Adenosine-triphosphate hydrolysis by purified Rubisco activase. *Archives of Biochemistry and Biophysics* **268**, 93-99 (1989).

10 Scales, J. C., Parry, M. A. J. & Salvucci, M. E. A non-radioactive method for measuring Rubisco activase activity in the presence of variable ATP: ADP ratios, including modifications for measuring the activity and activation state of Rubisco. *Photosynthesis Research* **119**, 355-365 (2014).

11 Li, C. S., Wang, D. F. & Portis, A. R. Identification of critical arginine residues in the functioning of Rubisco activase. *Archives of Biochemistry and Biophysics* **450**, 176-182 (2006).

12 Salvucci, M. E., van de Loo, F. J. & Stecher, D. Two isoforms of Rubisco activase in cotton, the products of separate genes not alternative splicing. *Planta* **216**, 736-744 (2003).

13 Blayney, M. J., Whitney, S. M. & Beck, J. L. NanoESI mass spectrometry of Rubisco and Rubisco activase structures and their interactions with nucleotides and sugar phosphates. *Journal of the American Society for Mass Spectrometry* **22**, 1588-1601 (2011).

14 Siegenthaler, U. & Sarmiento, J. L. Atmospheric carbon-dioxide and the ocean. *Nature* **365**, 119-125 (1993).
15 Cleland, W. W., Andrews, T. J., Gutteridge, S., Hartman, F. C. & Lorimer, G. H. Mechanism of Rubisco: The carbamate as general base. *Chemical Reviews* **98**, 549-561 (1998).
16 Kellogg, E. A. & Juliano, N. D. The structure and function of Rubisco and their implications for systematic studies. *American Journal of Botany* **84**, 413-428 (1997).
17 Taylor, T. C. & Andersson, I. Structural transitions during activation and ligand binding in hexadecameric Rubisco inferred from the crystal structure of the activated unliganded spinach enzyme. *Nature Structural Biology* **3**, 95-101 (1996).
18 Tabita, F. R., Hanson, T. E., Li, H., Satagopan, S., Singh, J. & Chan, S. Function, structure, and evolution of the Rubisco-like proteins and their Rubisco homologs. *Microbiology and Molecular Biology Reviews* **71**, 576-+ (2007).
19 Bauwe, H., Hagemann, M. & Fernie, A. R. Photorespiration: players, partners and origin. *Trends in Plant Science* **15**, 330-336 (2010).
20 Maurino, V. G. & Peterhansel, C. Photorespiration: current status and approaches for metabolic engineering. *Current Opinion in Plant Biology* **13**, 249-256 (2010).
21 Tabita, F. R., Satagopan, S., Hanson, T. E., Kreel, N. E. & Scott, S. S. Distinct form I, II, III, and IV Rubisco proteins from the three kingdoms of life provide clues about Rubisco evolution and structure/function relationships. *Journal of Experimental Botany* **59**, 1515-1524 (2008).
22 Duff, A. P., Andrews, T. J. & Curmi, P. M. G. The transition between the open and closed states of rubisco is triggered by the inter-phosphate distance of the bound bisphosphate. *Journal of Molecular Biology* **298**, 903-916 (2000).
23 Andersson, I. & Taylor, T. C. Structural framework for catalysis and regulation in Ribulose-1,5-bisphosphate carboxylase/oxygenase. *Archives of Biochemistry and Biophysics* **414**, 130-140 (2003).
24 Lorimer, G. H. Ribulosebisphosphate carboxylase - amino acid sequence of a peptide bearing the activator carbon-dioxide. *Biochemistry* **20**, 1236-1240 (1981).
25 Hartman, F. C., Stringer, C. D. & Lee, E. H. Complete primary structure of Ribulosebisphosphate carboxylase/oxygenase from rhodospirillium-rubrum. *Archives of Biochemistry and Biophysics* **232**, 280-295 (1984).
26 Spreitzer, R. J. & Salvucci, M. E. Rubisco: Structure, regulatory interactions, and possibilities for a better enzyme. *Annual Review of Plant Biology* **53**, 449-475 (2002).
27 Bracher, A., Starling-Windhof, A., Hartl, F. U. & Hayer-Hartl, M. Crystal structure of a chaperone-bound assembly intermediate of form I Rubisco. *Nature Structural & Molecular Biology* **18**, 875-U1500 (2011).
28 Newman, J. & Gutteridge, S. The purification and preliminary-X-ray diffraction studies of recombinant synechococcur Ribulose-1,5-bisphosphate carboxylase oxygenase from escherichia-coli. *Journal of Biological Chemistry* **265**, 15154-15159 (1990).

29 Gutteridge, S., Rhoades, D. F. & Herrmann, C. Site-specific mutations in a loop region of the C-terminal domain of the large subunit of Ribulose bisphosphate carboxylase oxygenase that influence substrate partitioning. *Journal of Biological Chemistry* **268**, 7818-7824 (1993).

30 Spreitzer, R. J. Role of the small subunit in ribulose-1,5-bisphosphate carboxylase/oxygenase. *Archives of Biochemistry and Biophysics* **414**, 141-149 (2003).

31 Berry, J. A., Lorimer, G. H., Pierce, J., Seemann, J. R., Meek, J. & Freas, S. Isolation, identification and synthesis of 2-carboxyarabinitol 1-phosphate, a diurnal regulator of ribulose-bisphosphate carboxylase activity. *Proceedings of the National Academy of Sciences of the United States of America* **84**, 734-738 (1987).

32 Gutteridge, S., Parry, M. A. J., Burton, S., Keys, A. J., Mudd, A., Feeney, J., Servaites, J. C. & Pierce, J. A noctural inhibitor of carboxylation in leaves. *Nature* **324**, 274-276 (1986).

33 Andralojc, P. J., Madgwick, P. J., Tao, Y., Keys, A. J., Ward, J. L., Beale, M. H., Loveland, J. E., Jackson, P. J., Willis, A. C., Gutteridge, S. & Parry, M. A. J. 2-Carboxy-D-arabinitol 1-phosphate (CA1P) phosphatase: evidence for a wider role in plant Rubisco regulation. *Biochemical Journal* **442**, 733-742 (2012).

34 Parry, M. A. J., Keys, A. J., Madgwick, P. J., Carmo-Silva, A. E. & Andralojc, P. J. Rubisco regulation: a role for inhibitors. *Journal of Experimental Botany* **59**, 1569-1580 (2008).

35 Pearce, F. G. Catalytic by-product formation and ligand binding by Ribulose Bisphosphate Carboxylases from different phylogenies. *Biochemical Journal* **399**, 525-534 (2006).

36 Savir, Y., Noor, E., Milo, R. & Tlusty, T. Cross-species analysis traces adaptation of Rubisco toward optimality in a low-dimensional landscape. *Proceedings of the National Academy of Sciences* **107**, 3475-3480 (2010).

37 Read, B. A. & Tabita, F. R. High substrate-specificity factor ribulose-bisphosphate carboxylate oxygenase from eukaryotic marine-algae and properties of recombinant cyanobacterial rubisco containing algal residue modifications. *Archives of Biochemistry and Biophysics* **312**, 210-218 (1994).

38 Jordan, D. B. & Ogren, W. L. Species variation in the specificity of ribulose-bisphosphate carboxylase-oxygenase. *Nature* **291**, 513-515 (1981).

39 Whitney, S. M., Baldett, P., Hudson, G. S. & Andrews, T. J. Form I Rubiscos from non-green algae are expressed abundantly but not assembled in tobacco chloroplasts. *Plant Journal* **26**, 535-547 (2001).

40 Edmondson, D. L., Badger, M. R. & Andrews, T. J. Slow inactivation of ribulosebisphosphate carboxylase during catalysis is not due to decarbamylation of the catalytic site. *Plant Physiology* **93**, 1383-1389 (1990).

41 Edmondson, D. L., Badger, M. R. & Andrews, T. J. Slow inactivation of ribulosebiphosphate carboxylase during catalysis is caused by accumulation of a slow, tight-binding inhibitor at the catalytic site. *Plant Physiology* **93**, 1390-1397 (1990).

42 Robinson, S. P. & Portis, A. R. Release of the nocturnal inhibitor, carboxyarabinitol-1-phosphate, form ribulose bisphosphate carboxylase oxygenase by rubisco activase. *Febs Letters* **233**, 413-416 (1988).

43 Mueller-Cajar, O., Stotz, M., Wendler, P., Hartl, F. U., Bracher, A. & Hayer-Hartl, M. Structure and function of the AAA(+) protein CbbX, a red-type Rubisco activase. *Nature* **479**, 194-U166 (2011).

44 Sage, R. F., Way, D. A. & Kubien, D. S. Rubisco, Rubisco activase, and global climate change. *Journal of Experimental Botany* **59**, 1581-1595 (2008).

45 IPCC. *Fourth assessment report: climate change*, 2007).

46 Law, R. D., Crafts-Brandner, S. J. & Salvucci, M. E. Heat stress induces the synthesis of a new form of ribulose-1,5-bisphosphate carboxylase/oxygenase activase in cotton leaves. *Planta* **214**, 117-125 (2001).

47 Crafts-Brandner, S. J. & Salvucci, M. E. Rubisco activase constrains the photosynthetic potential of leaves at high temperature and CO2. *Proceedings of the National Academy of Sciences of the United States of America* **97**, 13430-13435 (2000).

48 Salvucci, M. E. & Crafts-Brandner, S. J. Mechanism for deactivation of Rubisco under moderate heat stress. *Physiologia Plantarum* **122**, 513-519 (2004).

49 Salvucci, M. E., Osteryoung, K. W., Crafts-Brandner, S. J. & Vierling, E. Exceptional sensitivity of rubisco activase to thermal denaturation in vitro and in vivo. *Plant Physiology* **127**, 1053-1064 (2001).

50 Salvucci, M. E. & Crafts-Brandner, S. J. Relationship between the heat tolerance of photosynthesis and the thermal stability of rubisco activase in plants from contrasting thermal environments. *Plant Physiology* **134**, 1460-1470 (2004).

51 CraftsBrandner, S. J., vandeLoo, F. J. & Salvucci, M. E. The two forms of rubisco activase differ in sensitivity to elevated temperature. *Plant Physiology* **114**, 1055-1055 (1997).

52 Kallis, R. P., Ewy, R. G. & Portis, A. R. Alteration of the adenine nucleotide response and increased Rubisco activation activity of Arabidopsis Rubisco activase by site-directed mutagenesis. *Plant Physiology* **123**, 1077-1086 (2000).

53 Carmo-Silva, A. E. & Salvucci, M. E. The activity of Rubisco's molecular chaperone, Rubisco activase, in leaf extracts. *Photosynthesis Research* **108**, 143-155 (2011).

54 Kobza, J. & Edwards, G. E. Control of photosynthesis in wheat by CO2, O2 and light-intensity. *Plant and Cell Physiology* **28**, 1141-1152 (1987).

55 Feller, U., CraftsBrandner, S. & Salvucci, M. Heat treatment inhibits light activation of rubisco by rubisco activase. *Plant Physiology* **111**, 346-346 (1996).

56 Berry, J. & Bjorkman, O. Photosynthetic response and adaptation to temperature in higher-plants. *Annual Review of Plant Physiology and Plant Molecular Biology* **31**, 491-543 (1980).

57 Schrader, S. M., Kane, H. J., Sharkey, T. D. & von Caemmerer, S. High temperature enhances inhibitor production but reduces fallover in tobacco Rubisco. *Functional Plant Biology* **33**, 921-929 (2006).

58 Neuwald, A. F., Aravind, L., Spouge, J. L. & Koonin, E. V. AAA(+): A class of chaperone-like ATPases associated with the assembly, operation, and disassembly of protein complexes. *Genome Research* **9**, 27-43 (1999).
59 Hanson, P. I. & Whiteheart, S. W. AAA+ Proteins: Have engine, will work. *Nature Reviews Molecular Cell Biology* **6**, 519-529 (2005).
60 Snider, J. L. & Houry, W. A. AAA+ proteins: diversity in function, similarity in structure. *Biochemical Society Transactions* **36**, 72-77 (2008).
61 Beyer, A. Sequence analysis of the AAA protein family. *Protein Science* **6**, 2043-2058 (1997).
62 Bar-Nun, S. & Glickman, M. H. Proteasomal AAA-ATPases: Structure and function. *Biochimica Et Biophysica Acta-Molecular Cell Research* **1823**, 67-82 (2012).
63 White, S. R. & Lauring, B. AAA+ ATPases: Achieving diversity of function with conserved machinery. *Traffic* **8**, 1657-1667 (2007).
64 Ammelburg, M., Frickey, T. & Lupas, A. N. Classification of AAA+ proteins. *Journal of Structural Biology* **156**, 2-11 (2006).
65 Lupas, A. N. & Martin, J. AAA proteins. *Current Opinion in Structural Biology* **12**, 746-753 (2002).
66 Lupas, A. N., Martin, J. & Zwickl, P. AAA plus proteins. *Journal of Structural Biology* **156**, 1-1 (2006).
67 Rao, S. T. & Rossmann, M. G. Comparison of super-secondary structures in proteins. *Journal of Molecular Biology* **76**, 241-& (1973).
68 Iyer, L. M., Leipe, D. D., Koonin, E. V. & Aravind, L. Evolutionary history and higher order classification of AAA plus ATPases. *Journal of Structural Biology* **146**, 11-31 (2004).
69 Chen, B. Y., Sysoeva, T. A., Chowdhury, S., Guo, L. A., De Carlo, S., Hanson, J. A., Yang, H. & Nixon, B. T. Engagement of arginine finger to ATP triggers large conformational changes in NtrC1 AAA+ ATPase for remodeling bacterial RNA polymerase. *Structure* **18**, 1420-1430 (2010).
70 Walker, J. E., Saraste, M., Runswick, M. J. & Gay, N. J. Distantly related sequences in the alpha-subunits and beta-subunits of the ATP Synthase, Myosin, Kinases and other ATP-requiring snzymes and a common nucleotide binding fold. *Embo Journal* **1**, 945-951 (1982).
71 Story, R. M. & Steitz, T. A. Structure of the RecA protein-ADP complex. *Nature* **355**, 374-376 (1992).
72 McWilliam, H., Li, W., Uludag, M., Squizzato, S., Park, Y. M., Buso, N., Cowley, A. & Lopez, R. Analysis tool web services from the EMBL-EBI. *Nucleic Acids Research* **41**, W597-W600 (2013).
73 Wendler, P., Ciniawsky, S., Kock, M. & Kube, S. Structure and function of the AAA plus nucleotide binding pocket. *Biochimica Et Biophysica Acta-Molecular Cell Research* **1823**, 2-14 (2012).
74 Ogura, T., Whiteheart, S. W. & Wilkinson, A. J. Conserved arginine residues implicated in ATP hydrolysis, nucleotide-sensing, and inter-subunit interactions in AAA and AAA+ ATPases. *Journal of Structural Biology* **146**, 106-112 (2004).

75 Karata, K., Inagawa, T., Wilkinson, A. J., Tatsuta, T. & Ogura, T. Dissecting the role of a conserved motif (the second region of homology) in the AAA family of ATPases - Site-directed mutagenesis of the ATP-dependent protease FtsH. *Journal of Biological Chemistry* **274**, 26225-26232 (1999).

76 Rombel, I., Peters-Wendisch, P., Mesecar, A., Thorgeirsson, T., Shin, Y. K. & Kustu, S. MgATP binding and hydrolysis determinants of NtrC, a bacterial enhancer-binding protein. *Journal of Bacteriology* **181**, 4628-4638 (1999).

77 Tucker, P. A. & Sallai, L. The AAA+ superfamily;A myriad of motions. *Current Opinion in Structural Biology* **17**, 641-652 (2007).

78 Guo, F. S., Maurizi, M. R., Esser, L. & Xia, D. Crystal structure of ClpA, an Hsp100 chaperone and regulator of ClpAP protease. *Journal of Biological Chemistry* **277**, 46743-46752 (2002).

79 Niwa, H., Tsuchiya, D., Makyio, H., Yoshida, M. & Morikawa, K. Hexameric ring structure of the ATPase domain of the membrane-integrated metalloprotease FtsH from Thermus thermophilus HB8. *Structure* **10**, 1415-1423 (2002).

80 Reid, B. G., Fenton, W. A., Homwich, A. L. & Weber-Ban, E. U. ClpA mediates directional translocation of substrate proteins into the ClpP protease. *Proceedings of the National Academy of Sciences of the United States of America* **98**, 3768-3772 (2001).

81 Gibson, J. L. & Tabita, F. R. Analysis of the cbbXYZ operon in Rhodobacter sphaeroides. *Journal of Bacteriology* **179**, 663-669 (1997).

82 Van de Loo, F. J. & Salvucci, M. E. Activation of Ribulose-1,5-bisphosphate carboxylase/oxygenase (Rubisco) involves Rubisco activase Trp16. *Biochemistry* **35**, 8143-8148 (1996).

83 Zeymer, C., Barends, T. R. M., Werbeck, N. D., Schlichting, I. & Reinstein, J. Elements in nucleotide sensing and hydrolysis of the AAA+ disaggregation machine ClpB: a structure-based mechanistic dissection of a molecular motor. *Acta Crystallographica Section D* **70**, 582-595 (2014).

84 El Bakkouri, M., Gutsche, I., Kanjee, U., Zhao, B., Yu, M., Goret, G., Schoehn, G., Burmeister, W. P. & Houry, W. A. Structure of RavA MoxR AAA+ protein reveals the design principles of a molecular cage modulating the inducible lysine decarboxylase activity. *Proceedings of the National Academy of Sciences of the United States of America* **107**, 22499-22504 (2010).

85 Peng, W., Lin, Z., Li, W., Lu, J., Shen, Y. & Wang, C. Structural insights into the unusually strong ATPase activity of the AAA domain of the Caenorhabditis elegans fidgetin-like 1 (FIGL-1) protein. *Journal of Biological Chemistry* **288**, 29305-29312 (2013).

86 Krissinel, E. & Henrick, K. Inference of macromolecular assemblies from crystalline state. *Journal of Molecular Biology* **372**, 774-797 (2007).

87 Portis, A. R. Rubisco activase - Rubisco's catalytic chaperone. *Photosynthesis Research* **75**, 11-27 (2003).

88 Werneke, J. M. & Ogren, W. L. Structure of an arabidopsis-thaliana cDNA-encoding Rubisco activase. *Nucleic Acids Research* **17**, 2871-2871 (1989).

89 Zielinski, R. E., Werneke, J. M. & Jenkins, M. E. Coordinate expression of Rubisco activase and Rubisco during barley leaf cell-development. *Plant Physiology* **90**, 516-521 (1989).

90 Rundle, S. J. & Zielinski, R. E. Alterations in Barley Ribulose-1,5-Bisphosphate Carboxylase Oxygenase activase gene-expression during development and in response to illumination. *Journal of Biological Chemistry* **266**, 14802-14807 (1991).

91 To, K. Y., Suen, D. F. & Chen, S. C. G. Molecular characterization of Ribulose-1,5-bisphosphate carboxylase/oxygenase activase in rice leaves. *Planta* **209**, 66-76 (1999).

92 Zhang, N. & Portis, A. R. Mechanism of light regulation of Rubisco: A specific role for the larger Rubisco activase isoform involving reductive activation by thioredoxin-f. *Proceedings of the National Academy of Sciences of the United States of America* **96**, 9438-9443 (1999).

93 Zhang, N., Schurmann, P. & Portis, A. R. Characterization of the regulatory function of the 46-kDa isoform of Rubisco activase from Arabidopsis. *Photosynthesis Research* **68**, 29-37 (2001).

94 Wang, D. & Portis, A. R. Increased sensitivity of oxidized large isoform of Ribulose-1,5-bisphosphate carboxylase/oxygenase (Rubisco) activase to ADP inhibition is due to an interaction between its carboxyl extension and nucleotide-binding pocket. *Journal of Biological Chemistry* **281**, 25241-25249 (2006).

95 Carmo-Silva, A. E. & Salvucci, M. E. The regulatory properties of Rubisco activase differ among species and affect photosynthetic induction during light transitions. *Plant Physiology* **161**, 1645-1655 (2013).

96 Robinson, S. P. & Portis, A. R. Ribulose-1,5-bisphosphate carboxylase oxygenase activase protein prevents the invitro decline in activity of ribulose-1,5-bisphosphate carboxylase oxygenase. *Plant Physiology* **90**, 968-971 (1989).

97 Wang, D. F. & Portis, A. R. Two conserved tryptophan residues are responsible for intrinsic fluorescence enhancement in Rubisco activase upon ATP binding. *Photosynthesis Research* **88**, 185-193 (2006).

98 Van de Loo, F. J. & Salvucci, M. E. Involvement of two aspartate residues of rubisco activase in coordination of the ATP gamma-phosphate and subunit cooperativity. *Biochemistry* **37**, 4621-4625 (1998).

99 CraftsBrandner, S. J., vandeLoo, F. J. & Salvucci, M. E. The two forms of ribulose-1,5-bisphosphate carboxylase/oxygenase activase differ in sensitivity to elevated temperature. *Plant Physiology* **114**, 439-444 (1997).

100 Wang, Z. Y. & Portis, A. R. A fluorometric study with 1-anilononaphthalene-8-sulfonic acid (ANS) of the interactions of ATP and ADP with Rubisco activase. *Biochimica Et Biophysica Acta* **1079**, 263-267 (1991).

101 Salvucci, M. E., Chavan, A. J., Klein, R. R., Rajagopolan, K. & Haley, B. E. Photoaffinity-labeling of the ATP binding domain of Rubisco activase and a seperate domain involved in the activation of Ribulose-1,5-bisphosphate carboxylase/oxygenase. *Biochemistry* **33**, 14879-14886 (1994).

102 Salvucci, M. E., Rajagopalan, K., Sievert, G. & Haley, B. E. Identification of the ATP gamma-phosphate binding domain of Rubisco activase. *Plant Physiology* **102**, 142-142 (1993).

103 Salvucci, M. E. Subunit interactions of Rubisco activase - Polyethylene-glycol promotes self-association, stimulates ATPase and activation activities, and enhances interactions with Rubisco. *Archives of Biochemistry and Biophysics* **298**, 688-696 (1992).

104 Li, C. H., Salvucci, M. E. & Portis, A. R. Two residues of rubisco activase involved in recognition of the rubisco substrate. *Journal of Biological Chemistry* **280**, 24864-24869 (2005).

105 Barta, C., Dunkle, A. M., Wachter, R. M. & Salvucci, M. E. Structural changes associated with the acute thermal instability of Rubisco activase. *Archives of Biochemistry and Biophysics* **499**, 17-25 (2010).

106 Chakraborty, M., Kuriata, A. M., Henderson, J. N., Salvucci, M. E., Wachter, R. M. & Levitus, M. Protein oligomerization monitored by fluorescence fluctuation spectroscopy: self-assembly of Rubisco activase. *Biophysical Journal* **103**, 949-958 (2012).

107 Sweeney, T. R., Cisnetto, V., Bose, D., Bailey, M., Wilson, J. R., Zhang, X. D., Belsham, G. J. & Curry, S. Foot-and-Mouth Disease Virus 2C Is a Hexameric AAA plus Protein with a Coordinated ATP Hydrolysis Mechanism. *Journal of Biological Chemistry* **285**, 24347-24359 (2010).

108 Joly, N., Zhang, N. & Buck, M. ATPase site architecture is required for self-assembly and remodeling activity of a hexameric AAA plus transcriptional activator. *Molecular Cell* **47**, 484-490 (2012).

109 Stotz, M. *Structure of green type Rubisco activase from Nicotiana tabacum* PhD thesis, (2011).

110 Keown, J. R. & Pearce, F. G. Characterisation of Spinach Ribulose-1,5-Bisphosphate carboxylase/oxygenase activase isoforms reveals hexameric assemblies with increased thermal stability. *Biochemical Journal* **464**, 413-423 (2014).

111 Lilley, R. M. & Portis, A. R. ATP hydrolysis activity and polymerization state of Ribulose-1,5-Bisphosphate Carboxylase Oxygenase activase - Do the effects of Mg2+, K+, and activase concentrations indicate a functional similarity to Actin? *Plant Physiology* **114**, 605-613 (1997).

112 Wang, Z. Y., Snyder, G. W., Esau, B. D., Portis, A. R. & Ogren, W. L. Species-dependent variation in the interaction of substrate-bound Ribulose-1,5-bisphosphate carboxylase oxygenase (Rubisco) and Rubisco activase. *Plant Physiology* **100**, 1858-1862 (1992).

113 Portis, A. R., Li, C. S., Wang, D. F. & Salvucci, M. E. Regulation of Rubisco activase and its interaction with Rubisco. *Journal of Experimental Botany* **59**, 1597-1604 (2008).

114 Esau, B. D., Snyder, G. W. & Portis, A. R. Activation of Ribulose-1,5-Bisphosphate Carboxylase/Oxygenase (Rubisco) with chimeric activase proteins. *Photosynthesis Research* **58**, 175-181 (1998).

115 Ott, C. M., Smith, B. D., Portis, A. R. & Spreitzer, R. J. Activase region on chloroplast Ribulose-1,5-bisphosphate carboxylase/oxygenase - nonconservative substitution in the large subunit alters species specificity of protein interaction. *Journal of Biological Chemistry* **275**, 26241-26244 (2000).

116 Portis, A. R. The regulation of Rubisco by Rubisco activase. *Journal of Experimental Botany* **46**, 1285-1291 (1995).

117 Larson, E. M., Obrien, C. M., Zhu, G. H., Spreitzer, R. J. & Portis, A. R. Specificity for activase is changed by a Pro-89 to Arg substitution in the large subunit of Ribulose-1,5-bisphosphate carboxylase/oxygenase. *Journal of Biological Chemistry* **272**, 17033-17037 (1997).

118 Wachter, R. M., Salvucci, M. E., Carmo-Silva, A. E., Barta, C., Genkov, T. & Spreitzer, R. J. Activation of interspecies-hybrid Rubisco enzymes to assess different models for the Rubisco-Rubisco activase interaction. *Photosynthesis Research* **117**, 557-566 (2013).

119 Gloria Esquivel, M., Genkov, T., Nogueira, A. S., Salvucci, M. E. & Spreitzer, R. J. Substitutions at the opening of the Rubisco central solvent channel affect holoenzyme stability and CO2/O-2 specificity but not activation by Rubisco activase. *Photosynthesis Research* **118**, 209-218 (2013).

120 Portis, A. R. in *Annual Plant Reviews* Vol. 7 (ed M. T. McManus) 30-52 (Sheffield Academic Press, Protein-protein interaction in plant biology, 2001).

121 Buchen-Osmond, C., Portis, A. & Andrews, J. in *Research in photosynthesis: proceedings of the IXth International Congres.* (ed Norio Murata) 653-656.

122 Gasteiger, E., Gattiker, A., Hoogland, C., Ivanyi, I., Appel, R. D. & Bairoch, A. ExPASy: the proteomics server for in-depth protein knowledge and analysis. *Nucleic Acids Research* **31**, 3784-3788 (2003).

123 Catanzariti, A. M., Soboleva, T. A., Jans, D. A., Board, P. G. & Baker, R. T. An efficient system for high-level expression and easy purification of authentic recombinant proteins. *Protein Science* **13**, 1331-1339 (2004).

124 Baker, R. T., Catanzariti, A. M., Karunasekara, Y., Soboleva, T. A., Sharwood, R., Whitney, S. & Board, P. G. in *Ubiquitin and Protein Degradation, Part A* Vol. 398 *Methods in Enzymology* (ed R. J. Deshaies) 540-554 (2005).

125 Barta, C., Carmo-Silva, A. E. & Salvucci, M. E. in *Photosynthesis Research Protocols, Second Edition* Vol. 684 *Methods in Molecular Biology* (ed R. Carpentier) 363-374 (2011).

126 Servaites, J. C. Crystalline ribulose bisphosphate carboxylase oxygenase of high integrity and catalytic activity from nicotiana tabacum. *Archives of Biochemistry and Biophysics* **238**, 154-160 (1985).

127 Lilley, R. M. & Walker, D. A. Improved spectrophotometric assay for Ribulose-bis-phosphate carboxylase. *Biochimica Et Biophysica Acta* **358**, 226-229 (1974).

128 Kane, H. J., Wilkin, J. M., Portis, A. R. & Andrews, T. J. Potent inhibition of ribulose-bisphosphate carboxylase by an oxidized impurity in ribulose-1,5-bisphosphate. *Plant Physiology* **117**, 1059-1069 (1998).

129 Laue, T. M., Shah, B. D., Ridgeway, T. M. & Pelletier, S. L. Analytical ultracentrifugation in biochemistry and polymer science. 90-125 (1992).

130 Schuck, P. Size-distribution analysis of macromolecules by sedimentation velocity ultracentrifugation and Lamm equation modeling. *Biophysical Journal* **78**, 1606-1619 (2000).
131 Schuck, P., Perugini, M. A., Gonzales, N. R., Howlett, G. J. & Schubert, D. Size-distribution analysis of proteins by analytical ultracentrifugation: Strategies and application to model systems. *Biophysical Journal* **82**, 1096-1111 (2002).
132 Schuck, P. On the analysis of protein self-association by sedimentation velocity analytical ultracentrifugation. *Analytical Biochemistry* **320**, 104-124 (2003).
133 Cole, J. L. in *Methods in Enzymology* Vol. Volume 384 (eds L. Johnson Michael & Brand Ludwig) 212-232 (Academic Press, 2004).
134 Cole, A. B., Folimonova, S. Y., Watson, B. S., Sumner, L. W. & Nelson, R. S. Silencing of rubisco activase, an up-regulated protein during Tobacco mosaic virus infection, does not attenuate TMV infection in Nicotiana benthamiana. *Phytopathology* **94**, S20-S20 (2004).
135 Kirby, N. M., Mudie, S. T., Hawley, A. M., Cookson, D. J., Mertens, H. D. T., Cowieson, N. & Samardzic-Boban, V. A low-background-intensity focusing small-angle X-ray scattering undulator beamline. *Journal of Applied Crystallography* **46**, 1670-1680 (2013).
136 Petoukhov, M. V., Konarev, P. V., Kikhney, A. G. & Svergun, D. I. ATSAS 2.1 - towards automated and web-supported small-angle scattering data analysis. *Journal of Applied Crystallography* **40**, S223-S228 (2007).
137 Konarev, P. V., Volkov, V. V., Sokolova, A. V., Koch, M. H. J. & Svergun, D. I. PRIMUS: a Windows PC-based system for small-angle scattering data analysis. *Journal of Applied Crystallography* **36**, 1277-1282 (2003).
138 Svergun, D. I., Petoukhov, M. V. & Koch, M. H. J. Determination of domain structure of proteins from X-ray solution scattering. *Biophysical Journal* **80**, 2946-2953 (2001).
139 Petoukhov, M. V., Franke, D., Shkumatov, A. V., Tria, G., Kikhney, A. G., Gajda, M., Gorba, C., Mertens, H. D. T., Konarev, P. V. & Svergun, D. I. New developments in the ATSAS program package for small-angle scattering data analysis. *Journal of Applied Crystallography* **45**, 342-350 (2012).
140 Petoukhov, M. V. & Svergun, D. I. Global rigid body modeling of macromolecular complexes against small-angle scattering data. *Biophysical Journal* **89**, 1237-1250 (2005).
141 Svergun, D., Barberato, C. & Koch, M. H. J. CRYSOL-a program to evaluate X-ray solution scattering of biological macromolecules from atomic coordinates. *Journal of Applied Crystallography* **28**, 768-773 (1995).
142 Mylonas, E. & Svergun, D. I. Accuracy of molecular mass determination of proteins in solution by small-angle X-ray scattering. *Journal of Applied Crystallography* **40**, S245-S249 (2007).
143 Feigin, L. A. & Svergun, D. I. *Structure analysis by small-angle X-ray and neutron scattering*. (1987).
144 Niesen, F. H., Berglund, H. & Vedadi, M. The use of differential scanning fluorimetry to detect ligand interactions that promote protein stability. *Nature Protocols* **2**, 2212-2221 (2007).

145 Erzberger, J. P., Mott, M. L. & Berger, J. M. Structural basis for ATP-dependent DnaA assembly and replication-origin remodeling. *Nature Structural & Molecular Biology* **13**, 676-683 (2006).
146 Kress, W., Mutschler, H. & Weber-Ban, E. Assembly pathway of an AAA+ protein: Tracking ClpA and ClpAP complex formation in real time. *Biochemistry* **46**, 6183-6193 (2007).
147 Keown, J. R., Griffin, M. D. W., Mertens, H. D. T. & Pearce, F. G. Small oligomers of Ribulose-bisphosphate carboxylase/oxygenase (Rubisco) activase are required for biological activity. *The Journal of biological chemistry* **288**, 20607-20615 (2013).
148 Dam, J. & Schuck, P. Sedimentation velocity analysis of heterogeneous protein-protein interactions: sedimentation coefficient distributions c(s) and asymptotic boundary profiles from Gilbert-Jenkins theory. *Biophysical Journal* **89**, 651-666 (2005).
149 Dam, J. & Schuck, P. in *Methods in Enzymology* Vol. Volume 384 (eds L. Johnson Michael & Brand Ludwig) 185-212 (Academic Press, 2004).
150 Brookes, E., Demeler, B., Rosano, C. & Rocco, M. The implementation of SOMO (SOlution MOdeller) in the UltraScan analytical ultracentrifugation data analysis suite: enhanced capabilities allow the reliable hydrodynamic modeling of virtually any kind of biomacromolecule. *European Biophysics Journal* **39**, 423-435 (2010).
151 Mertens, H. D. T. & Svergun, D. I. Structural characterization of proteins and complexes using small-angle X-ray solution scattering. *Journal of Structural Biology* **172**, 128-141 (2010).
152 Gardemann, A., Schimkat, D. & Heldt, H. W. Control of CO2 fixation regulation of stromal fructose-1,6-bisphosphatase in spinach by pH and Mg 2+ concentration. *Planta* **168**, 536-545 (1986).
153 Michelet, L., Zaffagnini, M., Morisse, S., Sparla, F., Perez-Perez, M. E., Francia, F., Danon, A., Marchand, C. H., Fermani, S., Trost, P. & Lemaire, S. D. Redox regulation of the Calvin-Benson cycle: something old, something new. *Frontiers in Plant Science* **4** (2013).
154 Ishijima, S., Uchlbori, A., Takagi, H., Maki, R. & Ohnishi, M. Light-induced increase in free Mg2+ concentration in spinach chloroplasts: Measurement of free Mg2+ by using a fluorescent probe and necessity of stromal alkalinization. *Archives of Biochemistry and Biophysics* **412**, 126-132 (2003).
155 Frolov, A. & Tikhonov, A. Influence of light-induced changes in stromal and lumenal pH on electron transport kinetics in chloroplasts: mathematical modeling. *Biophysics* **52**, 398-405 (2007).
156 Monroe, N., Han, H., Gonciarz, M. D., Eckert, D. M., Karren, M., Whitby, F. G., Sundquist, W. I. & Hill, C. P. The oligomeric state of the active Vps4 AAA ATPase. *Journal of Molecular Biology* **426**, 510-525 (2014).
157 Rokka, A., Zhang, L. X. & Aro, E. M. Rubisco activase: an enzyme with a temperature-dependent dual function? *Plant Journal* **25**, 463-471 (2001).
158 Bowman, G. D., O'Donnell, M. & Kuriyan, J. Structural analysis of a eukaryotic sliding DNA clamp-clamp loader complex. *Nature* **429**, 724-730 (2004).

159 Bochman, M. L., Bell, S. P. & Schwacha, A. Subunit organization of Mcm2-7 and the unequal role of active Sites in ATP hydrolysis and viability. *Molecular and Cellular Biology* **28**, 5865-5873 (2008).
160 Maisel, T., Joseph, S., Mielke, T., Bürger, J., Schwarzinger, S. & Meyer, O. The CoxD protein, a novel AAA+ ATPase involved in metal cluster assembly: hydrolysis of nucleotide-triphosphates and oligomerization. *Plos One* **7**, e47424 (2012).
161 Hattendorf, D. A. & Lindquist, S. L. Analysis of the AAA sensor-2 motif in the C-terminal ATPase domain of Hsp104 with a site-specific fluorescent probe of nucleotide binding. *Proceedings of the National Academy of Sciences* **99**, 2732-2737 (2002).
162 Nishida, S., Fujimitsu, K., Sekimizu, K., Ohmura, T., Ueda, T. & Katayama, T. A nucleotide switch in the Escherichia coli DnaA protein initiates chromosomal replication: evidnece from a mutant DnaA protein defective in regulatory ATP hydrolysis in vitro and in vivo. *Journal of Biological Chemistry* **277**, 14986-14995 (2002).
163 Pérez-Martín, J. & de Lorenzo, V. ATP binding to the σ54-dependent activator XylR triggers a protein multimerization cycle catalyzed by UAS DNA. *Cell* **86**, 331-339 (1996).
164 Bock, R. M., Ling, N., Morell, S. A. & Lipton, S. H. Ultraviolet absorption spectra of adenosine-5′-triphosphate and related 5′-ribonucleotides. *Archives of Biochemistry and Biophysics* **62**, 253-264 (1956).
165 Jiang, R., Yang, H., Sun, F. & Chen, T. Searching for interpretable rules for disease mutations: a simulated annealing bump hunting strategy. *Bmc Bioinformatics* **7** (2006).
166 Vistica, J., Dam, J., Balbo, A., Yikilmaz, E., Mariuzza, R. A., Rouault, T. A. & Schuck, P. Sedimentation equilibrium analysis of protein interactions with global implicit mass conservation constraints and systematic noise decomposition. *Analytical Biochemistry* **326**, 234-256 (2004).
167 Cole, J. L., Lary, J. W., P. Moody, T. & Laue, T. M. in *Methods in Cell Biology* Vol. Volume 84 (eds J. Correia Dr. John & Dr. H. William Detrich, III) 143-179 (Academic Press, 2008).
168 SEDPHAT. *http://www.analyticalultracentrifugation.com/sedphat/statistics.htm*, 2005).
169 Rambo, R. P. & Tainer, J. A. Accurate assessment of mass, models and resolution by small-angle scattering. *Nature* **496**, 477-481 (2013).
170 Shen, J. B., Orozco, E. M. & Ogren, W. L. Expression of the 2 isoforms of spinach Ribulose 1,5-bisphosphate carboxylase activase and essentiality of the conserved lysine in teh concensus nucleotide-binding domain. *Journal of Biological Chemistry* **266**, 8963-8968 (1991).
171 Esau, B. D., Snyder, G. W., Portis, A. R. & Ogren, W. L. Identification of residues controlling substrate preference in rubisco activase. *Plant Physiology* **102**, 142-142 (1993).
172 Zhang, N., Kallis, R. P., Ewy, R. G. & Portis, A. R. Light modulation of Rubisco in Arabidopsis requires a capacity for redox regulation of the larger Rubisco

activase isoform. *Proceedings of the National Academy of Sciences of the United States of America* **99**, 3330-3334 (2002).

173 Salvucci, M. E., Werneke, J. M., Ogren, W. L. & Portis, A. R. Purification and species distribution of Rubisco activase. *Plant Physiology* **84**, 930-936 (1987).

174 Andersson, I. Catalysis and regulation in Rubisco. *Journal of Experimental Botany* **59**, 1555-1568 (2008).

175 IPCC. *Summary for policymakers. in: climate change 2013: the physical science basis. contribution of working group I to the fifth assessment report of the intergovernmental panel on climate change*. (2013).

176 Karl, T. R., Melillo, J. M. & Peterson, T. C. Global climate change impacts in the United States. (2009).